The Dissertation Committee for Jung Joo Byun
certifies that this is the approved version of the following dissertation:

Laminar Burning Velocities and Laminar Flame Speeds of Multi-Component Fuel Blends at Elevated Temperatures and Pressures

Committee:

Ronald D. Matthews, Supervisor

Matthew J. Hall, Supervisor

Janet L. Ellzey

Ofodike A. Ezekoye

Charles E. Roberts

Laminar Burning Velocities and Laminar Flame Speeds of Multi-Component Fuel Blends at Elevated Temperatures and Pressures

by

Jung Joo Byun, B.S.; M.S.

DISSERTATION

Presented to the Faculty of the Graduate School of

The University of Texas at Austin

in Partial Fulfillment

of the Requirements

for the Degree of

DOCTOR OF PHILOSOPHY

THE UNIVERSITY OF TEXAS AT AUSTIN

May 2011

Dedicated to

Hye Jin, Elaina, Mom, Dad,

And

The Heavenly Father.

Acknowledgments

This dissertation is dedicated to all my sources of inspiration that contributed to the process. First of all, I want to thank God for guiding me.

I would like to thank my advisers Dr. Ronald D. Matthews and Dr. Matthew J. Hall for their guidance and insight. More importantly, it was their thoughtfulness and understanding during my doctoral studies at the University of Texas at Austin that had the most positive effect on me. I also want to thank the dissertation committee members, Dr. Janet L. Ellzey, Dr. Ofodike A. Ezekoye and Dr. Charles E. Roberts, for their advice and service.

I am very grateful to Dr. Charles E. Roberts for giving me the invaluable opportunity to work in the Southwest Research Institute, where I developed my knowledge in combustion as well as in conducting engineering research. To the others at the Southwest Research Institute, Dr. Terrence Alger II, Dr. Shin Hyuk Joo, Mark Walls and Dwight T. Freeman, I am blessed to have received their support in combustion chamber experiments.

I would also like to thank Dr. Ho-Myung Chang at Hongik University for his endless support, guidance and encouragement.

I am forever indebted to my friends who have accompanied me to this moment from my days at Hongik University, Korea Advanced Institute of Science and Technology (KAIST) and the University of Texas at Austin .

I thank my pastors, Joseph Kim, Ilsun Kim, and Hachul Kim as well as all the families in Christ at the Austin Korean Presbyterian Church for their prayers, encouragement and love.

My parents Dr. Hee Joon Byun and Hye Sik Shin, my brother Dong Joo Byun, and my sister Jae Eun Byun, have been with me my entire life and continue to love me in the name of family.

Finally, I wholeheartedly thank my dear wife, Hye Jin Jung, and our beautiful daughter, Elaina, for being patient and always supporting me. They are true gifts from God.

Laminar Burning Velocities and Laminar Flame Speeds of Multi-Component Fuel Blends at Elevated Temperatures and Pressures

Publication No. _____

Jung Joo Byun, Ph.D.
The University of Texas at Austin, 2011

Supervisors: Ronald D. Matthews
Matthew J. Hall

Iso-octane, *n*-heptane, ethanol and their blends were tested in a constant volume combustion chamber to measure laminar burning velocities. The experimental apparatus was modified from the previous version to an automatically-controlled system. Accuracy and speed of data acquisition were improved by this modification. The laminar burning velocity analysis code was also improved for minimized error and fast calculation. A large database of laminar burning velocities at elevated temperatures and pressures was established using this improved experimental apparatus and analysis code.

From this large database of laminar burning velocities, laminar flame speeds were extracted. Laminar flame speeds of *iso*-octane, *n*-heptane and blends were investigated and analysed to derive new correlations to predict

laminar flame speeds of any blending ratio. Ethanol and ethanol blends with *iso*-octane and/or *n*-heptane were also examined to see the role of ethanol in the blends.

Generally, the results for *iso*-octane and *n*-heptane agree with published data. Additionally, blends of *iso*-octane and *n*-heptane exhibited flame speeds that followed linear blending relationships. A new flame speed model was successfully applied to these fuels. Ethanol and ethanol blends with *iso*-octane and/or *n*-heptane exhibited a strongly non-linear blending relationship and the new flame speed model was not applied to these fuels. It was shown that the addition of ethanol into *iso*-octane and/or *n*-heptane accelerated the flame speeds.

Table of Contents

List of Tables

List of Figures

Chapter 1

Introduction

1.1 Motivation

The first goal of this research was to build an experimental apparatus with the capability of taking large amounts of data relating to premixed combustion processes and to establish a large database of laminar burning velocities of *iso*-octane, *n*-heptane, ethanol and their various blends. The laminar burning velocity is the calculated flame velocity in a constant volume chamber using pressure as the primary data measurement(pressure measuring method). This method is described in Subsection 2.1.6.2, Chap. 3 and Chap. 4. This laminar burning velocity includes effects of ignition and stretch in the beginning of combustion, where the radius of the flame is small. Also it includes effects of chamber wall and cellularity generation, where the flame radius is large. Due to these effects near the beginning and end of combustion, this flame velocity is not purely a fuel property. However, the laminar burning velocity data near the beginning and end of combustion are useful in research on the effects of ignition, stretch and quenching in real engines. From the mid 1990s, the stretch effect on the spherical flame has been investigated [2, 3, 24, 28, 30, 37, 38, 40, 49, 50, 56]. Hasse et al. [25] had research on the effect of ignition and Kelley and Law [35] conducted research on the effect of

ignition and of chamber walls on the spherical flames. Also, Bradely et al. [6] and Jomaas et al. [31] did research on the cellularity on the expanding flames. Establishing a large database of laminar burning velocities also helps the engine designer choose fuels. Even though this velocity is not the exact laminar flame speed, which is a fuel property, it can be achieved at a wide range of temperatures and pressures up to engine-like conditions. This flame velocity can be used to predict the relative engine performance. Stanglmaier et al. [48] used the spherical chamber to determine laminar burning velocities of multicomponent fuels that can be generally described as premium gasoline. These fuels were also tested in an instrumented 4-cylinder SI engine at 13,000 RPM. With this engine, MBT timing of these fuels was measured and these were in good qualitative agreement with measured laminar burning velocities.

The second goal of this research was to extract the laminar flame speed from the laminar burning velocity database and to analyse these data to determine a new method to predict the laminar flame speed of blended fuels. The laminar flame speed is one of the fuel-oxidizer mixture properties. It is defined as the velocity at which unburned gases move through the combustion wave in the direction normal to the wave surface [18]. It has been researched for several decades; however, there have been limitations of those results such as low pressure, low temperature and insufficient data. In a real engine, the burning velocity is higher than the corresponding laminar flame speed because of turbulence. The laminar flame speed is used in turbulent burning models which consider turbulent flames to be composed of laminar "flamelets" that

are wrinkled and stretched by the turbulent flow field [39]. Recent studies into the effect of flame stretch and wrinkling on premixed turbulent combustion rely heavily on the laminar flame speed. The laminar flame speed also affects the ignition delay time, wall quench layer thickness and required ignition energy [14]. The efforts to develop a new fuel for higher performance and less pollution has been made by developing new fuels or blending existing fuels [8]. According to previous research, the engine power production potential of a fuel is influenced by fuel characteristics such as specific energy content, stoichiometric ratio, volatility and latent heat of vaporization. In addition, it is recognized that a rapid heat release is desirable for maximizing the thermodynamic efficiency and to reduce knock. This burn rate effect is quantified by the MBT timing. This flame propagation rate is related to instantaneous turbulence intensity, bulk flow within the chamber and laminar flame speed. Among these factors, only the laminar flame speed is a fundamental thermochemical property of the fuel-oxidizer mixture [48].

A great deal of data exists for the laminar flame speed of gaseous fuels at low pressures and temperatures. These data were generally determined by using a laminar burner device. Figure 1.1 shows the laminar flame speed of methane-air mixtures [1, 10, 15, 21, 47, 51], and Figure 1.2 shows the laminar flame speed of *iso*-octane-air mixtures at room temperature and atmospheric pressure [17, 20, 41]. All data show the highest value of laminar flame speed at about 1.1 equivalence ratio; however, the variance in the laminar flame speed value varies by up to 25%, showing the need for more accurate and more

repeatable results from an extended database.

In internal combustion engines the unburned gas temperature can be as high as 1000 K and the pressure ranges from 1 to 35 atm, with variations in fuel/air equivalence ratios from 0.6 to 1.4 [13]. Currently, the laminar flame speeds for fuels over the full range of pressures and temperatures of an internal combustion engine are not available. Also, as new fuels, including blended fuels, are developed, new techniques to measure the laminar flame speed at elevated pressures and temperatures to simulate more engine-like condition are required. In this research, an automatically controlled experimental apparatus was established to perform as many tests as possible and to make a large database of laminar flame speeds for primary reference fuels and their blends.

Based on this database, a new physically-based flame-speed blending model for *iso*-octane, *n*-heptane and their blends was developed, as explained in Chap. 5. So far, most laminar flame speed models have been functions of pressure, temperature and the equivalence ratio. These models cannot be directly used for blended fuels. This is because the temperature and pressure exponents are not expected to be linear in the fuel blend composition. Temperature and pressure are not independent in the combustion process. Therefore, a narrow range of initial conditions must be tested in order to examine engine-like conditions at every fuel blend composition. A new laminar flame speed model, which is a function of thermodynamic properties, state properties and reaction rate, is developed for *iso*-octane, *n*-heptane and blends. This is explained in detail in Subsection 5.2.1. Laminar flame speeds of ethanol and

blends with *iso*-octane or *n*-heptane were also examined to see the effect of ethanol in blends. This is explained in Subsection 5.2.2.

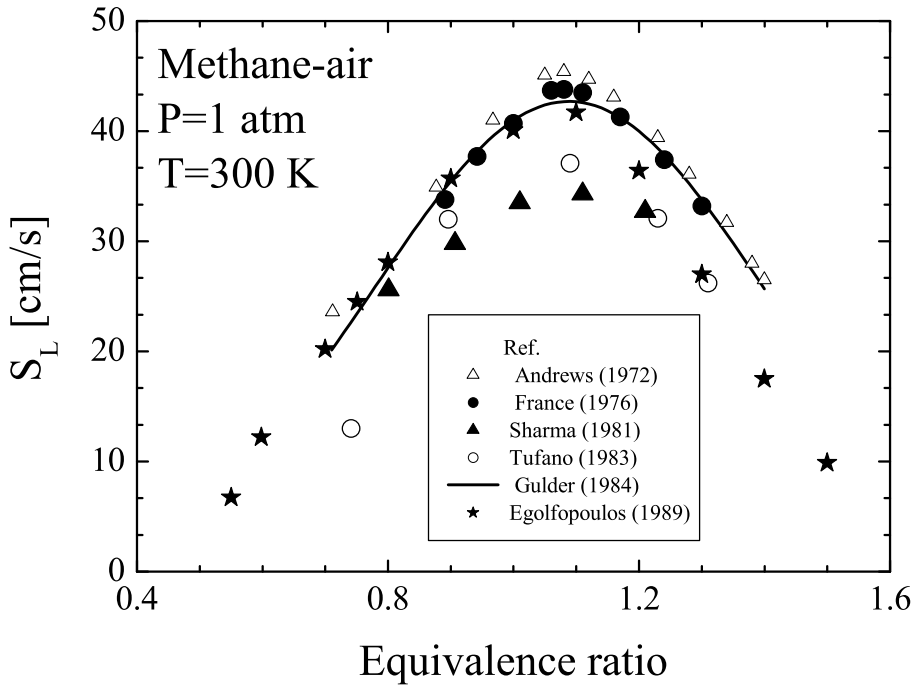

Figure 1.1: Laminar flame speed of methane-air mixtures at room temperature and atmospheric pressure.

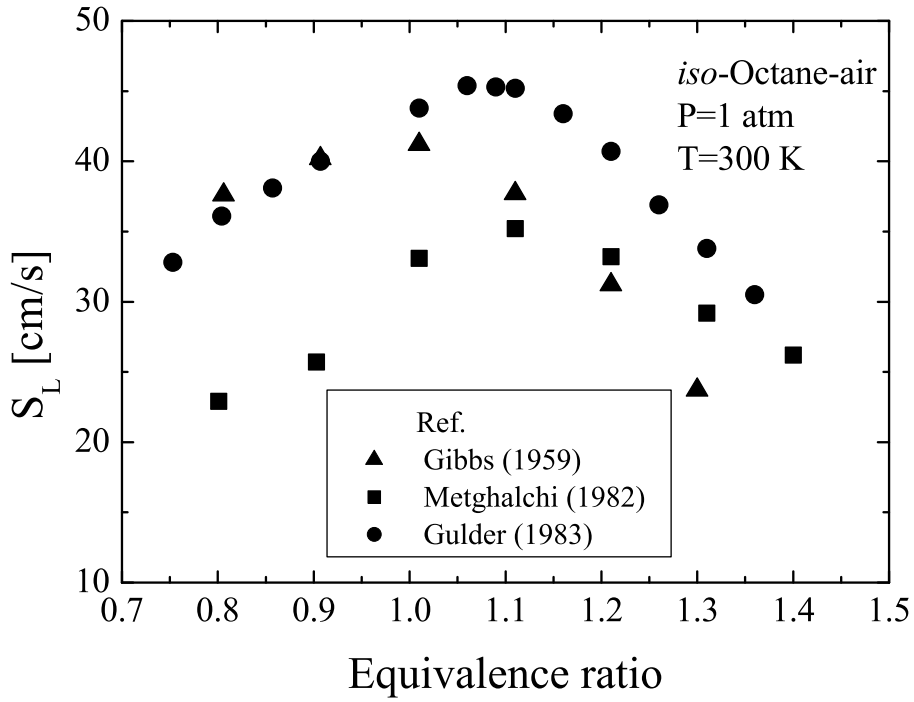

Figure 1.2: Laminar flame speed of *iso*-octane-air mixtures at room temperature and atmospheric pressure.

1.2 Scope

This study sought to acquire large data sets for fuels of interest to the automotive industry. Further, the flame speed measurements were analyzed to extract laminar flame speed over a broad range of temperatures, pressures and equivalence ratios. Blended fuel results were included. Finally, a flame speed model is presented.

This dissertation consists of six chapters.

Chapter 2 Literature Review contains a general classification of laminar flame speed measurement methods, followed by a review of analyses by other researchers. Several types of laminar flame speed measurement methods are introduced. A review of laminar flame speed measurements at elevated temperatures and pressures is also provided with classification with fuel type, pressure and temperature range and type of method.

In *Chapter 3 Experimental Apparatus*, the constant volume combustion chamber and automatically controlled, annexed devices are introduced. The drawings and control methods for these components are discussed in detail. Also, the analytical and empirical methods to verify the homogeneous mixing of fuel and air in the chamber, before the combustion event, are explained.

Chapter 4 Laminar Burning Velocity Calculation contains the explanation of the laminar burning velocity calculation code. Overall and detailed calculation procedures are introduced. Also, validation of experiment and calculation, by comparing the methane flame speed data from this research to

those from CHEMKIN [33], is shown.

The main results of this research are addressed in *Chapter 5 Laminar Burning Velocity Database and Laminar Flame Speed Analysis*. Firstly, the laminar burning velocity database is introduced. Secondly, the laminar flame speed analysis with a new correlation to predict laminar flame speeds of *iso*-octane and *n*-heptane blends with any blending ratio is introduced. Finally, the effect of ethanol in blends is also discussed.

Chapter 6 Conclusions and Recommendations present the conclusions from this dissertation. Several future activities are also proposed.

Chapter 2

Literature Review

2.1 Laminar Flame Speed Measurement Methods

Numerous experimental methods have been developed to measure the laminar flame speed of fuel-oxidant mixtures. The methods for measuring the laminar flame speed can be classified into two categories as follows [9]:

1. Stationary flames: in these methods, a premixed mixture flows into a stationary flame with a velocity that is equal to the burning velocity. Flat-flame burners and counter-flow burners are in this category.

2. Moving flames: in these methods, the flame moves through the mixture. The techniques include: cylindrical tube, soap bubble, constant pressure chamber and constant volume chamber methods.

2.1.1 Flat-flame burner method

In this method, a porous metal disc is placed at the exit of a large flow tube and it creates flat flames. After achieving a flat flame by adjusting flow rate, flame diameter is measured. The area of the flame is divided into the unburned mixture volume flow rate to have the laminar flame speed. The flame experiences reduced stability at higher flame speeds. A cooling porous

plug and extending results to the zero cooling condition with extrapolation is performed to measure the fast flame speed [18].

Bosschaart and de Goey [4] used a plenum chamber that consisted of a specific perforation pattern. This chamber was cooled to have the same temperature as the unburned gas mixture. The heat flux method was used to measure the flame speed in order to avoid uncertainty introduced by the extrapolation method. Results were presented for the laminar flame speed of methane-air mixture at $T_u = 295$ K, $P_u = 1.0$ bar with a wide range of equivalence ratio.

2.1.2 Counter-flow burner method

In this method, two axisymmetric counterflow burners make symmetrical and planar flames. The axial velocity profile along the centerline of the flow is measured using laser Doppler velocimetry. From this axial velocity profile, laminar flame speed is achieved by linear extrapolation in a laminar flame speed-strain rate graph.

With this method, Zhu et al. [57] determined the laminar flame speed of methane-(Ar, N2, CO2)-air mixtures over the pressure range from 0.25 to 2 atm and flame temperature range of 1,550 to 2,250 K. Egolfopoulos et al. [10] used the counterflow burner method to measure laminar flame speeds of Methane-Air mixtures under reduced and elevated pressures. Also Egolfopoulos et al. [12] measured laminar flame speeds of C2-Hydrocarbons(Ethane, Ethylene, Acetylene) and Propane with oxygen and nitrogen. The pressure

range was 0.25 atm to 3 atm. With calculated laminar flame speed data, kinetic schemes were validated. Egolfopoulos et al. [11] used this method for the laminar flame speed of ethanol and research on oxidation kinetics at atmospheric pressure. The unburned mixture temperatures were 298 K, 363 K, 428 K and 453 K. Vagelopoulos and Egolfopoulos [52] determined the laminar flame speed of carbon monoxide-hydrogen-air and carbon monoxide-methane-air mixtures. They investigated the effect of hydrogen and methane addition to CO-air flames. Because added H radicals increased branching and accelerated CO oxidation reaction rate, the addition of hydrogen and methane increased the laminar flame speed of CO-air flames. Wang et al. [53] measured the laminar flame speed of benzene-air flames at a temperature of 363 K and atmospheric pressure. They also conducted research on lean extinction and flammability limit of benzene. Saso et al. [46] determined the laminar flame speed of trifluoromethane-methane mixtures at atmospheric pressure with this method. Fluorinated hydrocarbon compounds are alternate fire suppressants and research on the effect of these compounds on flame was performed for an effective extinguishment of fire with minimized toxic fluoride generation. Hirasawa et al. [26] used the counter-flow burner method to determine the laminar flame speeds of atmospheric binary fuel blends of ethylene, *n*-butane and toluene. A flame-temperature based mixing rule was derived, and calculated flame speed was compared with other results from experiments. Huang et al. [27] investigated the laminar flame speed of primary reference fuels, *iso*-octane, *n*-heptane and their blends, reformer gas and reformer gas-*iso*-octane-

air mixtures using the counterflow burner method. They found that adding small amounts of reformer gas increased the flame speed of hydrocarbon-air mixtures. The temperature and pressure were 298 K and 1 atm, respectively. Freeh et al. [16] measured laminar flame speed using a counterflow flame for *iso*-octane-air and *n*-decane-air mixtures at preheated temperatures ranging 323 K to 400 K, all at 1 atm pressure. With different amounts of nitrogen dilution, they obtained different adiabatic flames temperatures. The activation energies of *iso*-octane-air mixtures at atmospheric pressure and at two temperatures, 300 K and 360 K, were determined as a function of equivalence ratio using this approach.

2.1.3 Cylindrical tube method

In this method, fuel-oxidant mixture is burned in a horizontal tube that has one opened end. The ignition occurs at opened end and the flame speed is the rate of the flame into the unburned gas. The difficulty with this method is in defining flame area because of the curved flame front. Since the flame is moving in the tube, the speed of flame moving should be subtracted from the measured velocity to have laminar flame speed. To measure the flame velocity, soap solution can be used. The soap solution is applied in the small hole drilled on the tube cap and by measuring the rate of growth of the soap bubble, the velocity of unburned gas can be obtained. This method has uncertainties because of tube wall effects and distortion by buoyancy [18].

2.1.4 Soap bubble method

To solve the problem due to the wall effects, the soap bubble method was developed. In this method, fuel-oxidant mixture is placed in the bubble film and ignited at the center. The flame propagates from the center with spherical shape at constant pressure. The laminar flame speed can be obtained from mass conservation at flame, $S_L A\rho_0 = u_r A\rho_f$ where, S_L is the laminar flame speed, u_r is observed velocity and ρ_0, ρ_f are density of unburned and burned gas, respectively. This method has disadvantages : There is large uncertainty in the density ratio, and only fast flame can be used to avoid convective effect. Water in the bubble can be evaporated, and it can alter the composition of the mixture [18].

2.1.5 Constant pressure chamber method

This method uses two concentric cylindrical vessels. The outer vessel is much larger than inner vessel and there are holes on the wall of the inner vessel. These holes are initially sealed with small resistance. When the pressure of inner vessel is increased and the pressure difference between inner and the outer vessel is reached to a certain level, the seal is broken and the pressure is released to the outer vessel to maintain a nearly constant pressure. Kelley and Law [35] used this method to determine unstretched laminar flame speed for n-butane-air mixtures at 1 atm of pressure. They also conducted research on the effect of ignition at the beginning of the flame and effect of the chamber wall at the end of the flame for a typical outwardly propagating flame in a

closed chamber.

2.1.6 Constant volume chamber method

This method uses a constant volume chamber. In many cases, the shape of the chamber is spherical. It is generally accepted that the constant volume chamber method permits the determination of the laminar flame speed of a combustible mixture with the best precision, 5 to 10%, and over wide ranges of pressure and temperature. This method is best suited to measuring flame speeds of average velocity ranging from 20 to 80 cm/s [9]. In this method, fuel-oxidant mixture is supplied into the closed chamber with desired initial pressure and ignited at the center. The flames propagate outwardly with a spherical shape. This method can be classified into two categories in terms of the tracing flame method as follows:

1. Optical photography method : The image of the flame in the chamber is taken by a high speed optical device, and laminar flame speed is calculated from these images.

2. Pressure method : The pressure change in the chamber is measured with a high speed pressure transducer, and laminar flame speed is calculated from measured pressures.

2.1.6.1 Optical photography method

In this method, a high speed optical device is used to take the flame image during combustion. In most cases, Schlieren photography is used as

the optical imaging method. Schlieren images of the first part of burning in the chamber are taken for a few milliseconds before the temperature and pressure are significantly changed. With these photos, one laminar flame speed is calculated for each combustion test. In many studies, the response of flames to stretch have been analysed with the method by Clavin and Williams, Pelce and Clavin and Matalon and Matkowsky. In this method, it is shown that the burnt gas Markstein length, L_b that expresses the influence of stretch in the flame speed can be described as

$$S_{b0} - S_b = L_b \cdot \kappa,$$

where S_{b0} is the unstretched flame speed of the burnt mixture and S_b is the propagating speed which is determined by differentiation of the radii over time from taken image. Stretch rate κ is defined at any point of the flame surface as the Lagrangian time derivative of the logarithm of the area of an infinitesimal element of the surface surrounding the point is given by

$$\kappa = \frac{1}{A} \cdot \frac{dA}{dt} = \frac{2}{r_b} \cdot \frac{dr_b}{dt},$$

where A is the flame front surface area [3].

With this analysis, S_{b0} is determined by extrapolating of S_b - κ graph. The laminar flame speed is determined by the continuity law of a planar unstretched flame

$$S_L = S_{u0} = S_{b0} \cdot \frac{\rho_b}{\rho_u}.$$

where ρ_b and ρ_u are the burnt and unburnt densities respectively.

Table 2.1 shows the previous laminar flame speed studies using the constant volume chamber method with optical photography.

2.1.6.2 Pressure measuring method

In this method, like the optical photography method, the fuel-oxidant mixture is ignited inside the constant volume chamber; however, pressure is measured to calculate laminar flame speeds. A high speed piezo-electric pressure transducer is generally used. The advantage of this method is that it allows the burning velocity to be evaluated over a range of pressures (and corresponding temperatures) from a single fuel-oxidant mixture burning. Also, this method demonstrates an engine-like condition at high pressures and high temperatures. In this research, this method is used and explained in more detail in Chap. 3.

Ryan et al. [43] used this method to measure the laminar flame speeds of *iso*-octane, *n*-heptane, methanol, methane and propane at elevated temperatures and pressures. They supplied a liquid fuel into the chamber with a hypodermic syringe and measured the pressure change during combustion with Kistler Model 609A water cooled piezoelectric pressure transducer. Pressure was up to 0.6 MPa and Temperature was up to 570 K. Rhodes and Keck [42] determined laminar flame speeds of indolene-air-diluent mixtures at high

Table 2.1: Laminar flame speed studies using the constant volume chamber method (Optical photography method).

Ref.	Fuel	P & T range	Optical device
[24]	Methane	0.5-4atm, 298K	High speed motion picture shadowgraphy
[6]	*iso*-Octane, *iso*-Octane and *n*-Heptane mixtures	1-10bar, 358-450K	Schlieren
[19]	Methane, *iso*-Octane	0.1-10MPa, 300-400K	Schlieren
[9]	Dimethyl ether	1bar, 295K	Photoelectric rapid visualization
[37]	Natural gas	1-10atm, 358-480K	Schlieren
[40]	Propane	1atm, 273K	High speed chemiluminescence imaging
[23]	Ethanol, *iso*-Octane, *n*-Heptane	1atm, 325K	Schlieren
[38]	Methane	1-10atm, 358-480K	Schlieren
[29]	Natural gas, Hydrogen	1atm, 300K	Schlieren
[28]	Dimethyl ether	0.08-0.15MPa, 285K	Schlieren
[31]	Acetylene, Propane, Hydrogen	4,5,10atm, 300K	Schlieren
[56]	Methanol	1atm, 300K	Schlieren
[50]	Methane	1atm, 300K	Shadowgraph
[30]	*n*-Heptane, *iso*-Octane, Methane, Ethane, *iso*-Butane, Propane, Butane	10, 25bar, 373K	Schlieren
[3]	*iso*-Octane, Methanol, Ethanol	10bar, 373K	Schlieren
[7]	Ethanol	0.1-1.4MPa, 250-500K	Schlieren

pressures and temperatures with this method. They used a gas tight syringe to supply fuel and the Kistler 603B1 piezoelectric pressure transducer to measure pressure history during combustion. To check the spherical shape of the flame, three ionization probes were used at three different points. Buoyancy effect to the burned gas was tested because the density of the hot burned gas is only 20 % of the unburned gas. From their research, it was found that buoyancy was noticeable when the measured flame speeds were less than 25 cm/s. It became severe when the flame speed was less than 12 cm/s. Stone et al. [49] used this method to measure the laminar burning velocity of methane. They used a separate vessel to mix fuel, air and diluent and measured dynamic pressure with a Kistler 701A quartz pressure transducer. They simply assumed the linear relationship between the mass fraction of mixture burnt and the pressure rise. The pressure range was 0.5 to 10.4 bar and temperature range was 295 to 454 K. Elia et al. [13] also tested methane-air-diluent mixtures with this method to achieve the laminar flame speeds at elevated pressures and temperatures. The measurement was taken in the range of pressure from 0.75 to 70 atm and temperature from 298 to 550 K. In their constant volume chamber device, two ionization probes, located at the top and bottom of the vessel, determined the arrival time of the flame front. These data provided information regarding the buoyancy effects. A Kistler 603B1 piezoelectric quartz pressure transducer measured the dynamic pressure inside the chamber. Stanglmaier et al. [48] used the spherical chamber to determine laminar flame speeds of *iso*-octane and three multicomponent fuels. They used *iso*-octane as a validating fuel and

compared laminar flame speeds of *iso*-octane with other laminar flame speeds from previous research. Saeed and Stone [44, 45] developed multiple burned gas zone models to describe premix laminar combustion in a closed spherical vessel. EQM model(equal mass zones model) and EQR model(equal radius zones model) were developed for the method to discretize the vessel. EQM model has the same mass, and EQR model has the same increase in radius in every zone. These two methods were validated by showing a good agreement of the final temperature in the first zone from two models with temperature predicted by STANJAN. Han et al. [22] also used a constant volume combustion chamber; however, they did not use multiple laminar flame speeds from one combustion event. They determined only one laminar flame speeds at the initial condition by extrapolating laminar flame speed-pressure data back to the initial pressure. The range of initial temperature was 298 to 498 K, and the range of initial pressure was 1 to 5 atm. Methane was used as a fuel. The effect of temperature, pressure, EGR and reformer gas was investigated in this research.

2.2 Laminar Flame Speed at Elevated Pressures and Temperatures

In the internal combustion engine, pressure varies from 1 to 35 atm and unburnt gas temperature varies from 500 to 1000 K. Precise measurement of laminar flame speeds at elevated pressures and temperatures is useful for practical applications. However, studies of laminar flame speeds at elevated

pressures and temperatures to simulate real engine operation are scarce. A common method to determine laminar flame speeds at high pressures and temperatures is using a constant volume chamber since a metal vessel can hold high pressures. When the pressure method is used, many laminar flame speed data points at high pressures and temperatures can be obtained during a single combustion event. Table 2.2 shows laminar flame speed studies that determined laminar flame speeds at elevated pressures and temperatures with fuel names, pressure and temperature ranges and method types. As shown in this table, all methods were with a constant volume chamber with either optical photography or pressure measuring method.

Fig. 2.1 shows laminar flame speed of *iso*-octane at elevated pressures and temperatures from previous studies. From the laminar flame speed results of Stanglmaier [48] with $T_0 = 550$ K, $P = 15$ atm and Jerzembeck [30] with $T_0 = 373$ K, $P = 15$ bar, it is found that the laminar flame speed is proportional to the initial temperature. To see the effect of the initial pressure on the laminar flame speed, laminar flame speeds, which are less than 30 cm/s, are shown in Fig. 2.2. As seen in Jerzembeck's results with various initial pressures, the laminar flame speed is inversely proportional to pressure.

Fig. 2.3 shows laminar flame speeds of *iso*-octane, *n*-heptane and ethanol at elevated pressures and temperatures from previous studies. Based on this figure, ethanol is faster than *iso*-octane and *n*-heptane is faster than *iso*-octane. However, these results do not have sufficient data points to figure out the generalized characteristics of laminar flame speed at elevated tem-

Table 2.2: Studies that determined laminar flame speed at elevated pressure and temperatures.

Ref.	Fuel	P & T range	Method
[43]	*iso*-Octane, *n*-Heptane, Methanol, Methane and Propane	0.3-2MPa, 470-570K	Const. Vol. Pressure
[42]	Indolene	0.4-12atm, 350-550K	Const. Vol. Pressure
[6]	*iso*-Octane, *iso*-Octane and *n*-Heptane mixtures	1-10bar, 358-450K	Const. Vol. Optical
[49]	Methane	0.5-10.4bar, 293-454K	Const. Vol. Pressure
[19]	Methane, *iso*-Octane	0.1-1MPa, 300-400K	Const. Vol. Optical
[13]	Methane	0.75-70atm, 298-550K	Const. Vol. Pressure
[48]	*iso*-Octane, Multicomponent fuels	-25atm, -800K	Const. Vol. Pressure
[37]	Natural gas	1-10atm, 358-480K	Const. Vol. Optical
[38]	Methane	1-10atm, 358-480K	Const. Vol. Optical
[45]	Methanol	0.5-3.5bar, 298-425K	Const. Vol. Pressure
[22]	Methane	1-5atm, 298-498K	Const. Vol. Pressure
[3]	*iso*-Octane, Methanol, Ethanol	10bar, 373K	Const. Vol. Optical
[7]	Ethanol	0.1-1.4MPa, 250-500K	Const. Vol. Optical
[30]	*n*-Heptane, *iso*-Octane, Methane, Ethane, *iso*-Butane, Propane, Butane	10, 25bar, 373K	Const. Vol. Optical

peratures and pressures. Also, the research on blends of these fuels was not conducted sufficiently to see the effect of added fuel in blends. In this study, a large number of data points were taken for pure and blended fuels to investigate the laminar flame speed characteristics of these fuels. Deriving a blending model that can be used to predict the laminar flame speed for any blending ratio was also attempted. These are explained in detail in the following chapters.

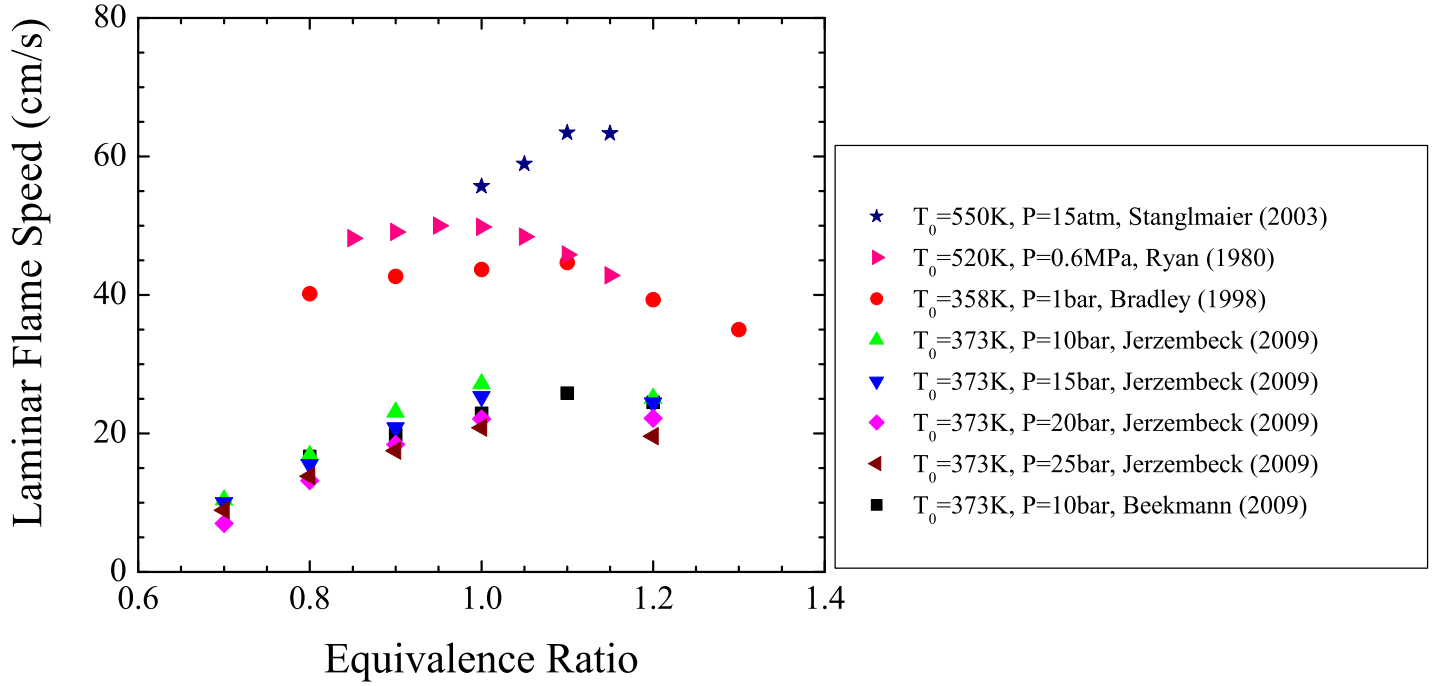

Figure 2.1: Laminar flame speed of *iso*-octane at elevated pressures and temperatures from previous studies.

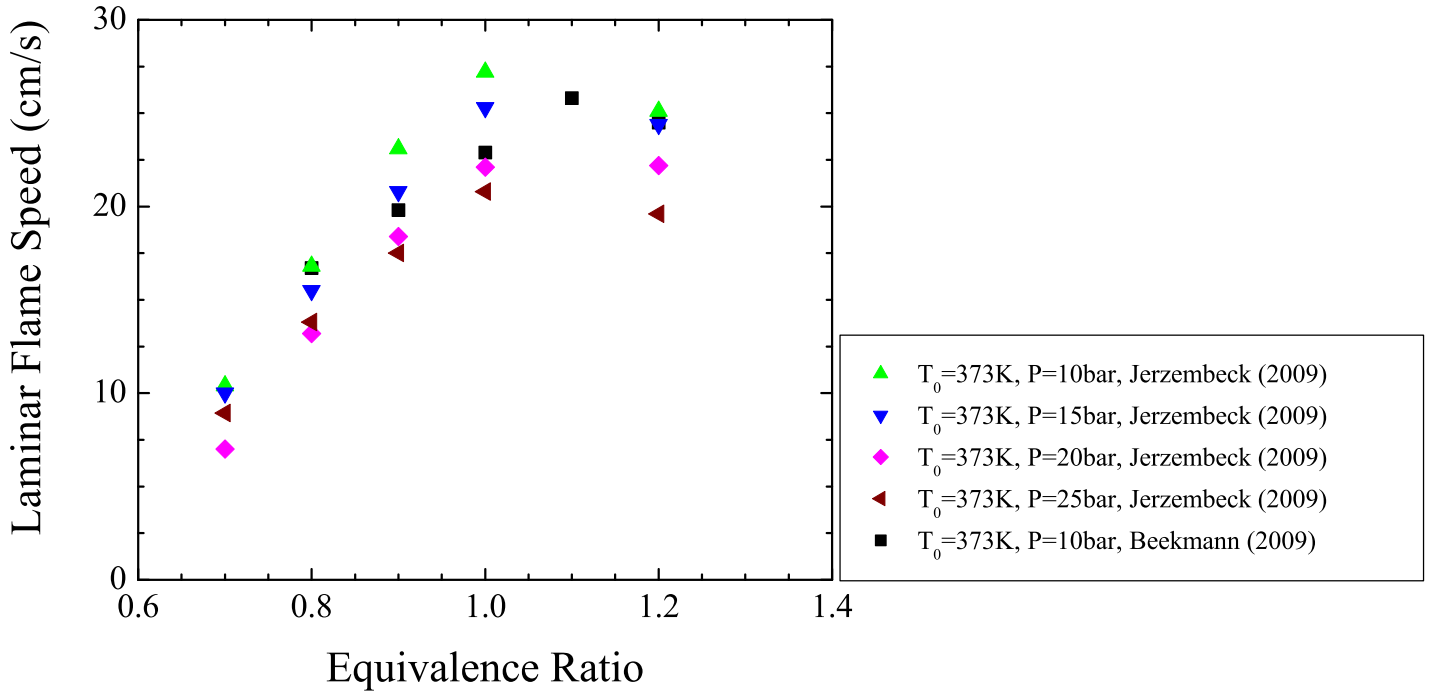

Figure 2.2: Laminar flame speed of *iso*-octane at elevated pressures and temperatures from previous studies (LFS<30 cm/s).

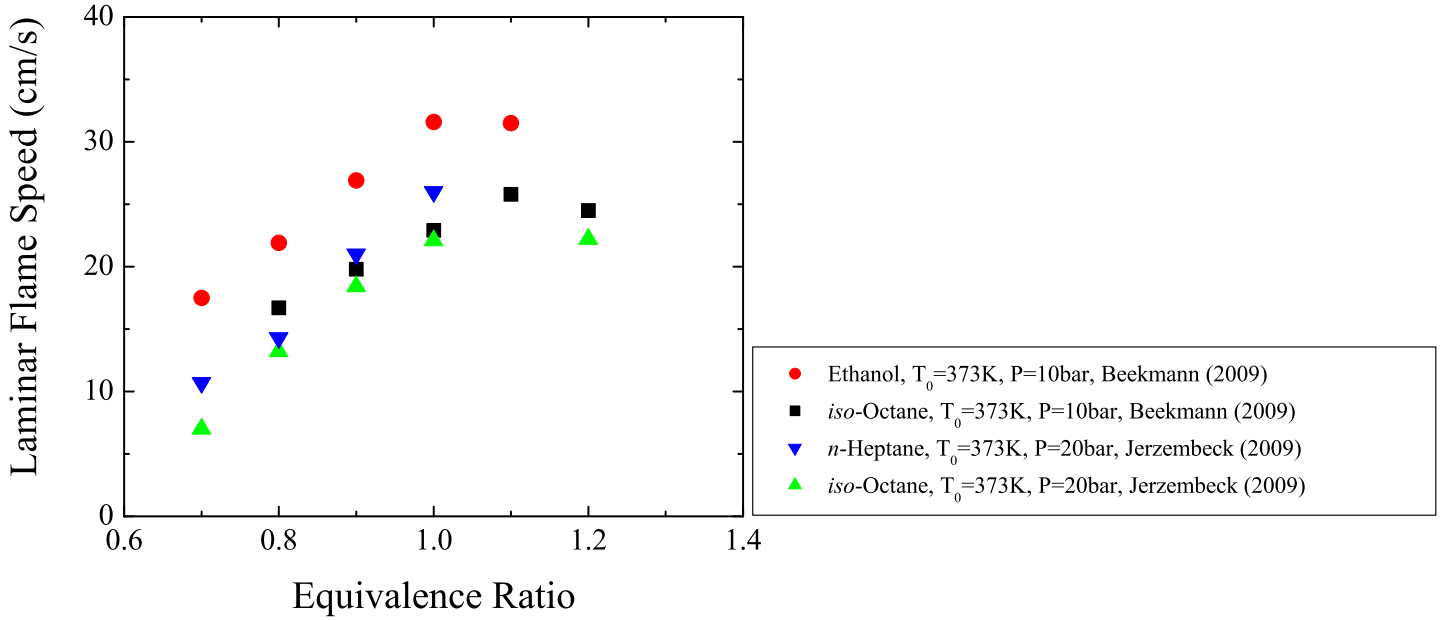

Figure 2.3: Laminar flame speed of *iso*-octane, *n*-heptane and ethanol at elevated pressures and temperatures from previous studies.

Chapter 3

Experimental Apparatus

3.1 Combustion Chamber

As explained in Chap. 1, a constant volume combustion chamber was used for the laminar burning velocity measuring device. The whole device setup is illustrated schematically in Fig. 3.1. Also a picture of the actual setup is shown in Fig. 3.2.

The spherical chamber was constructed by Ryan [43] and modified as required. This chamber was made of 303 stainless steel and consisted of two flanged hemispheres. The inside diameter of the chamber is 12.7 cm and there are several access holes for intake, exhaust, fuel injector, piezo-electric pressure transducer, ignition system and temperature probe. In addition, two observation windows with 1-1/4 inch diameter, which allows for observations directly through the middle of the chamber, were installed . Two spark plugs with extended electrodes were positioned so that the ignition occurs at the center of the chamber. The chamber is wrapped with heating tape and the temperature of the chamber is controlled electronically to maintain the desired initial gas temperature inside the chamber. Because of the high variety of gas temperatures during experiments, temperature of the chamber surface is

used as a reference temperature to control the heater. K-type thermocouples are used to monitor the surface temperature and gas temperature within the chamber.

There are two air-operated high pressure valves and three 3-way solenoid valves in this system. Two air-operated high pressure valves control the opening and closing of intake and exhaust. These valves are operated by 30-100 psi air and can hold up to 680 atm at high temperature, up to 650 °C. Two 3-way solenoid valves control operating air that lifts up a diaphragm inside these air-operated high pressure valves. The other 3-way solenoid valve controls the path of the exhaust either to a vent or vacuum pump.

A direct fuel injector which is from the Audi motor company and an accumulator are used to supply fuel into the chamber. Fig. 3.3 shows the structure of the fuel injection system schematically. High pressure of 50 bar nitrogen pressurizes the fuel and the desired amount of fuel is injected into the chamber according to the pulse width signal from an injector drive. One of the observation window holes was used to install the fuel injector. A pressure transducer monitors fuel pressure near the injector. Due to the limitation of the opening time of the fuel injector, the injection process is equally divided into 3 steps. Fuel is injected 3 times during the injecting process.

A piezo-electric pressure transducer and amplifier are used to measure the pressure history during combustion. This pressure transducer set only measures pressure changes. The initial pressure, which is taken by an air pressure transducer when this piezo-electic pressure transducer is reset, is added

to these dynamic pressure data to calculate the absolute pressures. A water cooling system is installed in the piezo-electic pressure transducer to protect it from the heat.

The equivalence ratio of the mixture is measured after each experiment by making the combusted products exhaust through an automotive wide-range oxygen sensor(UEGO). This sensor is calibrated for each fuel. The method of calibrating this sensor and measuring equivalence ratio are explained in more detail in Section 3.2. Fig. 3.4 shows a close-up view of the spherical combustion chamber.

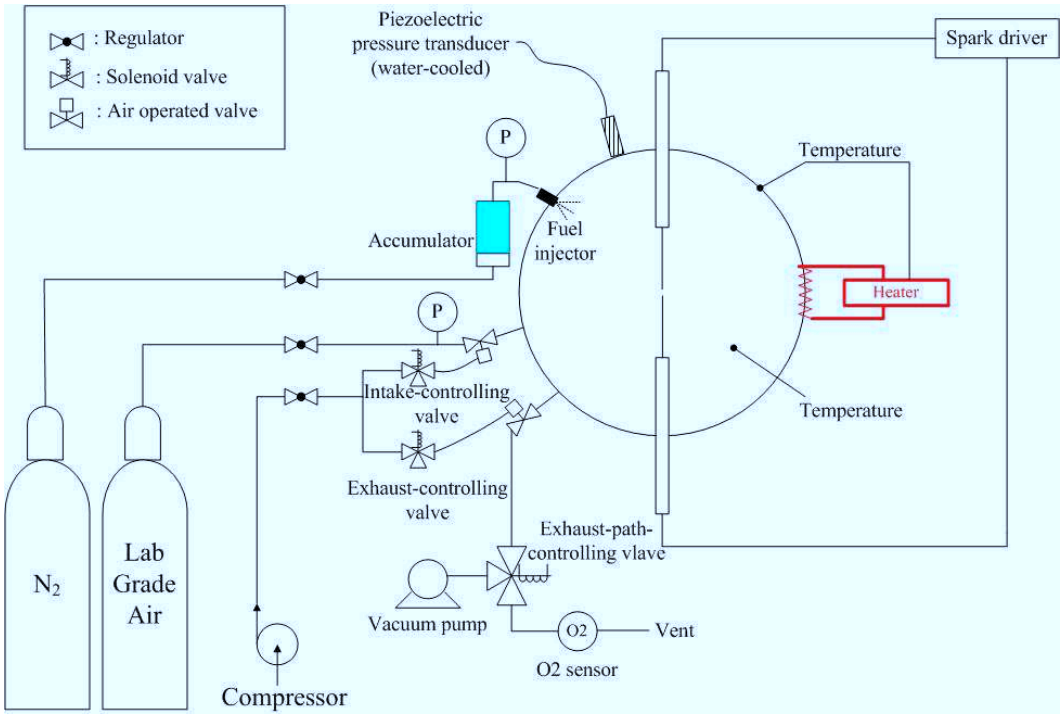

Figure 3.1: Schematic diagram of the experimental apparatus.

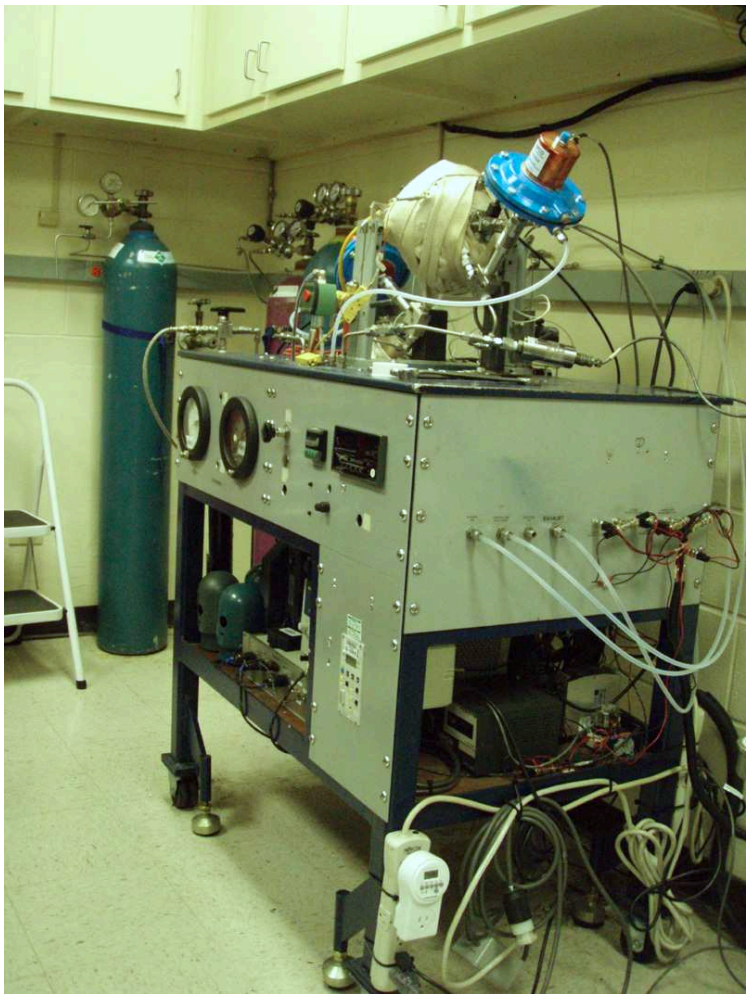

Figure 3.2: Picture of the experimental apparatus.

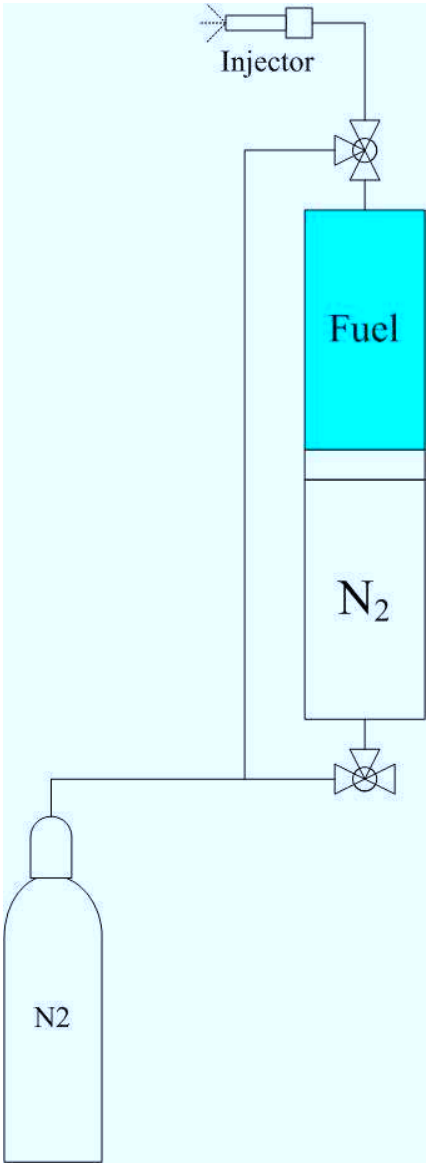

Figure 3.3: Fuel injection system.

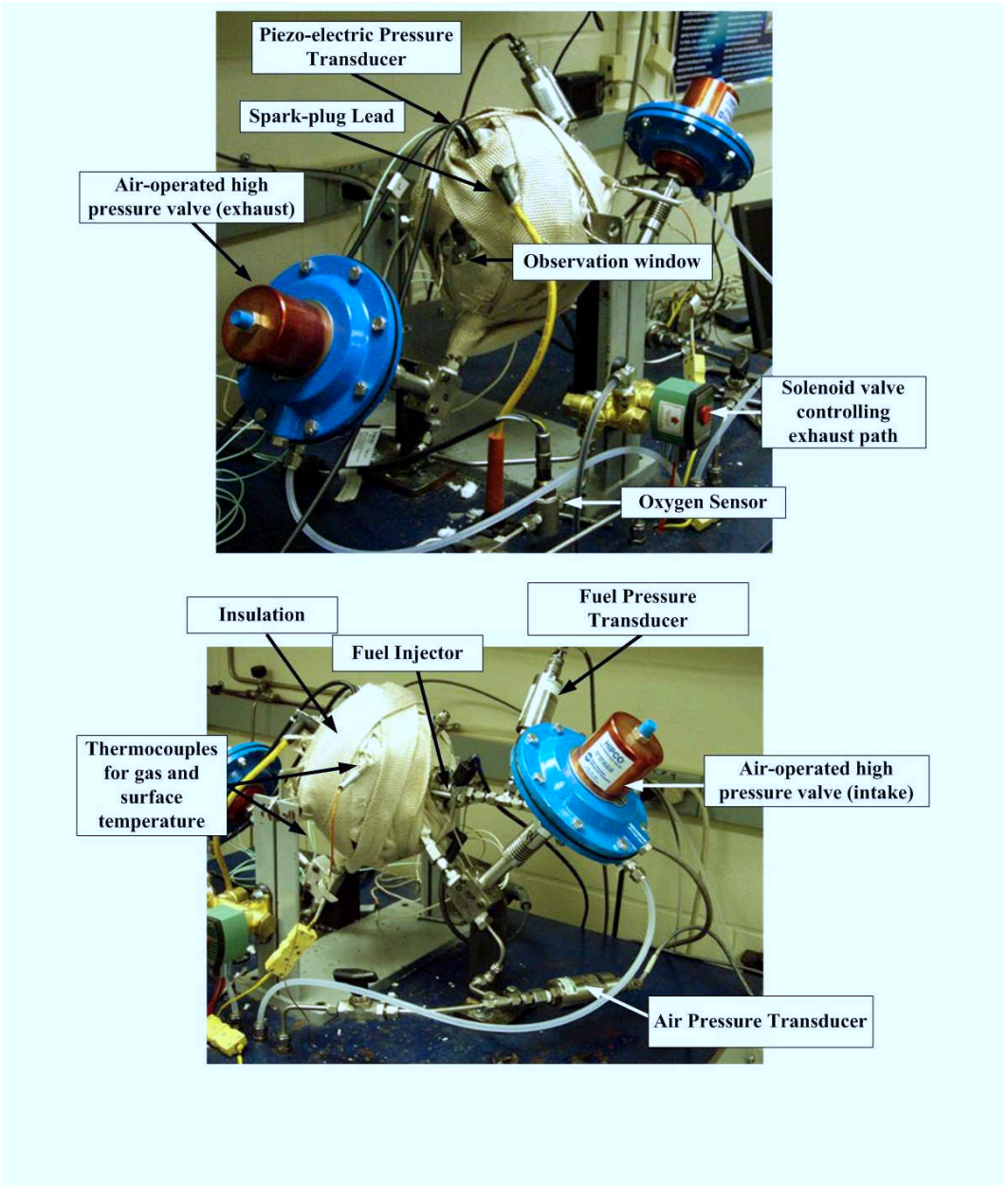

Figure 3.4: Close-up view of the spherical combustion chamber.

3.2 Experimental Procedure

3.2.1 Oxygen sensor calibration

As explained in Section 3.1, an automotive wide-range oxygen sensor (UEGO) was used to measure the equivalence ratio of the air-fuel mixture. Because this commercialized oxygen sensor was designed for conventional gasoline, calibrating for every fuel was required before the main combustion experiments. To calibrate this oxygen sensor, collecting bags were used to collect combusted products, and they were analysed by Horiba Exhaust Gas Analyzer. Because there was a required minimum amount of combusted product to analyse, at least 10 tests were performed with the same initial condition for the single bag. Fig. 3.5 shows the collecting bag for the combusted products, and Fig. 3.6 shows Horiba Exhaust Gas Analyzer.

For each fuel, at least 5 cases of equivalence ratio were tested. The smallest equivalence ratio was about 0.82. The largest equivalence ratio was about 1.30. The stoichiometric case was in the middle. This equivalence ratio range is with a given gain and offset by the oxygen sensor manufacturer. After enough combusted products were collected in the bag, they were analysed with the Horiba Exhaust Gas Analyzer to have the accurate equivalence ratio. New gain and offset settings were derived with linear fitting for the testing fuel with at least 5 data points of the relationship between equivalence ratios from the given gain and offset by the oxygen sensor manufacturer and those from Horiba Exhaust Gas Analyzer.

Fig. 3.7 shows a result of the oxygen sensor calibration with ethanol

and table 3.1 shows the results for every tested fuel. *Iso*-octane and *n*-heptane and their blends showed almost the same gain and offset for the oxygen sensor. As mentioned, the readable range of this oxygen sensor was 0.82 to 1.30 with given gain and offset by the oxygen sensor company. However, 0.82 was actually about 0.70 and 1.30 was actually about 1.60 for *iso*-octane, *n*-heptane, ethanol and their blends with the new offset and gain. For methane, the readable range of this oxygen sensor was 0.75 to 1.40.

Table 3.1: Gain and offset of the oxygen sensor for each fuel.

Fuel	Gain	Offset
Given by oxygen sensor company	0.2301	0.42857
iso-Octane, *n*-Heptane and their blends	0.4244	-0.01334
iso-Octane or *n*-Heptane-Ethanol blend	0.4884	-0.16493
iso-Octane-*n*-Heptane-Ethanol blend	0.4423	-0.06981
Ethanol	0.4688	-0.13918
Methane	0.3145	0.21924

3.2.2 Main combustion experiment

After the oxygen sensor calibration, the main combustion experiments measuring pressure history while air-fuel mixture was burning were performed. Nine test fuels, including *iso*-octane, *n*-heptane, ethanol and their various blends, were tested for this main experiment. One fuel, methane, was tested for the verification of the experiments and laminar flame speed calculation. Ethanol is an important engine bio-fuel, either alone, or in a fuel blend, but there are only limited measured data of its characteristics at high pressures and temperatures [7]. Those tests were with various equivalence ratios, initial

pressure and initial temperature combinations. Table 3.2 shows parameters of the main laminar burning velocity experiments in this research. Three repeated tests were conducted with each case, and the total number of tests was about three thousands. This large number of tests could be done because of the modification of the experimental apparatus. The most innovative improvement of the experimental apparatus in this research was automatically controlling all processes to maximize the number of experiments and to achieve accuracy of experimental results. National Instruments CompactRio-9004 was used to control the devices including solenoid valves, relays, the injector drive and the spark plug drive. NI LabView software was used to control CompactRio. Fig. 3.8 shows the snapshot of the LabView Control Panel.

Measurements were made for single-component, *iso*-octane, *n*-heptane and ethanol, and binary blends of *iso*-octane-*n*-heptane in 1/3, 1/1, 3/1 volume ratios, *iso*-octane-ethanol in 1/1 volume ratio, *n*-heptane-ethanol in 1/1 volume ratio and ternary blends of *iso*-octane-*n*-heptane-ethanol in 1/1/1 volume ratio over a wide range of equivalence ratios at elevated temperatures and pressures.

The experimental procedure of the single test was as follows. Before the tests were conducted, heaters were turned on, and the chamber was allowed to heat up for at least 2 hours prior to initiating the tests. While the chamber was being heated up, fuel in the accumulator and transfer lines was replaced with fresh fuel. The sealing of the spherical chamber was verified everyday before tests.

Table 3.2: Parameters of the main laminar burning velocity tests.

Fuel	*iso*-Octane, *n*-Heptane, Ethanol, 25(vol%)*iso*-Octane-75(vol%)*n*-Heptane, 50*iso*-Octane-50*n*-Heptane, 75*iso*-Octane-25*n*-Heptane, 50*iso*-Octane-50Ethanol, 50*n*-Heptane-50Ethanol, 33*iso*-Octane-33*n*-Heptane-33Ethanol
Initial temperature (°C)	170, 185, 200
Initial pressure (atm gage)	1, 3, 5, 7, 9
Equivalence ratio	7 cases between readable limits while stoichiometric case is in the middle

After all preparation steps, the following procedure was performed automatically. Here, all experimental devices can be found in Fig. 3.1 and Fig. 3.4.

A . Purge residual or burned gas in the chamber

i . Energize exhaust-controlling solenoid valve to let operating air open exhaust and wait until burned or any high pressure gas is exhausted.

ii . Energize intake-controlling solenoid valve to let operating air open intake and let lab grade air clean the chamber for a few seconds.

iii . De-energize intake-controlling solenoid valve to close intake and wait until residual clean air is exhausted.

iv . Turn on the vacuum pump.

v . Energize air-path-controlling solenoid valve to connect exhaust to vacuum pump and wait until the chamber is evacuated.

vi . De-energize exhaust-controlling solenoid valve to close exhaust and de-energize air-path-controlling solenoid valve to connect exhaust to vent.

vii . Energize intake-controlling solenoid valve to open intake and energize exhaust-controlling solenoid valve to open exhaust and let lab grade air clean the chamber again for a few seconds.

viii . De-energize intake-controlling solenoid valve to close intake.

B . Evacuate the chamber

i . Wait until residual clean air is exhausted.

ii . Energize air-path-controlling solenoid valve and wait until the chamber is evacuated.

iii . De-energize exhaust-controlling solenoid valve and turn off the vacuum pump.

iv . De-energize air-path-controlling solenoid valve.

C . Supply fuel and air

i . Supply fuel with injector by controlling pulse width of the signal.

ii . Energize intake-controlling solenoid valve and wait until pegging pressure of the chamber reaches to target initial pressure.

iii . De-energize intake-controlling solenoid valve and wait for sufficient amount of time to allow the mixture to be settled.

iv . Turn off the heater to avoid noise in piezo-transducer reading due to A/C power.

D . Ignite and measure Phi

i . Record initial pegging pressure and gas temperature.

ii . Reset charge amp.

iii . Ignite with recording pressure change with piezo-transducer for 0.25 second.

iv . Turn heater back on and energize exhaust-controlling solenoid valve and measure equivalence ratio.

E . Iterating

i . Go to step A. for the next experiment.

Fig. 3.9 shows a flowchart of one set of experiments. One set of experiments consists of seven pulse width fuel settings. Each pulse width case was tested three times to check the repeatability. After one set of tests with various injector pulse width, one file, FILE I, that contains data of chamber surface temperature, mixture temperature, initial pressure, equivalence ratio, fuel pressure and injector pulse width for each test was generated. After each test, File II that contains initial mixture temperature, sample rate and pressure history data was generated. Fig. 3.10 shows these files from one set of

tests. Fig. 3.11 is experimental result for a representative experiment, which was with *iso*-octane, initial pressure of 5 atm gage, initial temperature of 185 °C and approximately stoichiometric equivalence ratio. One test took approximately 6 minutes with a 3 minute waiting time for air-fuel mixing.

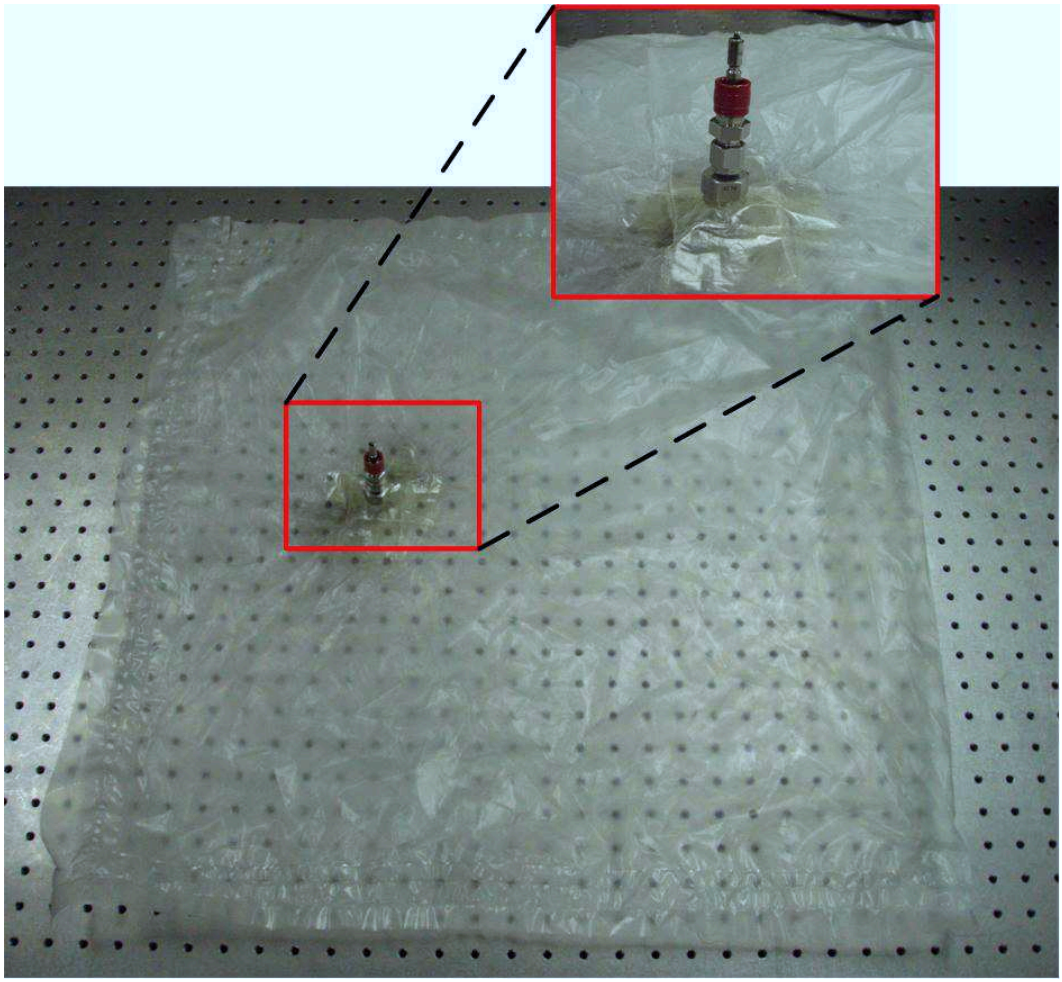

Figure 3.5: Combusted products collecting bag for oxygen sensor calibration.

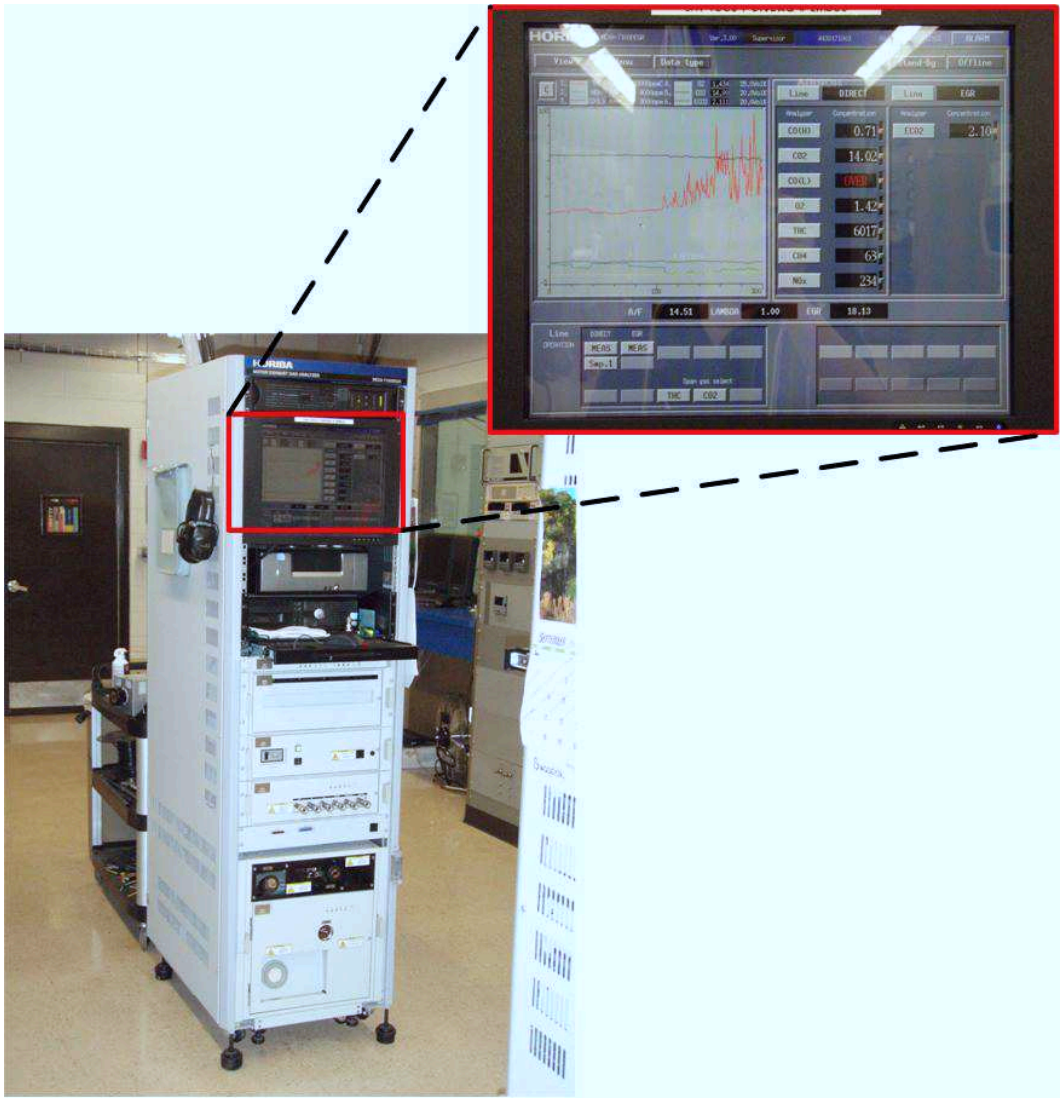

Figure 3.6: Horiba Exhaust Gas Analyzer.

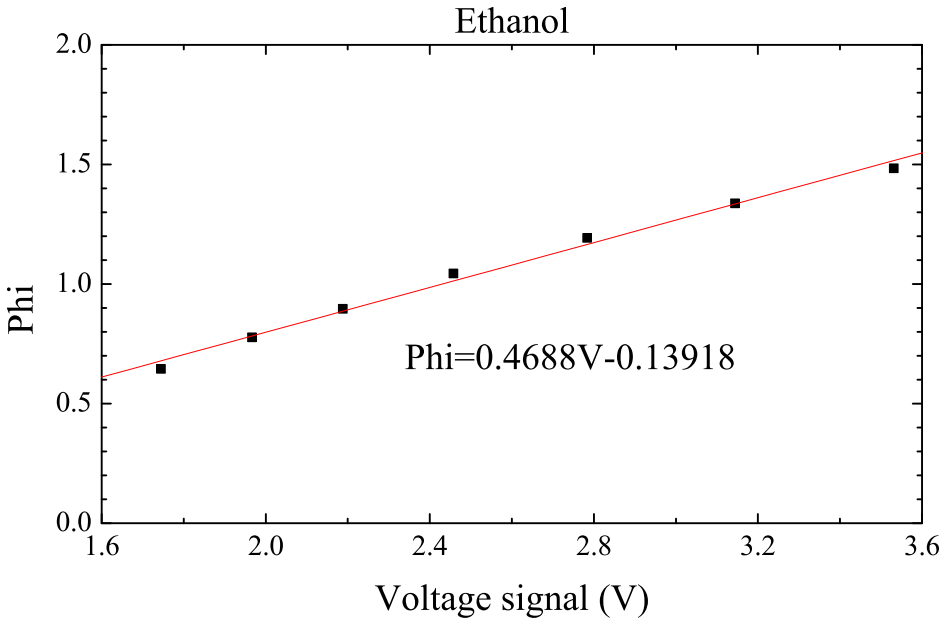

Figure 3.7: A result of the oxygen sensor calibration with ethanol.

Figure 3.8: Snapshot of the LabView control panel.

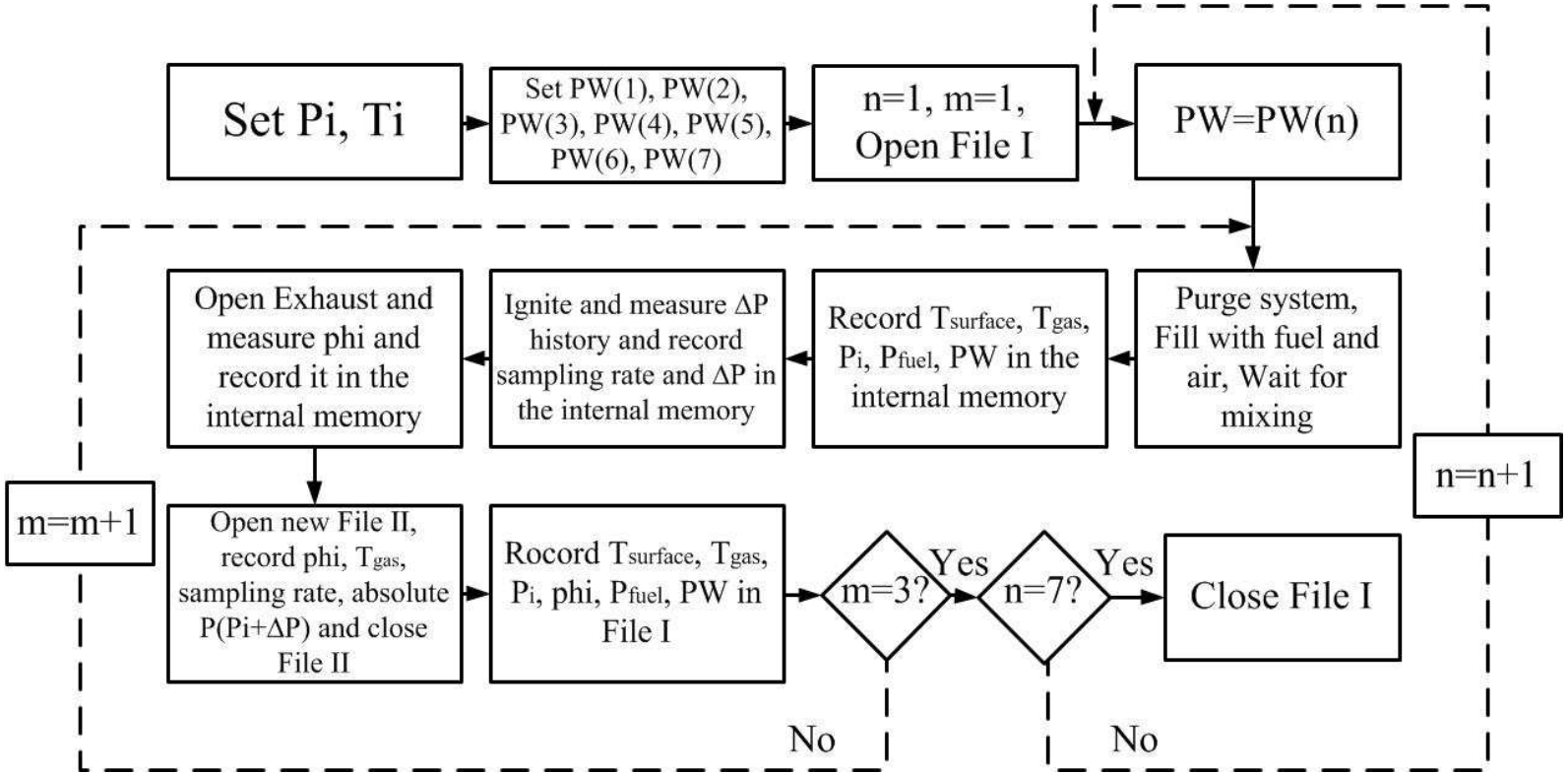

Figure 3.9: Flowchart of one set of experiments.

File I

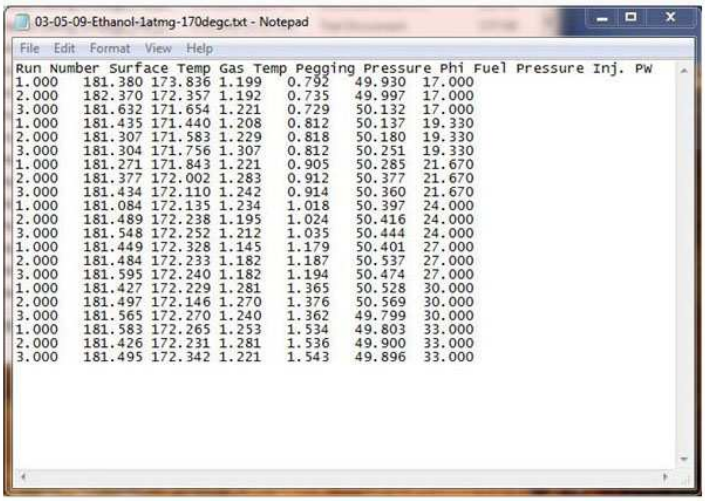

Set of File II

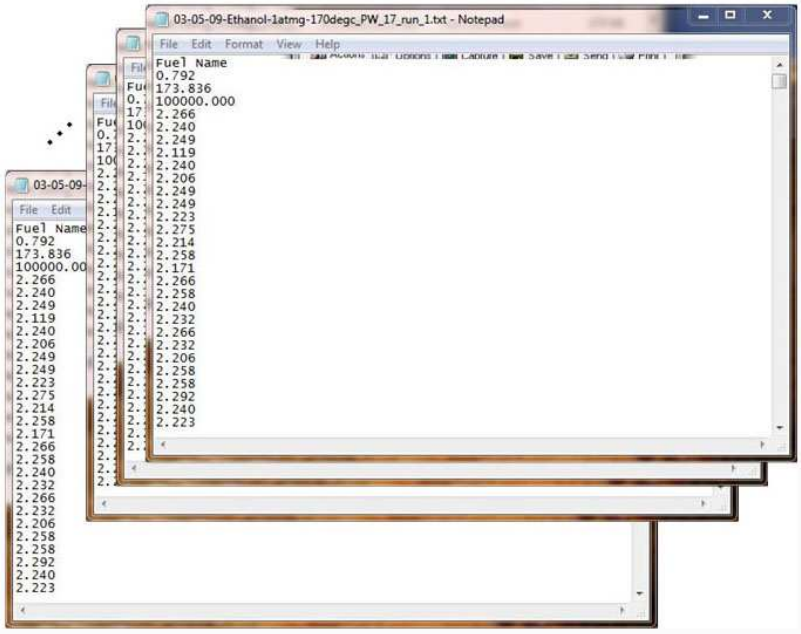

Figure 3.10: Result files from one set of tests.

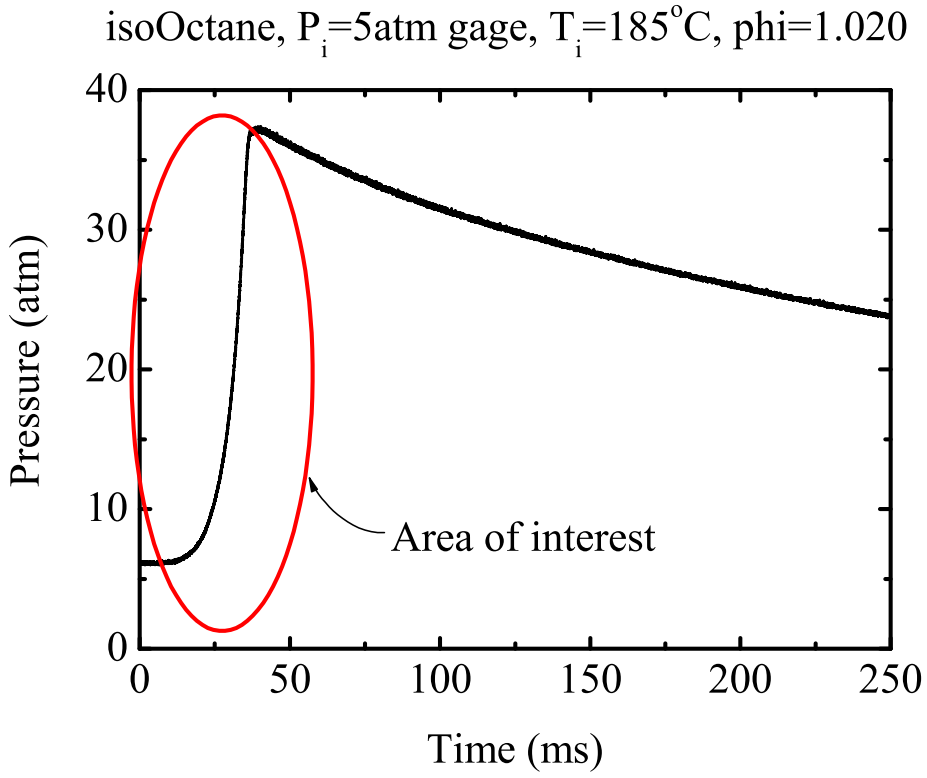

Figure 3.11: Experimental result for a representative experiment.

3.3 Verification of Mixing

To have a uniform equivalence ratio and spherical shape of the flame during combustion, it is required to verify the homogeneous mixing of air and fuel before ignition. To check the air-fuel mixing, Schlieren videos were taken during mixing and burning air-fuel mixtures. The fuel was *iso*-octane. Initial pressure was 7 atm gage. Initial temperature was 170 °C. All Schlieren videos are available at `http://user.chol.com/~cryogenic/Schlieren/`, and snapshots of those videos are in Fig. 3.12. The first video shows the inside of the chamber upon completion of the evacuation process. When the inside of the chamber is empty, a quiescent image is shown. The second video shows air flowing inside the chamber while both intake and exhaust are open. As vigorous flow occurs in the chamber, the high density variation inside the chamber is shown. The third video shows three fuel injections. As fuel is injected, short but clear density changes appear at around 2350 ms, 4750 ms and 7150 ms. The fourth video shows slowed video of 1 injection event starting at 2350 ms. The fifth video shows the Schlieren image inside the chamber from the last injection to air supplying for about 20 seconds. Air was supplied 2 seconds after the last fuel injection, and there were slight density variations inside the chamber. However, a few seconds later at the end of supplying air process, the Schlieren image was just like the one shown when the chamber is evacuated. It could be either because Schlieren image is sufficiently sensitive to detect small movements inside the chamber for mixings or the mixing may have been finalized only a few seconds upon air supply. Liquid fuel is sprayed

as small droplets by the injector. Those fuel droplets are easily evaporated due to low pressure and heat inside the chamber. Therefore, only a few seconds can be sufficient time to have an uniform air-fuel mixture inside the chamber. Another test was performed to verify this result. Tests with various waiting times, 0, 5, 10, 20, 30 seconds, were conducted with *iso*-octane at 7 atm gage initial pressure and 170 °C initial temperature. Their pressure histories during combustion were compared. These pressure histories are shown in Fig. 3.13. Pressure histories with 0 second and 5 second waiting times were different from histories with 10, 20, 30 second waiting times. Fig. 3.14 shows calculated laminar burning velocities at 30 milliseconds with these waiting times. As seen in this figure, from waiting time of 10 seconds, the value of laminar burning velocity started to be stabilized and had the almost same value from 20 milliseconds. From this result, it was found that a waiting time longer than 20 second was required to have a homogeneous air-fuel mixture.

Another point that needed to be checked was the minimum required mixing time to have a homogeneous initial mixture temperature. To check if a three-minutes wait-time is sufficient, analytical analysis was used as follows. Conservatively, a quiescent gas mixture was assumed in the spherical chamber. Only conduction was considered after the room temperature air-fuel mixture was supplied into the heated chamber. For the transient spherical heat conduction, the governing equation with initial and boundary conditions are as follows.

G.E :

$$\frac{1}{r^2}\frac{\partial}{\partial r}(r^2\frac{\partial T}{\partial r}) = \frac{1}{\alpha}\frac{\partial T}{\partial t}$$

I.C :

$$T(r, t = 0) = 300$$

B.Cs :

$$T(r = 0.0635, t > 0) = 573$$

$$\frac{\partial T}{\partial r}(r = 0, t) = 0$$

With Separation of Variables,

$$T = \sum_{n=1}^{\infty} \frac{C_n}{r} \sin(\lambda_n r) \exp^{-\alpha\lambda_n^2 t} + 573$$

where

$$C_n = \frac{-273 \int_0^{0.0635} r \sin(\lambda_n r) dr}{\int_0^{0.0635} \sin^2(\lambda_n r) dr}$$

$$\lambda_n = \frac{n\pi}{0.0635}$$

Fig. 3.15 shows the temperature profile in the chamber with various times. After 120 seconds, the gas in the chamber has a homogeneous temperature profile. Therefore, three-minutes was sufficient time to have a homogeneous temperature profile of the air-fuel mixture in the chamber.

From these three verification processes, a three-minutes waiting time for mixing before igniting the air-fuel mixture was proved to be sufficient.

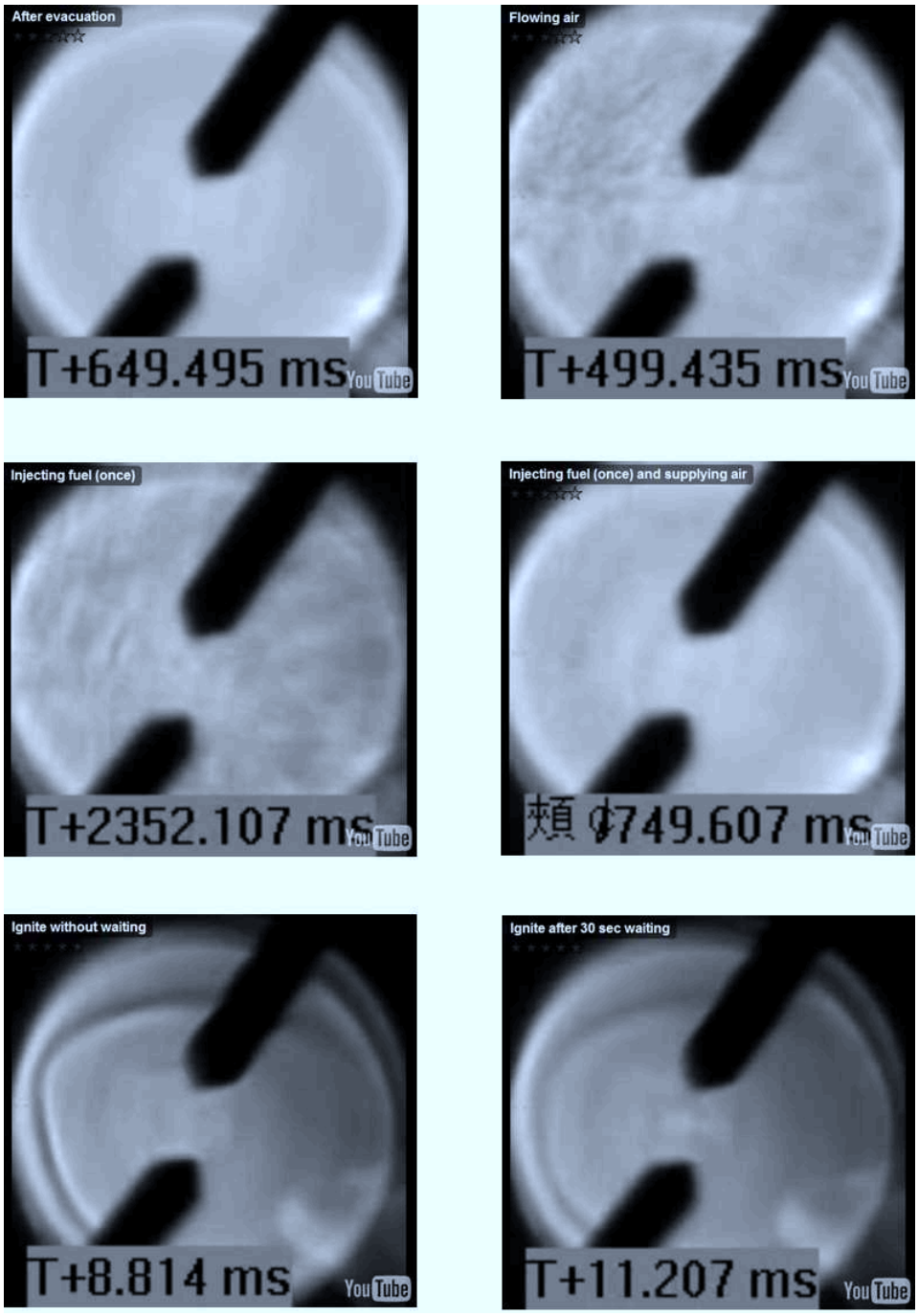

Figure 3.12: Snapshots of the Schlieren videos.

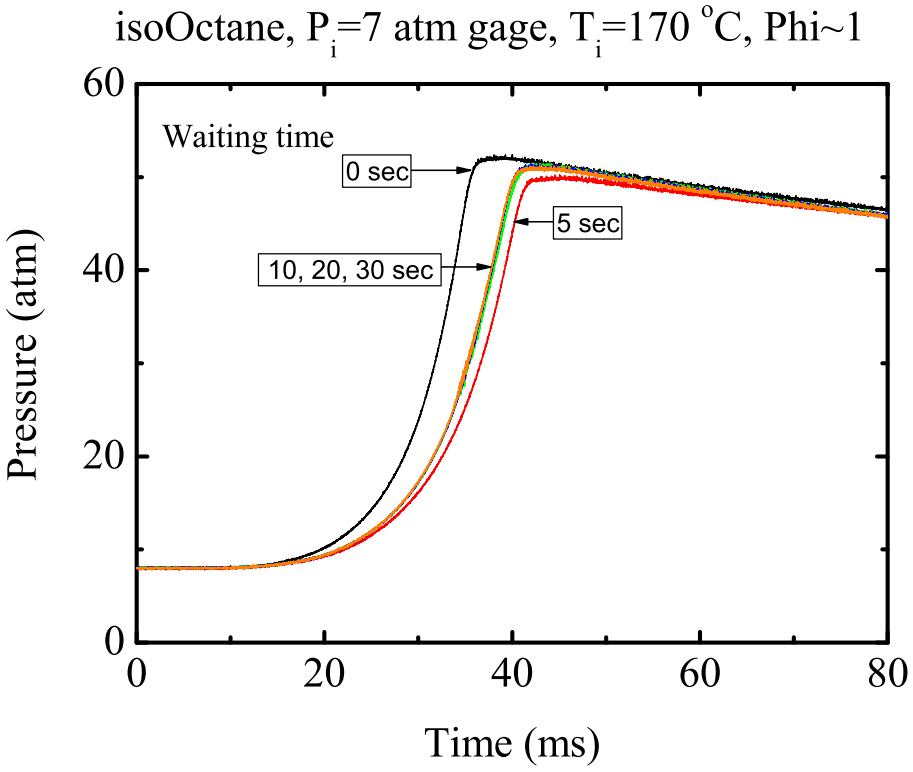

Figure 3.13: Pressure histories with various air-fuel mixing times.

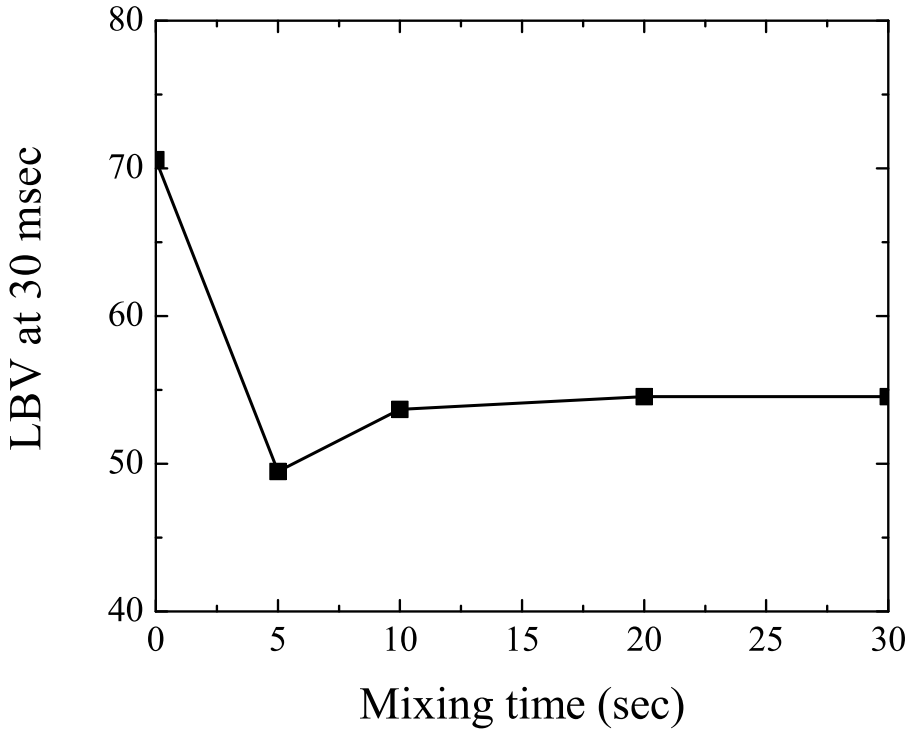

Figure 3.14: Laminar Burning Velocities at 30 milliseconds with various air-fuel mixing times.

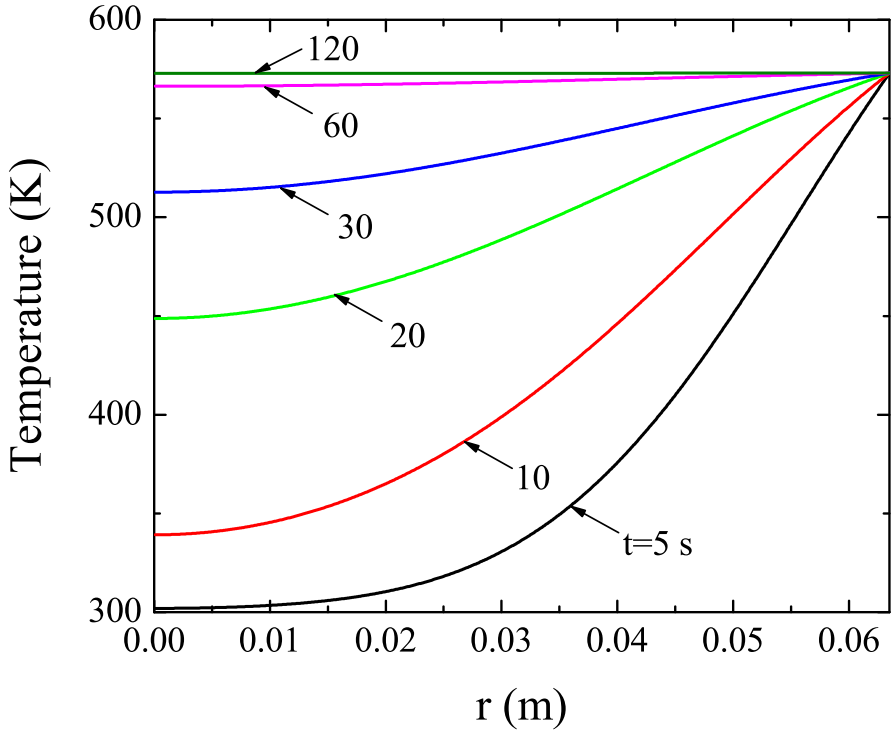

Figure 3.15: Temperature profiles in a quiescent air-fuel mixture with various waiting times.

Chapter 4

Laminar Burning Velocity Calculation

4.1 Analysis Code

The analysis code is based on the work by Ryan [43] and Roberts [48], but in this research it had been updated to have more accurate results from given experimental data. In this analysis code, the spherical flame is assumed to be ignited at the center and to move in the radial direction. Fig. 4.1 illustrates the numerical flame growth model and the shape of pressure history diagram at each moment. The kernel formation and end of combustion regimes are marked on this figure. These regimes have high uncertainty in flame speed calculation due to kernel formation and heat losses; therefore it was ignored in the analysis of laminar burning velocities. Detailed flame velocities, chamber pressure and flame velocity regimes for the representative experiment are shown. The laminar burning velocity and laminar flame speed regimes have been marked in Fig. 4.2. For the laminar burning velocity regime, the flame radius is approximately between 2.3 cm and 6.0 cm for this representative case. At the beginning and end of this regime, there are still stretch effects and wall effects. This regime could be used in future research on the effects of stretch and the engine wall. The laminar flame speed regime is the flame radius range between 3 cm and 4.5 cm. There is the least effect of the

experimental components in this range. This flame speed, the laminar flame speed, is a property of the fuel. If the radius differences between laminar burning velocity and laminar flame speed regimes are compared, the radius difference at the end (1.5 cm) is larger than that at the beginning (0.7 cm). That is because it is attempted to have the same laminar flame speed regime for all tested fuels in this research. In some cases cellularity is generated as flame propagates. Cellularity is a dimpled surface on the flame as shown in Fig. 4.3 [31]. This increases the surface area compared to the perfect sphere. This results in misleadingly high values of the laminar burning velocities. Also, as fuel blends have more *n*-heptane, auto ignition tends to occur at the end of combustion in the spherical chamber. Since there were more uncertainties at the end of the combustion, a larger portion at the end of the combustion was ignored in the laminar flame speed analysis. This restriction of data was required to have similar temperature and pressure ranges for all tested fuels to be comparable.

In the analysis code, the inside of the chamber is discretized into 250 computational spatial zones. A given zone is assumed to be within the unburned zone before the flame arrives to its location, and part of the burned zone after the flame passes. The flame zone is approximated by the energy release region, which is associated with the volume combusted by the flame during a computational time-step. Each zone calculation is explained in detail in Subsection 4.1.2.

4.1.1 Overall computational procedure

A flow chart of the overall computational procedure is shown in Fig. 4.4. The analysis code reads the experimental data including initial mixture temperature, sample rate, equivalence ratio and the pressure-time history before the calculation. After reading data, it filters the pressure history data to remove high frequency noise with two steps. The filtering technique is key to having reasonable and accurate laminar flame speed calculations. For the first step of filtering, raw pressure history data are smoothed. The newer technique of kernel regression method was replaced with the previous filtering method of 10-point-moving-average method. With the 10-point-moving-average method, the filtered data were slightly higher than the original raw data in many regions; however, with the kernel regression method, more reasonably filtered data were achieved. The next filtering step is forcing the pressure history data to monotonically increase. Since the combustion process is assumed to be adiabatic, the pressure cannot decrease during the combustion event. A decreasing pressure history would yield a negative mass burning rate in the laminar burning velocity calculation, and that is physically impossible for this process. Hence, decreasing pressure history data from signal noise are forced to have the same value as the previous one to prevent a negative mass burning rate during the calculation. Fig. 4.5 shows a comparison between raw and filtered pressure history data in several locations.

After reading and filtering the experimental data, calculations are started by entering a time-step loop with an initial guess for the burning mass dur-

ing the current time-step. In one time-step, there is a spatial-step loop that calculates subvolumes of the enflamed, burned and unburned regions. After volume calculations in each region, the sum of all calculated subvolumes is checked against the actual spherical chamber volume. If the sum of subvolumes does not match the overall chamber volume within a tolerance level, the entire spatial-step calculation is repeated with a new guess of burning mass. This new burning mass is obtained by a bisection routine. This process is repeated until convergence on the overall volume is attained. Upon successful convergence for a spatial-step calculation, the current time is checked against the final time. If the current time does not reach the final one, another flame speed calculation is made and advanced to the next time-step. This time-step loop is repeated until the current time-step reaches the final time-step.

4.1.2 Computational procedure of each zone

Detailed flow charts of each zone calculation are shown in Fig. 4.6, Fig. 4.7 and Fig. 4.8. Again, the purpose of these calculations at each zone is obtaining subvolumes to check the sum of them against the actual chamber volume. The ideal gas law with measured pressures from the experiments is used to calculate subvolumes at all regions. This process is repeated until the right burning mass during the current time-step is attained.

Fig. 4.6 shows the flowchart of the enflamed zone calculations. A guessed current burning mass is used for the mass. This is updated with a new mass until the sum of the subvolumes matches the overall chamber volume

within a tolerance level. The EQUIL program, a CHEMKIN implementation of the STANJAN code, is used to solve for the equilibrium temperature. This equilibrium temperature is used for the temperature of the mixture in this zone. Measured pressure is used for the mixture pressure. Subroutines in CHEMKIN [33], CKPCBS and CKCVBS, are used to calculate the gas constant. Using this mass, gas constant, temperature and pressure, the volume of this zone is calculated using the ideal gas law.

Fig. 4.7 shows the flowchart of burned zone calculations. The burned zone is made up of all incremental masses that are already burned. No mixing with unburned gas is allowed, and all previous burned masses remain distinct in this region. The temperature of each spatial step is calculated using the isentropic compression assumption. In this region, the specific heat ratio and gas constant at each spatial step are calculated with CKPCBS and CKCVBS subroutines in CHEMKIN. Again, the volume of this zone is calculated using the ideal gas law.

Fig. 4.8 shows the flowchart of the unburned zone calculations. The unburned zone is made up of equally distributed masses to maintain the balance of mass in the chamber. Again, no mixing with burned gas is allowed, and all unburned masses remain distinct in this region. The total mass of unburned mixture, which is the difference between the total mass in the chamber and sum of burned and unburned masses, divided by the number of spatial steps in this zone is used for the mass of each spatial step. The temperature of each spatial step is also calculated with the isentropic compression assump-

tion. Like the burned zone calculation, specific heat ratio and gas constants are calculated with CHEMKIN, and the ideal gas law is used for the subvolume calculation.

After the volume calculations of the three zones, the sum of all subvolumes is compared against the actual spherical chamber volume to check if the correct burning mass is attained at the current time-step.

4.1.3 Calculation of flame speeds

There are two kinds of flame speeds that are identified during each time-step. The first one is the "apparent" flame speed, which is simply the change in flame radius divided by the time-step size. This apparent flame speed includes effects due to laminar burning rate as well as the relative thermodynamic expansion or contraction of the unburned and burned gas regions. In other words, the laminar flame "rides" on the moving enflamed region. This flame speed can be inferred from traditional visual measurement methods. In the current calculation method, the apparent flame speed is computed by numerically following the motion of the enflamed region of the chamber.

The second flame speed, the laminar burning velocity (without expansion effects), is calculated with attained current burning mass after the completion of the current time-step loop. Fig. 4.9 shows the laminar flame speed calculation model. In this model, the volume of enflamed zone at the current time-step is considered. At the current time-step, the volume of the enflamed zone can be expressed with laminar flame speed, S_L, time-step size, Δt and

flame area, A_f as follows.

$$V_{f@t=t} = S_L \cdot \Delta t \cdot A_f$$

where A_f is the surface area of the current spherical flame which is calculated as $A_f = 4\pi r^2_{@t=t}$.

If the same volume is considered at one time-step before the current time-step, it can be also expressed with current burning mass, $M_{enflamed}$, gas constant, R, temperature, T and pressure, P as follows.

$$V_{f@t=t-1} = M_{enflamed} \cdot \left[\left(\frac{RT}{P} \right)_{t-1} \right]$$

With these two expression for the same volume of current time-step enflamed zone, the laminar burning velocity, S_L is calculated with following equation.

$$S_L = \frac{M_{enflamed} \cdot \left[\left(\frac{RT}{P} \right)_{t-1} \right]}{A_f \cdot \Delta t}$$

Fig. 4.2 shows a comparison between the apparent flame speed and the laminar burning velocity during a representative experiment. As the flame grows, the apparent flame speed decreases due to high resistance by the pressurized unburned mixture. The laminar burning velocity increases due to the high temperature of the unburned mixture. But the apparent flame speed is

always higher than the laminar burning velocity, because the laminar burning velocity is a part of the apparent flame speed.

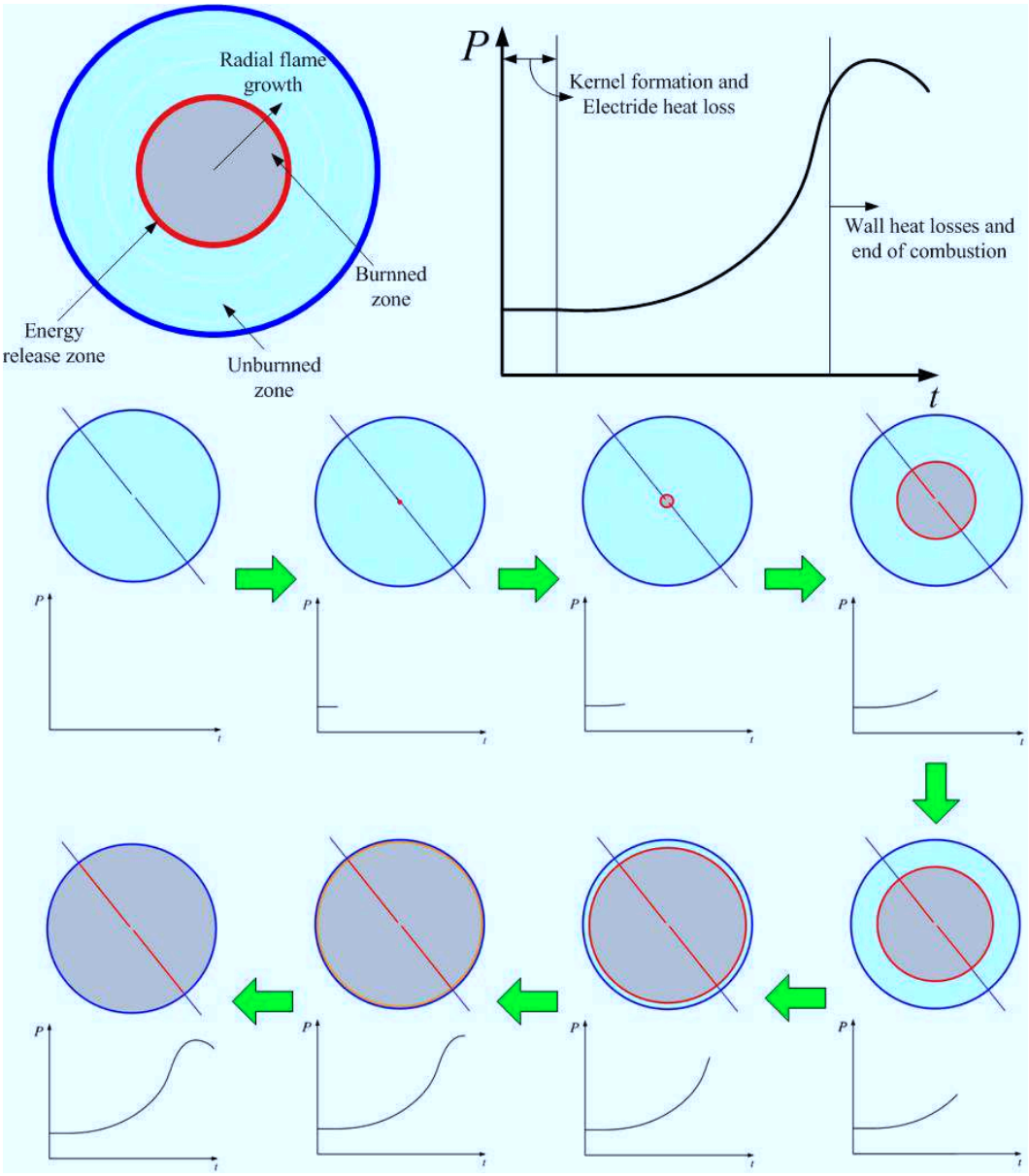

Figure 4.1: Schematic illustration of the numerical flame growth model.

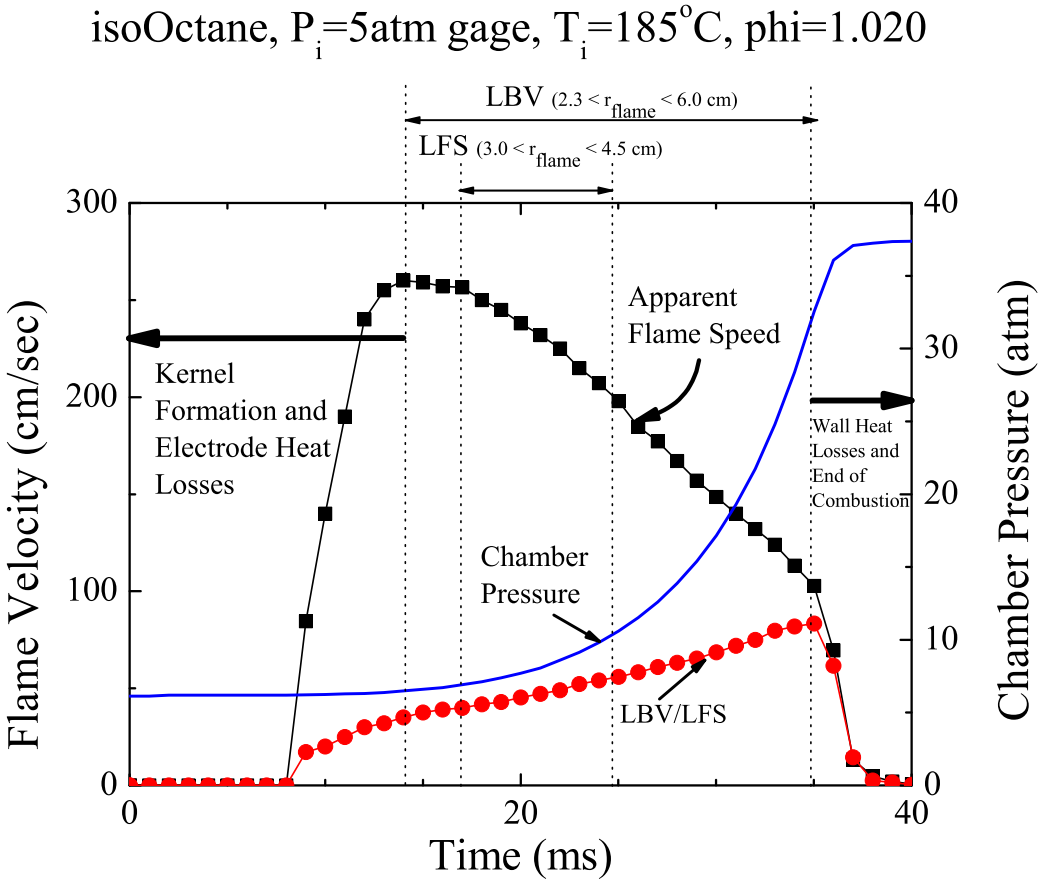

Figure 4.2: Flame velocities, chamber pressure and flame velocity regimes for the representative experiment.

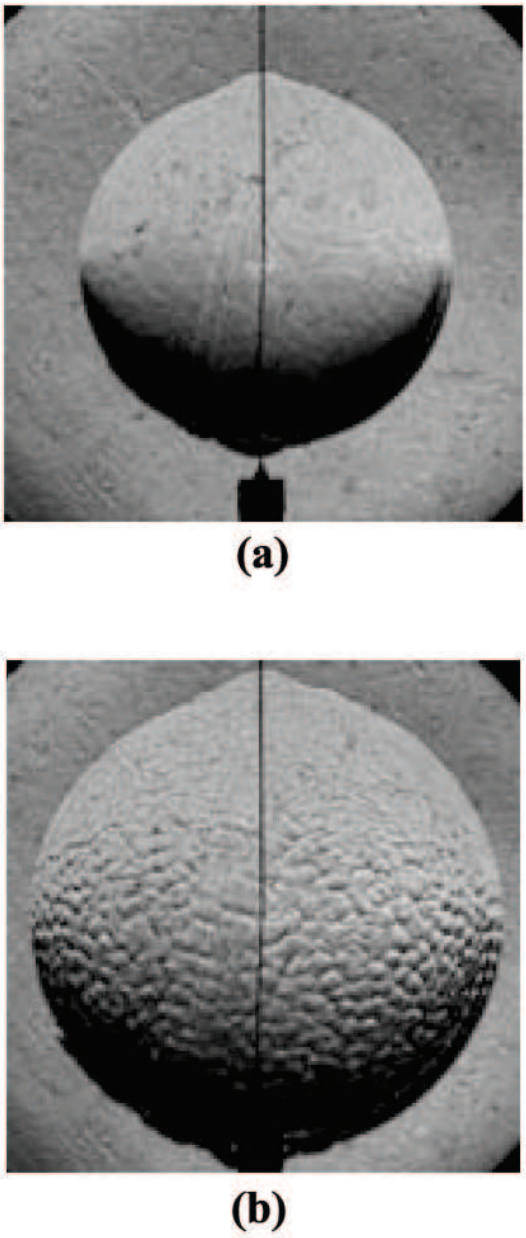

Figure 4.3: Cellularity : (a) smooth flame and (b) cellular flame.

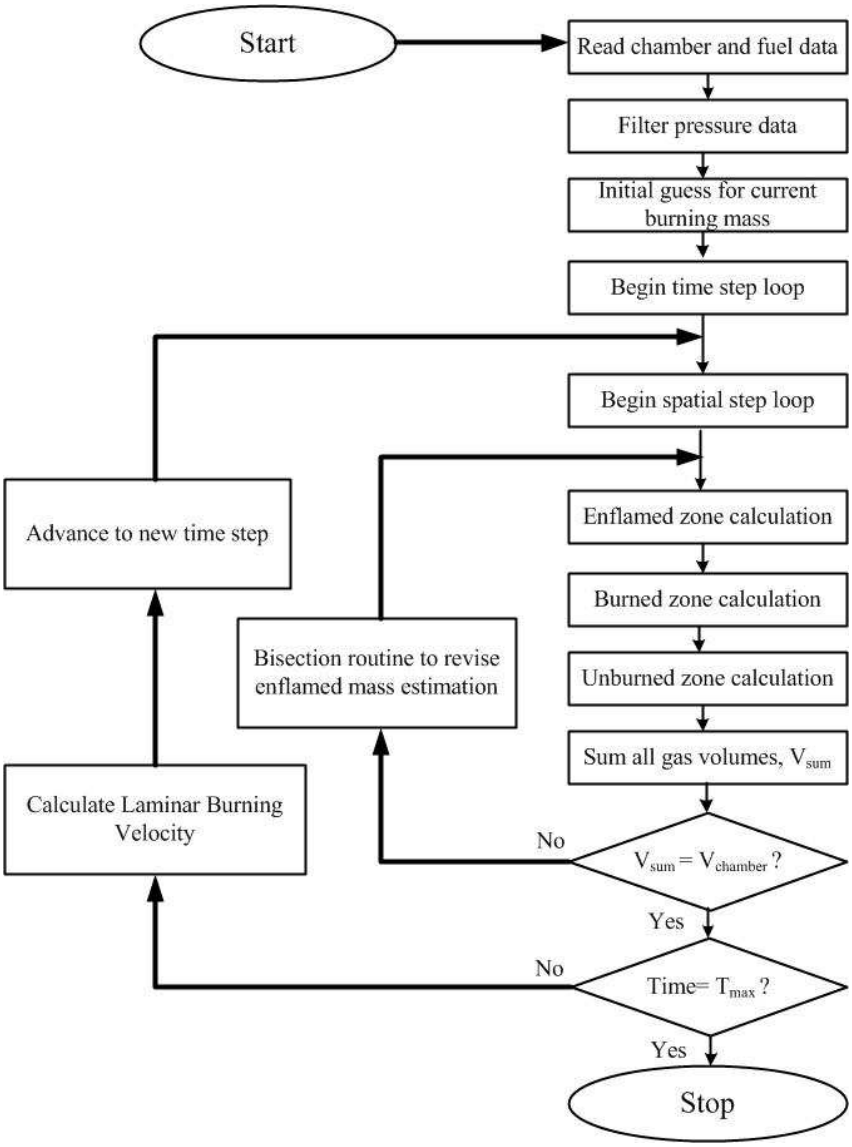

Figure 4.4: Flowchart of the computational procedure.

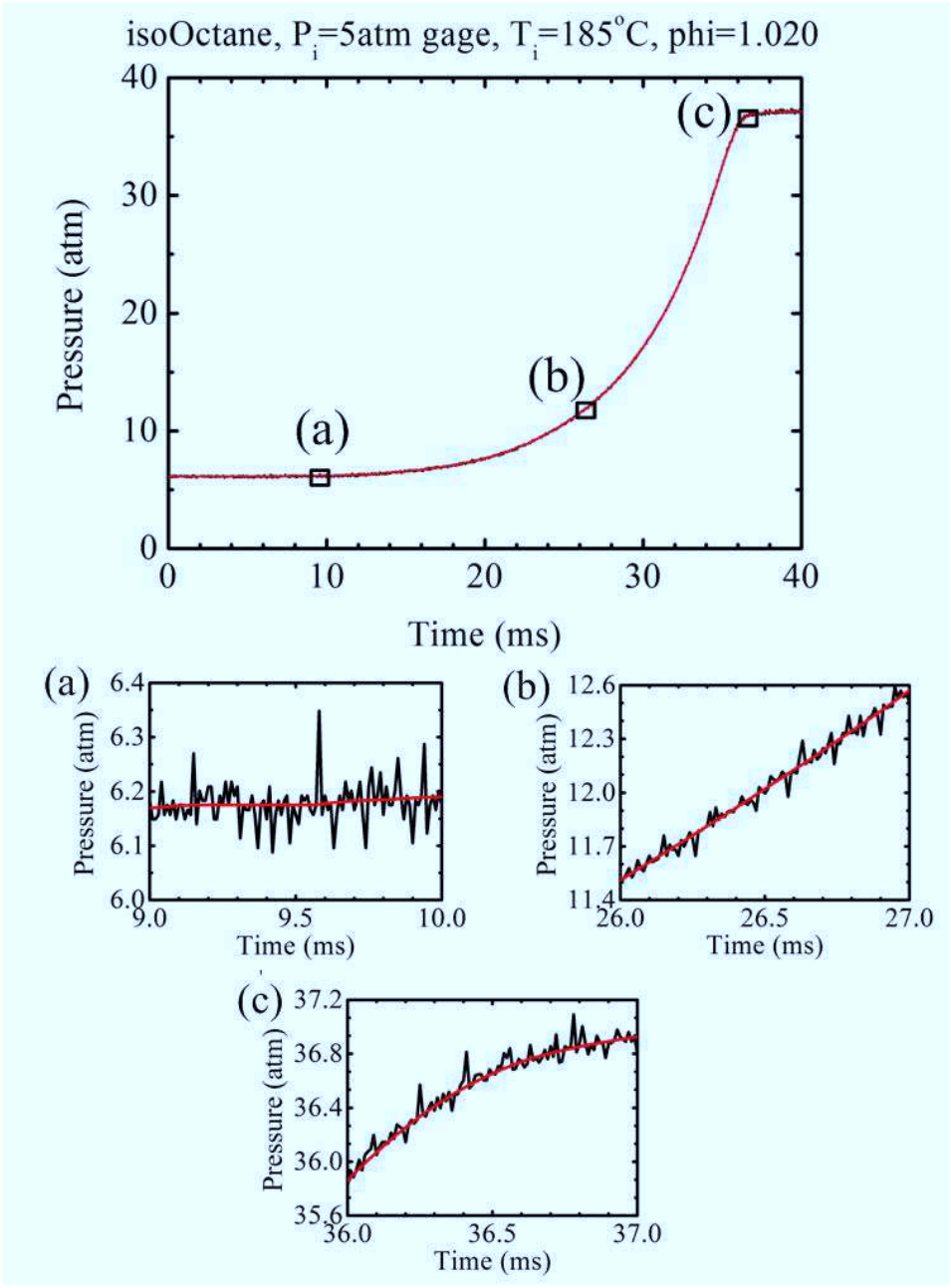

Figure 4.5: Comparison between raw and filtered pressure history data.

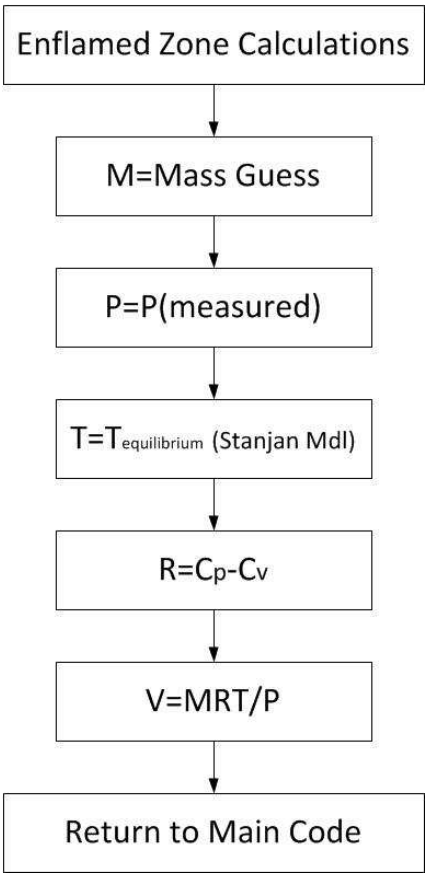

Figure 4.6: Flowchart of enflamed zone calculations.

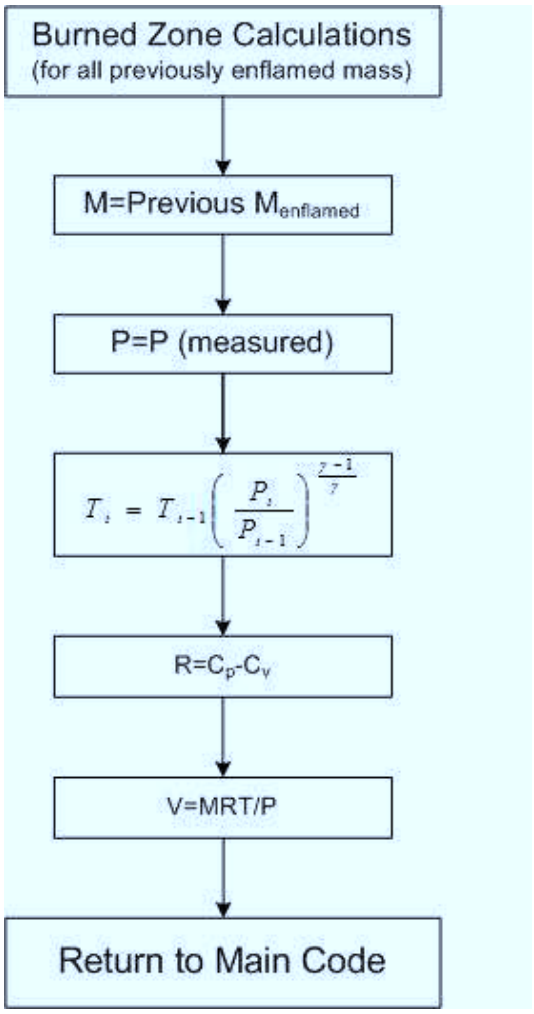

Figure 4.7: Flowchart of burned zone calculations.

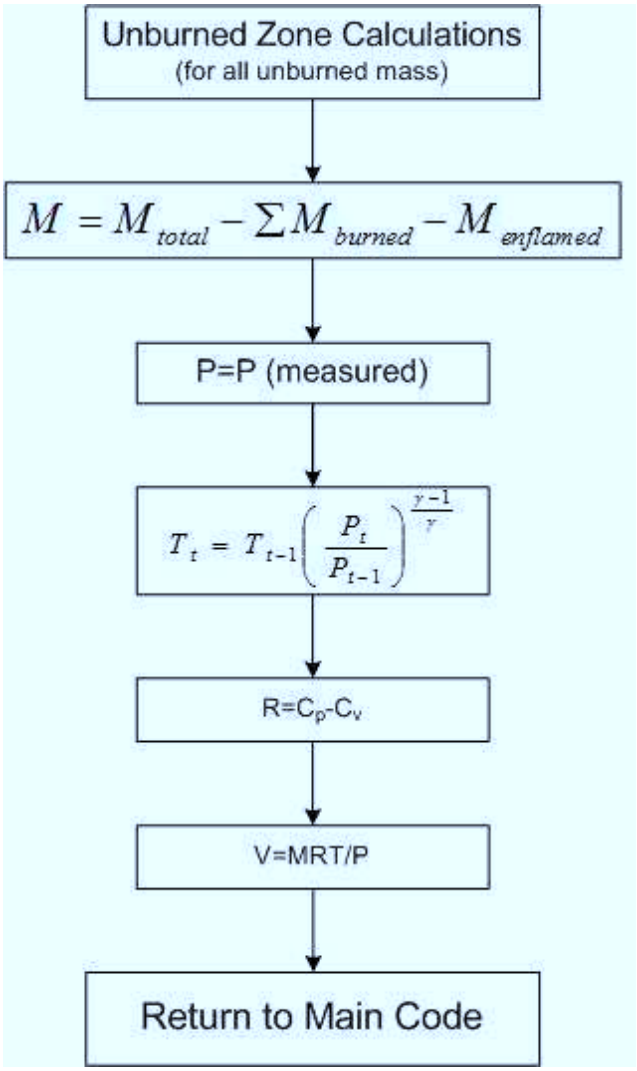

Figure 4.8: Flowchart of unburned zone calculations.

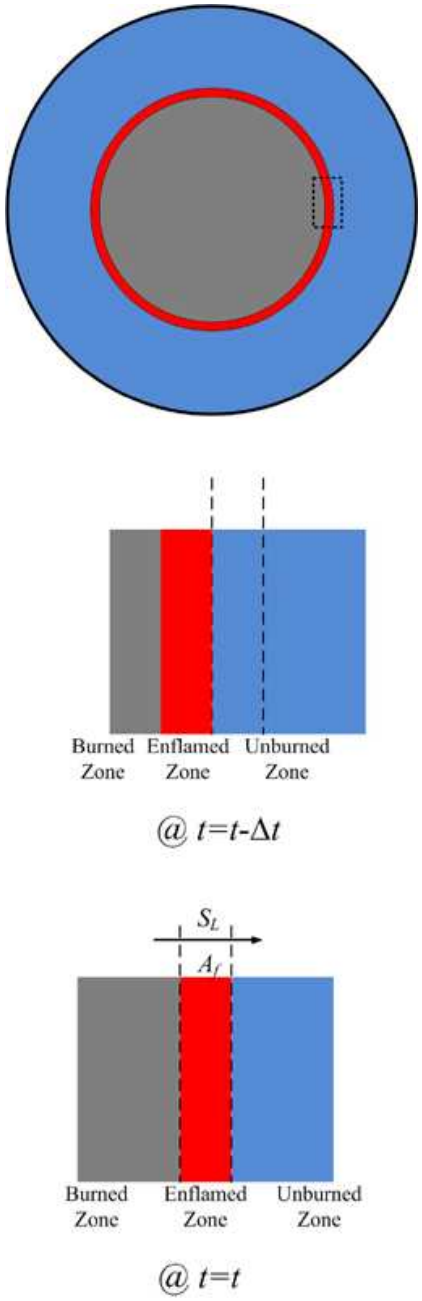

Figure 4.9: Laminar flame speed calculation model.

4.2 Validation of Calculated Laminar Burning Velocities

To validate the laminar burning velocity calculations as well as the experimental method, methane was tested and compared with the reference laminar flame speed data. Even though methane is one of the most investigated fuels, its characteristics at elevated pressures and temperatures have not been studied. In this research, the PREMIX code [32] was used for the calculation of laminar flame speeds of methane. This code is integrated with the CHEMKIN and Transport [34] subroutine libraries. GRI-Mech 3.0 [5] was used to describe the kinetics.

Table 4.1: Parameters of the calculated laminar burning velocities verification tests.

Fuel	Methane
Initial temperature (°C)	100
Initial pressure (atm gage)	5
Equivalence ratio	0.888, 0.948, 1.025, 1.123, 1.206

Table 4.1 lists the parameters of these tests. After each test with one equivalence ratio, laminar burning velocities were calculated with the analysis code. After that, laminar flame speeds were calculated at each pressure, temperature and equivalence ratio, with the PREMIX code. Appendix A contains the results of these calculations, and Fig. 4.10 shows comparisons between this experimental laminar burning velocity and the calculated laminar flame speed

from the PREMIX code for various methane-air equivalence ratios, with the flame radius range of 2.5 cm to 5.0 cm. Fig. 4.11 shows percent error from the comparison of these two flame speeds. As seen in Fig. 4.11, the calculated laminar burning velocities in the middle of the burning area are well matched with laminar flame speeds from the PREMIX code, mostly within 5 % error. However, even after eliminating beginning and end of burning, the first and last part of the selected laminar burning velocities do not have good agreement with the laminar flame speed from the PREMIX code. As explained in Chap. 1 and Section 4.1, it is because the calculated laminar burning velocities from the experimental data have a strong effect of ignition and stretch in the beginning and wall effect and have cellularity generation in the end of the combustion.

From this comparison, it is shown that if the laminar burning velocity data are narrowed down to use only the middle of the burning area, these data can be used as laminar flame speeds of the tested fuel. To validate the minimum flame radius for the laminar flame speed, which was 3 cm, a stretch analysis was conducted. Methane data with an equivalence ratio of 0.948 were used. As explained in Subsection 2.1.6.1, the unstretched laminar flame speed, S_{b0}, and propagating speed, S_b, are related as follows.

$$S_{b0} - S_b = L_b \cdot \kappa,$$

where L_b is the Markstein length and κ is the stretch rate. Using this relationship, S_{b0} is determined by extrapolating of a S_b - κ graph at various flame

radii of 1.5, 2.0, 2.5, 3.0 cm. Table 4.2 and Fig. 4.12 show the results of this analysis.

Table 4.2: Propagating flame speed and unstretched flame speed at various flame radii.

r_{flame} (cm)	S_b (cm/s)	S_{b0} (cm/s)	% error (%)
1.5	113.25	63.19	79.23
2.0	99.86	71.53	39.60
2.5	95.11	79.36	19.84
3.0	91.58	84.97	7.78

As flame radius increased, the error between unstretched flame speed and propagating speed decreased. At a flame radius of 3 cm, the % error was less than 10 % and it was shown that flame radius of 3 cm can be used as a minimum flame radius for determining the laminar flame speed with reasonable accuracy.

From this validation process, it is shown that the methods of the experiment and calculation work for the laminar burning velocity in the wide range of flame radius and for the laminar flame speed in the middle of combustion.

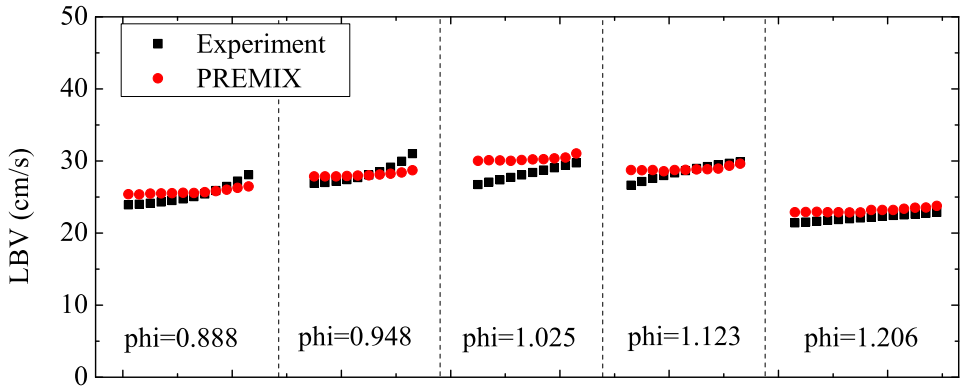

Figure 4.10: Comparison between experimental laminar burning velocity and calculated laminar flame speed from the PREMIX code using methane kinetics.

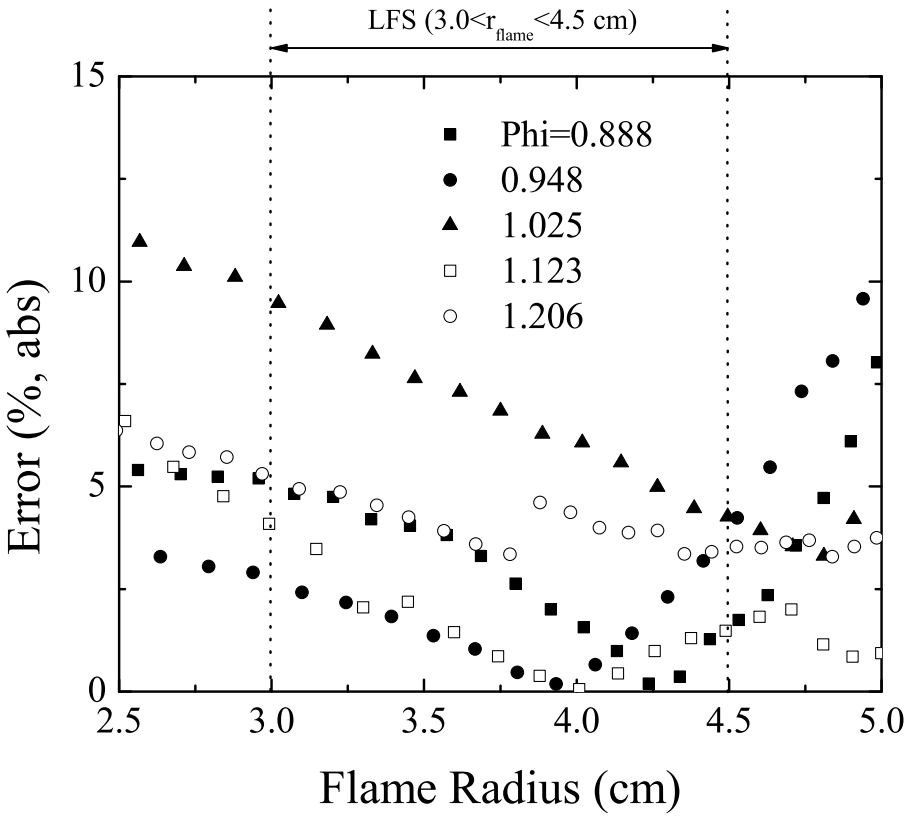

Figure 4.11: Error of the comparison between experimental laminar burning velocity and calculated laminar flame speed from the PREMIX code for methane.

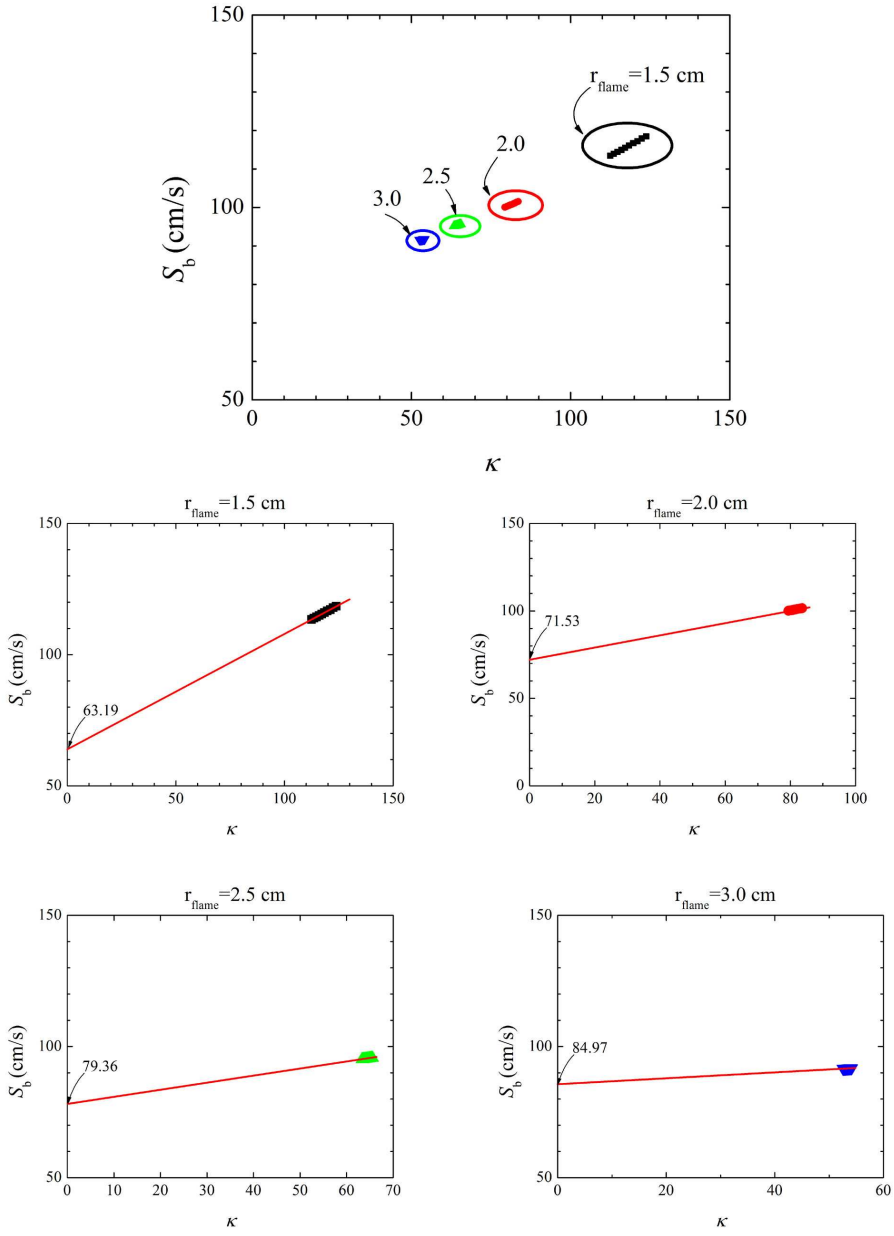

Figure 4.12: Results of stretch analysis.

Chapter 5

Laminar Burning Velocity Database and Laminar Flame Speed Analysis

5.1 Laminar Burning Velocity Database

From the experiments and calculations, a large database of laminar burning velocities was established. As defined in Chap. 1, the laminar burning velocity is the measured flame velocity in a constant volume chamber using the pressure measuring method. It includes the effects of ignition and stretch at the beginning of combustion, where the radius of the flame is small, and the effects of chamber wall and cellularity generation, where the flame radius is large. This flame velocity is not a fuel property. The effect of experimental components is included especially at the beginning and end of the combustion. In this research, 21,663 laminar burning velocity data points were measured for nine tested fuels with a wide range of equivalence ratios at elevated pressures and temperatures. Again, these fuels are three pure fuels, *n*-heptane, *iso*-octane and ethanol and six blended fuels: 25Hep75Oct, 50Hep50Oct, 75Hep25Oct, 50Hep50Eth, 50Oct50Eth and 33Hep33Oct33Eth. This large number of laminar burning velocity data can be used in research related to ignition, stretch, engine wall effects and cellularity generation. Also the data can be used in the relative comparison of fuels in prediction of engine

performance with each fuel. Table 5.1 shows the number of individual data points, range of the equivalence ratio, pressure and temperature for tested fuels in the laminar burning velocity database. More than 2,000 data points were collected for each fuel and most equivalence ratios were in the readable range of the UEGO sensor ($0.70 < \text{phi} < 1.60$). The highest pressure was up to 40 atm, and the highest temperature was up to 660 K.

Table 5.1: Number of data points, range of equivalence ratio, pressure and temperature for tested fuels in the laminar burning velocity database.

Fuel	Number of data points	Phi range	P range (atm)	T range (K)
n-Heptane	2,130	0.720 - 1.572	2.18 - 39.26	464.08 - 659.73
iso-Octane	2,583	0.717 - 1.606	2.16 - 40.37	464.24 - 654.70
Ethanol	3,363	0.667 - 1.558	2.08 - 35.13	450.81 - 623.62
25Hep75Oct	2,411	0.740 - 1.547	2.25 - 40.12	463.49 - 657.58
50Hep50Oct	2,280	0.735 - 1.592	2.22 - 39.97	464.21 - 659.82
75Hep25Oct	2,159	0.734 - 1.542	2.17 - 39.62	464.67 - 654.03
50Hep50Eth	2,297	0.717 - 1.571	2.21 - 39.74	452.22 - 634.53
50Oct50Eth	2,265	0.736 - 1.606	2.10 - 41.05	451.60 - 632.57
33Hep33Oct33Eth	2,175	0.744 - 1.568	2.18 - 39.14	451.48 - 638.93
Total	21,663			

The tabulated database is available at `http://user.chol.com/~cryogenic/LBVdb/`. The laminar burning velocity database is the starting point for the subsequent laminar flame speed study.

5.2 Laminar Flame Speed Analysis

5.2.1 *Iso*-octane, *n*-heptane and blends

For *iso*-octane and *n*-heptane, measurements were made for the two single-components and binary blends in 1/3, 1/1, 3/1 volume ratios over a

wide range of equivalence ratios at elevated temperatures and pressures.

As explained in Chap. 1, the laminar flame speed, which is a fuel property, was extracted from the laminar burning velocity database. Table 5.2 shows the number of data points in the laminar burning velocity database and the number of extracted laminar flame speeds for each fuel. As explained in Chap. 4, the flame radius range of 3 cm to 4.5 cm was used to extract laminar flame speeds from the laminar burning velocity database. The equivalence ratio range of 0.8 to 1.2 was added as a criterion to narrow down the laminar burning velocity to the laminar flame speed for data analysis. This was because it was found that slow flame speeds at both ends of the equivalence ratio had high uncertainties. With these laminar flame speeds, a new physically-based flame-speed blending model was developed. Again, the purpose of this analysis is to develop a new correlation to predict laminar flame speeds of blended fuels.

Table 5.2: Number of data points of laminar burning velocity and laminar flame speed for *iso*-octane, *n*-heptane and blends.

	Laminar Burning Velocity 2.3 < Flame Radius < 6.0 cm				
Fuel	*n*-Heptane	75Hep25Oct	50Hep50Oct	25Hep75Oct	*iso*-Octane
Number of data points	2,130	2,159	2,280	2,411	2,583
	Laminar Flame Speed 3 < Flame Radius < 4.5 cm				
Fuel	*n*-Heptane	75Hep25Oct	50Hep50Oct	25Hep75Oct	*iso*-Octane
Number of data points	288	307	314	322	364

Before deriving a new flame-speed model for blends, some graphs of laminar burning velocities and other properties were drawn to see their re-

lationships. In this analysis, not laminar flame speeds but laminar burning velocities were used because there is much more laminar burning velocity data to analyse. This is a qualitative analysis. Fig. 5.1 shows laminar burning velocity and flame temperature of *iso*-octane, *n*-heptane and their blends with initial temperature of 185 °C and initial pressure of 3, 5 and 7 atm. Here, flame temperature is taken from the calculated adiabatic flame temperature with the Chemical Equilibrium with Applications (CEA) program at each condition [54]. For each set of data, the flame temperature profile is similar to the laminar burning velocity profile. From that, it concludes that the flame temperature works as a key part in defining the flame speed. However, from all fuels at each initial pressure, the flame temperature is similar to each other even though the laminar burning velocity varies with highest for pure *n*-heptane and lowest for pure *iso*-octane. Based on this result, it is found there is another factor that makes the laminar burning velocity distinctive in fuels except flame temperature.

It is also known that thermal diffusivity of the mixture affects the laminar flame speed. It is also verified with a graph. Fig. 5.2 is at the same cases with Fig. 5.1 for laminar burning velocity and thermal diffusivity. Here, thermal conductivity and specific heat data for thermal diffusivity of fuels were from Yaws [55]. For each set of data, it is not clear if the thermal diffusivity works significantly in defining the laminar burning velocity, since thermal diffusivity does not vary with fuel type. Thermal diffusivity is predicted to be proportional to the burning velocity with some power. But from Fig. 5.2,

it is inversely proportional to the burning velocity. As thermal diffusivity decreased, the laminar burning velocity increased. It is because the effect of flame temperature previously discussed overrides the effect of decreasing thermal diffusivity. Thus, for *iso*-octane and *n*-heptane, the dominant flame speed variable seems to be flame temperature. Like flame temperature, the thermal diffusivity is similar to each other in the tested fuels at each initial pressure even though the laminar burning velocity varies by the type of fuel. This result shows that there is another factor that makes the laminar burning velocity distinctive in fuels, as discussed in the following paragraph.

Mallard and Le Chatelier developed the laminar-flame theory to find the laminar flame speed in 1883 [36]. In their theory, they used heat conduction as the dominant driving force to make the flame propagate. The flame was divided into two zones; the preheat zone and the reaction zone as indicated in Fig. 5.3. Preheat zone(Zone I) is where the air-fuel mixture is heated by conduction and reaches ignition at the ignition boundary. T_0 is the unburned mixture temperature. T_{ig} is the ignition temperature. T_f is the flame temperature, and δ_r is the length of reaction zone. Mallard and Le Chatelier derived the following correlation using mass conservation and energy balance at zone I and II.

$$S_L = \frac{\lambda}{\rho C_p} \frac{T_f - T_{ig}}{T_{ig} - T_0} \frac{1}{\delta_r} \tag{5-1}$$

Here, the length of reaction zone, δ_r is expressed as follows

$$\delta_r = S_L \frac{1}{d\epsilon/dt} \tag{5-2}$$

where $d\epsilon/dt$ is the rate of reaction.

From the Arrhenius law, the reaction rate with n-th order chemical reaction has the relationship of

$$\frac{d\epsilon}{dt} \propto e^{-\frac{E_a}{R_u T_f}} P^{n-1} \tag{5-3}$$

where E_a is an activation energy, R_u is an universal gas constant, and P is pressure. Here, flame temperature T_f is used for the temperature because most chemical reactions take place around the flame temperature.

Substituting Eq. 5-2 and Eq. 5-3 into Eq. 5-1, the final from is

$$S_L = S_{L0} \sqrt{\frac{\lambda}{\rho C_p} \frac{T_f - T_{ig}}{T_{ig} - T_0} e^{-\frac{E_a}{R_u T_f}} P^{n-1}} \tag{5-4}$$

In this correlation, for the pressure dependence,

$$S_L \propto \sqrt{\frac{1}{\rho} P^{n-1}} \propto \sqrt{P^{n-2}}$$

This equation implies that the laminar flame speed is independent of pressure for second-order chemical reactions.

Based on Eq. 5-4, a new correlation for the laminar flame speed for blends of n-heptane and *iso*-octane was derived.

The form of the new correlation is as follows.

$$S_L = S_{L0}\alpha^{k_1}\left(\frac{T_f - T_{ig}}{T_{ig} - T_0}\right)^{k_2} k_3 e^{-\frac{E_a}{R_u T_f}} P^{k_4}$$

Firstly, fitting the *iso*-octane laminar flame speed data with this correlation was attempted. S_{L0} and T_{ig} were set at 24 cm/s and 720 K, respectively. From fitting, the values for the parameters, k_1, k_2, k_3, k_4 and Ea were determined as follows.

k_1	k_2	k_3	k_4	Ea
0.20008	1.27777	3.7173	-8.2234E-26	16816.95963

Fig. 5.4 shows the result of fitting. Appendix B shows the numerical values of laminar flame speeds from experiments and fitting with percent error in these two values.

To verify the new correlation with these parameters, laminar flame speeds from this research were compared with previously published data. Because no previous laminar flame speeds at the temperature range of this research was available, extrapolated laminar flame speeds to the highest available temperature were used for the comparison. The temperature and pressure were 347 K and 10 bar, respectively. Fig. 5.5 shows the graph of laminar flame speed from this research and previous research for a wide range of equivalence ratios. The values of laminar flame speed had good agreement with most of the previously researched data; however, the peak value of the laminar flame

speed in this research was at a slightly lower equivalence ratio. To investigate this disagreement, the pressure effect on the flame temperature was examined. Fig. 5.6 shows the flame temperature of *iso*-octane at different initial pressures, and Fig. 5.7 shows the zoomed in area of peak flame temperatures. As shown in these two graphs, the peak flame temperature occurs at a left-shifted equivalence ratio as initial pressure increases. Since the laminar flame speed is highly dependent on the flame temperature, the moved peak point of the flame temperature due to the high initial pressure is reasonable. As indicated in Fig. 5.5, the initial pressure is as high as 10 bar, and the left-shifted peak point of laminar flame speed in this research is also reasonable.

The derived parameters for *iso*-octane with the new correlation were used to predict laminar flame speeds of blended fuels. Various attempts were made to achieve a good fit with laminar flame speed data. The best fit was as follows. k_1, k_2, k_3, k_4 and Ea were fixed as the values that were found in *iso*-octane analysis. Only T_{ig} was used as a parameter for fitting with the new correlation to other fuels. Fig. 5.6, Fig. 5.7, Fig. 5.8 and Fig. 5.9 show the results of fitting with 75 *iso*-octane and 25 *n*-heptane, 50 *iso*-octane and 50 *n*-heptane, 25 *iso*-octane and 75 *n*-heptane blends and pure *n*-heptane, respectively. Tabulated data for these fitting are shown in Appendix C to Appendix F.

After all fitting processes were done, T_{ig} at each fuel was found and shown in Table 5.3 and Fig. 5.12. As shown in Fig. 5.12, T_{ig} and octane numbers of *iso*-octane and *n*-heptane blends have a linear relationship. Laminar

flame speed for any *n*-heptane, *iso*-octane blends can be predicted with T_{ig} at the octane number of this blend.

Table 5.3: Ignition temperatures with octane number of *iso*-octane and *n*-heptane blends.

Octane Number	0	25	50	75	100
T_{ig} (K)	696.09	701.17	707.98	713.59	720.00

The fitting result of these octane number and T_{ig} relationships was shown in Fig. 5.12 and the fitting result was as follows.

$$T_{ig}(K) = 695.72 + 0.24097 N_{Octane}$$

Figures from Fig. 5.13 to Fig. 5.22 show laminar burning velocities that were calculated with the new model. From Fig. 5.13 to Fig. 5.20, it is shown that *n*-heptane is the fastest fuel and *iso*-octane is the slowest fuel and blends are between these two pure fuels at various unburned air-fuel mixture temperatures and pressures throughout the wide range of equivalence ratio. Fig. 5.21 shows the effect of pressure on the laminar flame speed. It is shown that as pressure increases, the laminar flame speed decreases. Fig. 5.22 shows the effect of unburned air-fuel mixture temperature on the laminar flame speed. It is shown that as unburned air-fuel mixture temperature increases, the laminar flame speed also increases.

5.2.2 Ethanol and blends

For ethanol, laminar flame speed measurements were made for 1) pure ethanol, binary blends either 2) with *iso*-octane or 3) with *n*-heptane in 1/1 volume ratio, and 4) ternary blends with both *iso*-octane or *n*-heptane in a 1/1/1 volume ratio over a wide range of equivalence ratios at the elevated temperatures and pressures.

Like *iso*-octane and *n*-heptane blends, ethanol blends were examined with qualitative analysis to see the effect of flame temperature and thermal diffusivity on the laminar burning velocity. Fig. 5.23 and Fig. 5.24 show laminar burning velocity and flame temperature/thermal diffusivity of *iso*-octane, *n*-heptane, ethanol and their blends with an initial temperature of 185 °C and initial pressures of 3, 5 and 7 atm. From these two figures, flame temperature is a key factor in defining flame speed but thermal diffusivity did not show a clear effect on the flame speed.

Laminar flame speed analysis with the proposed correlation was attempted. Again, k_1, k_2, k_3, k_4 and Ea were fixed, and only T_{ig} was the parameter to fit the data. It was expected that this analysis may not have the linear relationship in blends to predict laminar flame speed in other blending ratios because ethanol, which has an O-H bond, is different from the other tested fuels. However, this analysis was performed to see the effect of ethanol in *iso*-octane and/or *n*-heptane blends. Fig. 5.25, Fig. 5.26, Fig. 5.27 and Fig. 5.28 show the results of fitting with 50 *n*-heptane and 50 ethanol, 33 *n*-heptane and 33 *iso*-octane and 33 ethanol, 50 *iso*-octane and 50 ethanol

and pure ethanol, respectively. Determined T_{ig}s of these fuels are tabulated in Table 5.4. The T_{ig}-Octane number relationship is shown in Fig. 5.29. In Fig. 5.29, the octane numbers of blends were estimated with the volume ratio of each fuel. As seen, the estimated octane number and T_{ig} have a non-linear relationship, as expected. Since this could be because of a poor laminar flame speed correlation, the experimental data were evaluated.

Table 5.4: Ignition temperatures with *iso*-octane, *n*-heptane and ethanol blends.

Fuel	*n*-Heptane	50Hep50Eth	33Hep33Oct33Eth	*iso*-Octane	50Oct50Eth	Ethanol
T_{ig} (K)	696.09	700.60	704.12	720.00	704.90	704.31

To check the non-linear behavior of ethanol in *iso*-octane and/or *n*-heptane blends, laminar burning velocity of *n*-heptane, *iso*-octane, ethanol and their binary blends with an initial temperature of 185 °C and initial pressures of 3, 5 and 7 atm are shown in Fig. 5.30. At an initial pressure 5 atm, adding ethanol (case 10), a "slow fuel", to *n*-heptane (case 6), "fast fuel", makes the blend (case 7) faster than *n*-heptane. Also, mixing two slow fuels, ethanol and *iso*-octane (case 8), made faster fuels (case 9) than these two fuels alone. The same phenomenon was found in the case of 7 atm initial pressure. From this analysis, it is found that ethanol works as an accelerating fuel even though it is a slow fuel by itself. This non-linearity was also found in other research. Beeckmann et al. [3] measured the laminar flame speed of ethanol, *iso*-octane and their blend in a 1/9 volume ratio and the results are shown in Fig. 5.31.

As seen in this figure, blended fuel with 10 % of ethanol in *iso*-octane was faster than *iso*-octane and ethanol in most equivalence ratios.

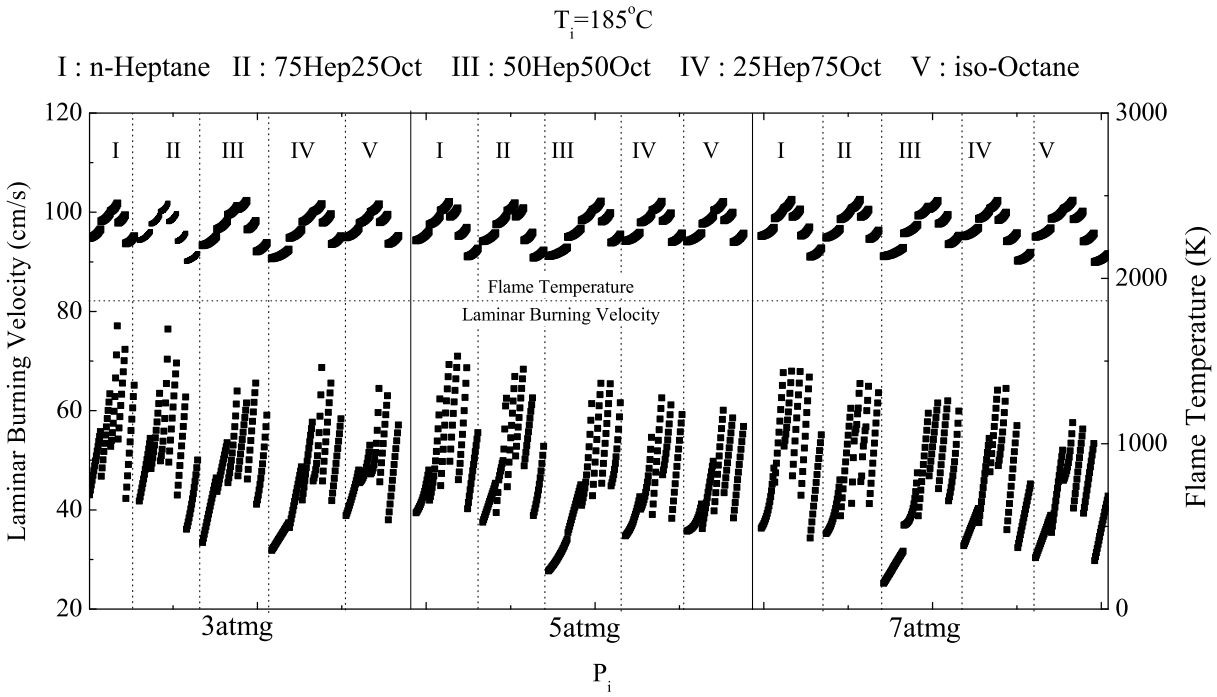

Figure 5.1: Laminar burning velocity and flame temperature of *iso*-octane, *n*-heptane and blends (Ti=185 °C, Pi=3,5,7 atmg).

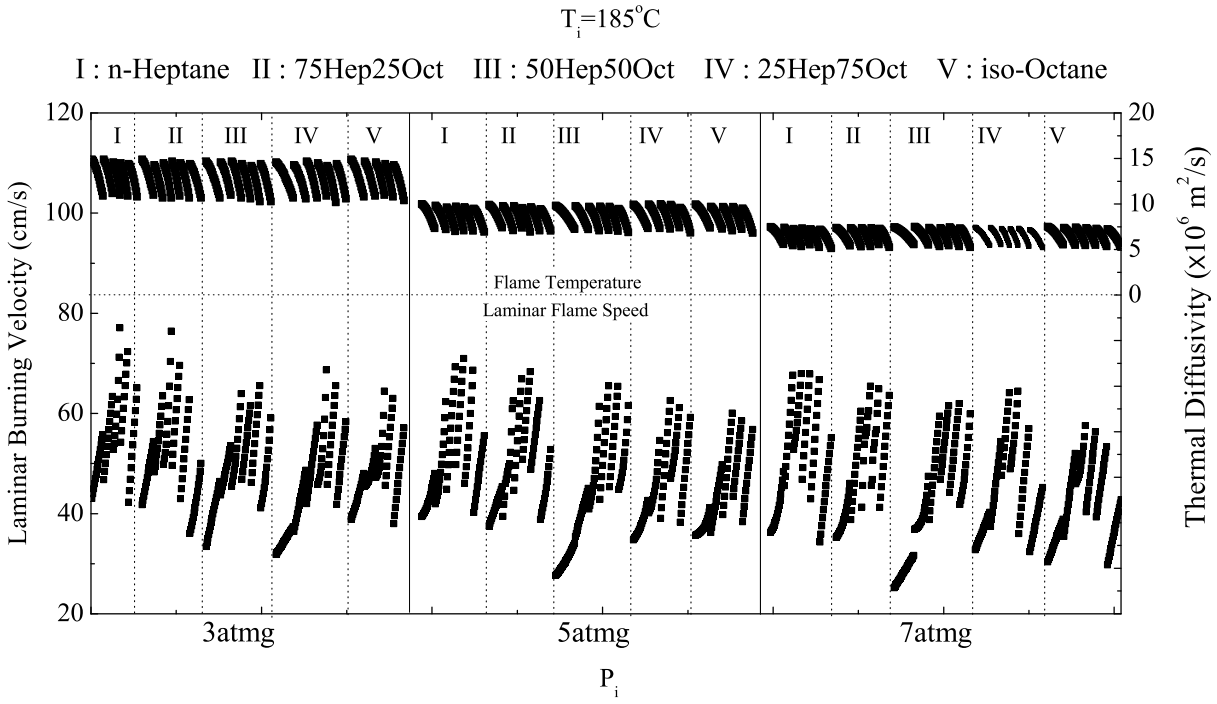

Figure 5.2: Laminar burning velocity and thermal diffusivity of *iso*-octane, *n*-heptane and blends (Ti=185 °C, Pi=3,5,7 atmg).

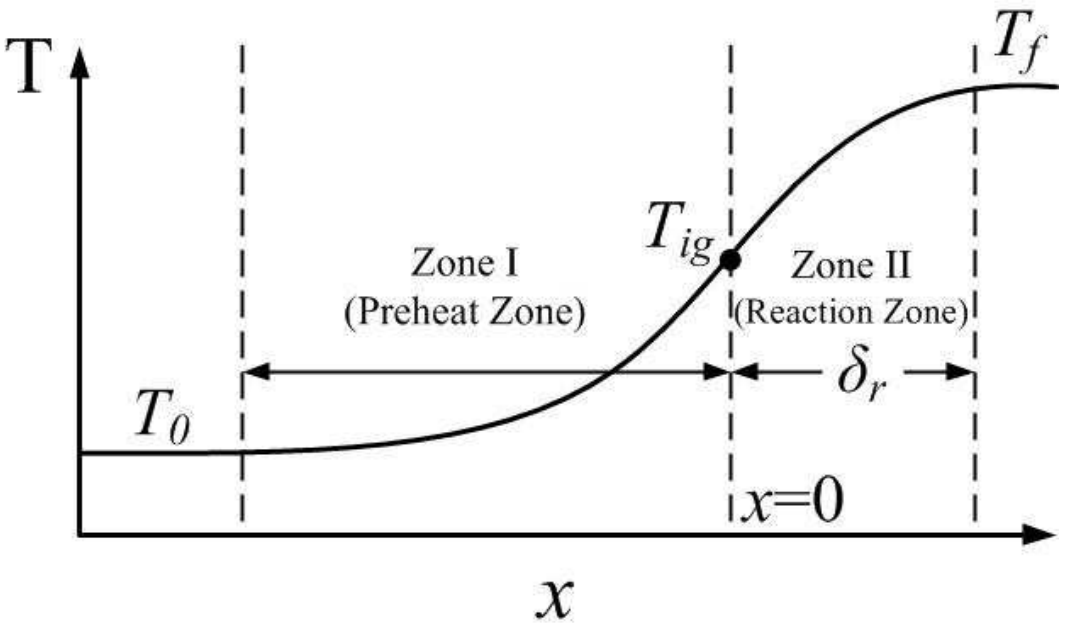

Figure 5.3: Schematic diagram of the temperature variation across a typical laminar flame [36].

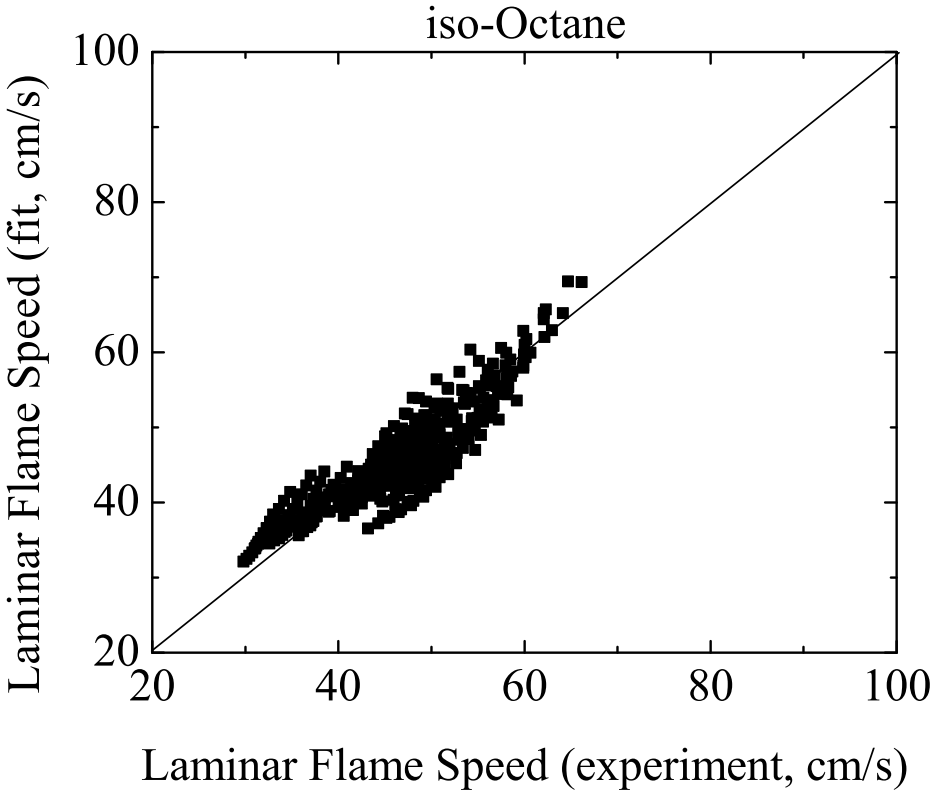

Figure 5.4: Fitting result for *iso*-octane.

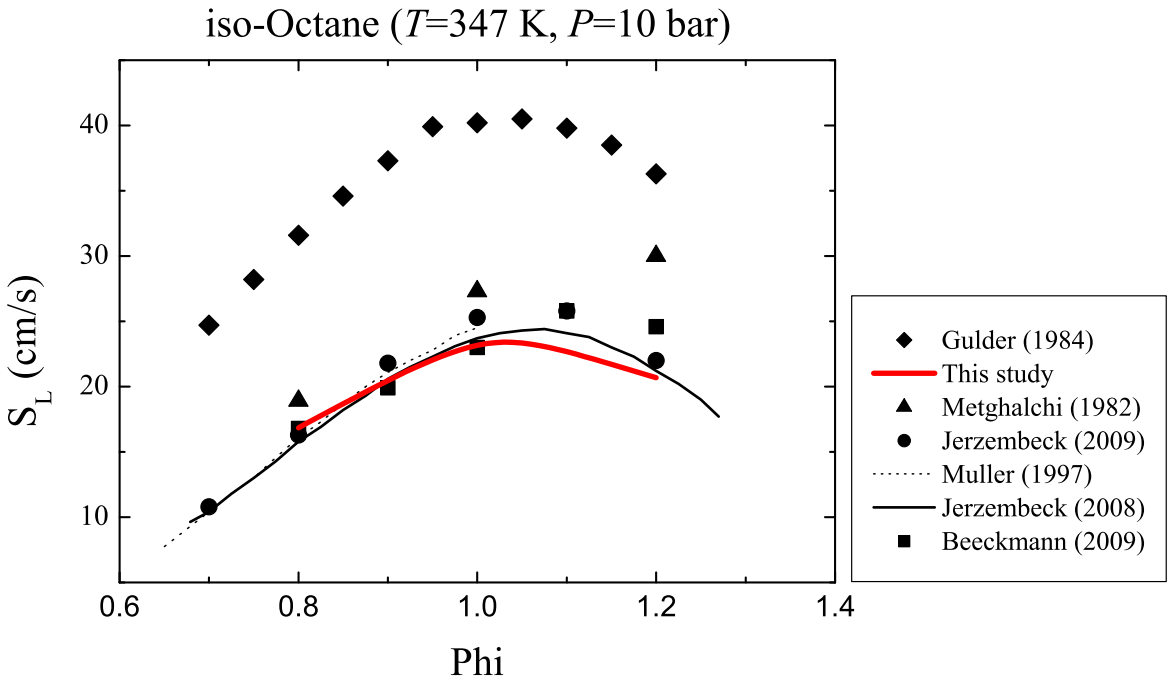

Figure 5.5: Laminar Flame Speeds of this study and previous researches at Ti=373 K, Pi=10 bar.

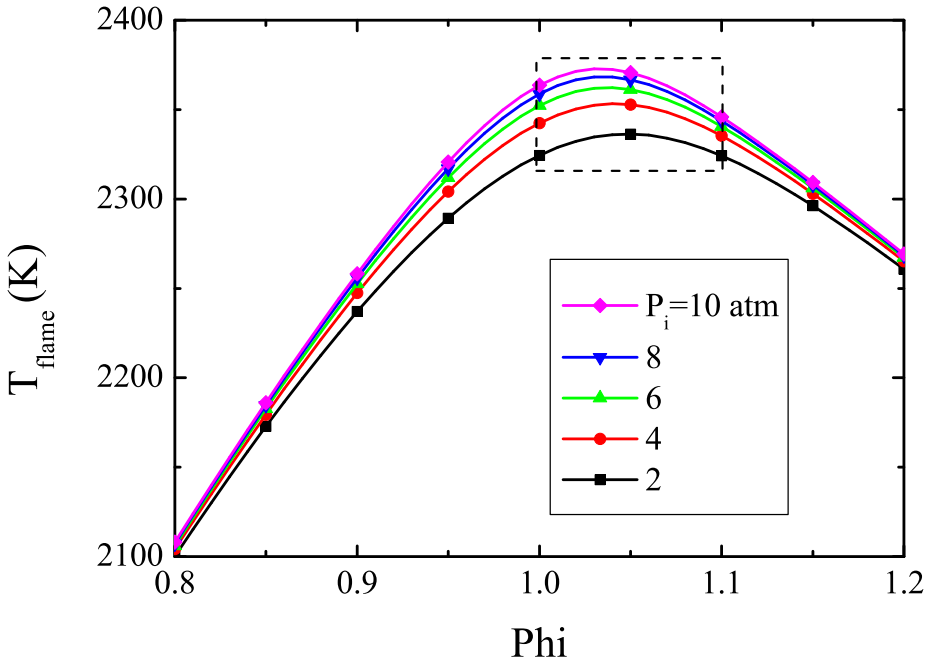

Figure 5.6: Flame temperature variation of *iso*-octane with various initial pressures.

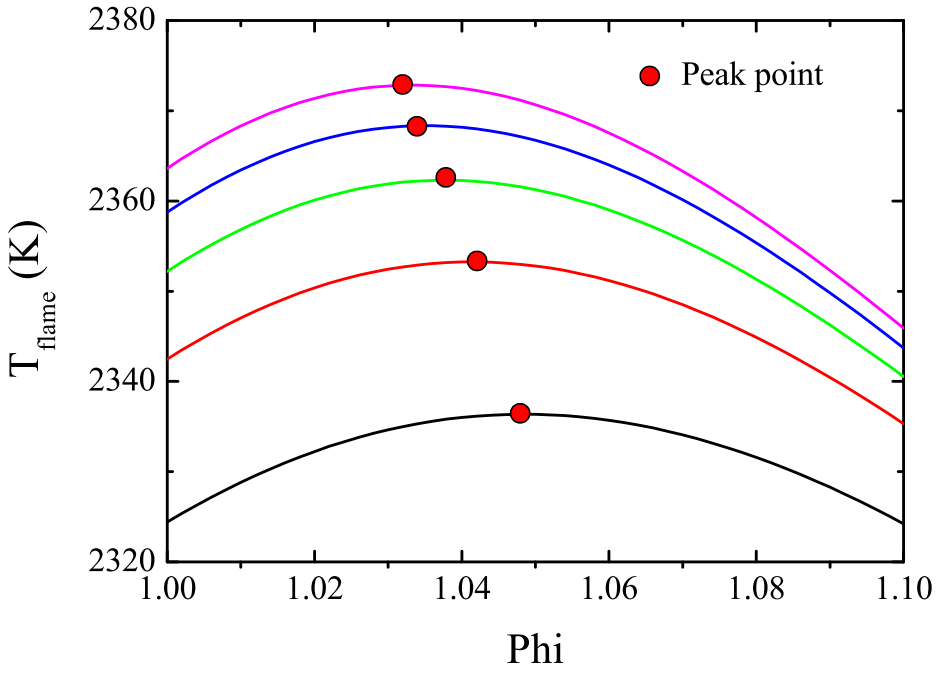

Figure 5.7: Flame temperature variation of *iso*-octane with various initial pressures(zoomed in).

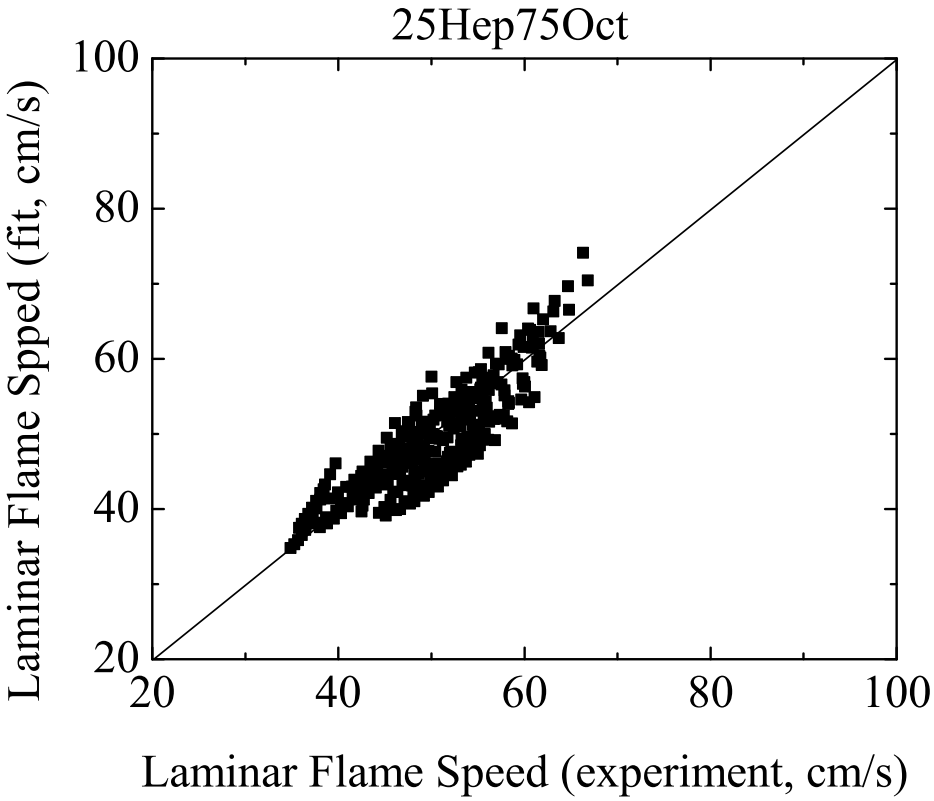

Figure 5.8: Fitting result of 75 *iso*-octane and 25 *n*-heptane blend.

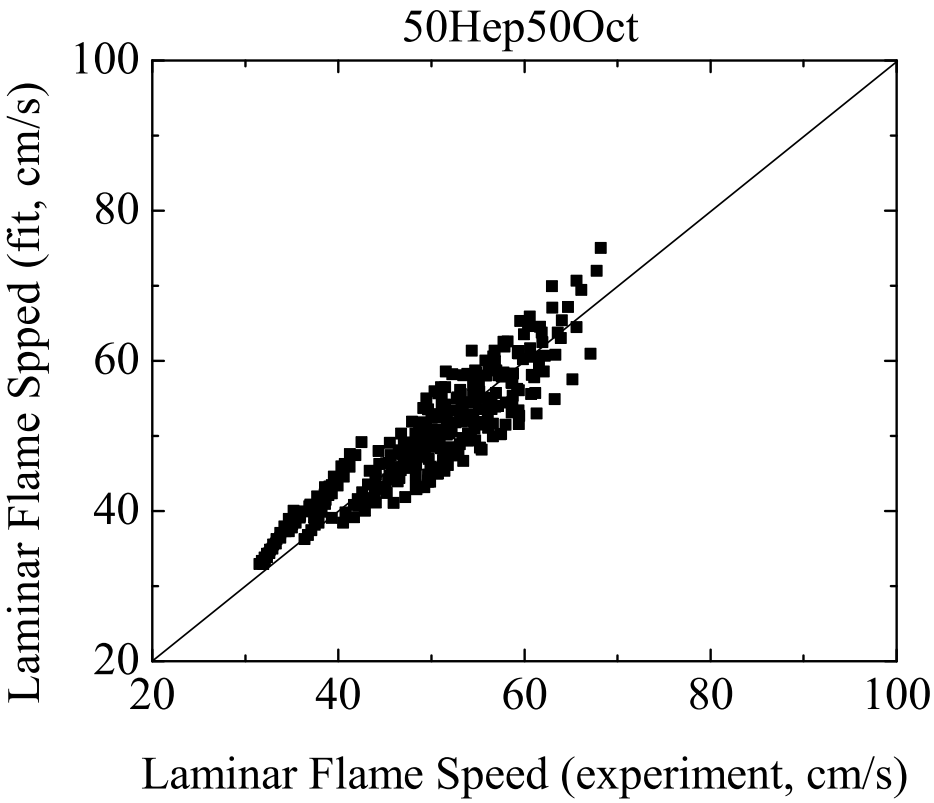

Figure 5.9: Fitting result of 50 *iso*-octane and 50 *n*-heptane blend.

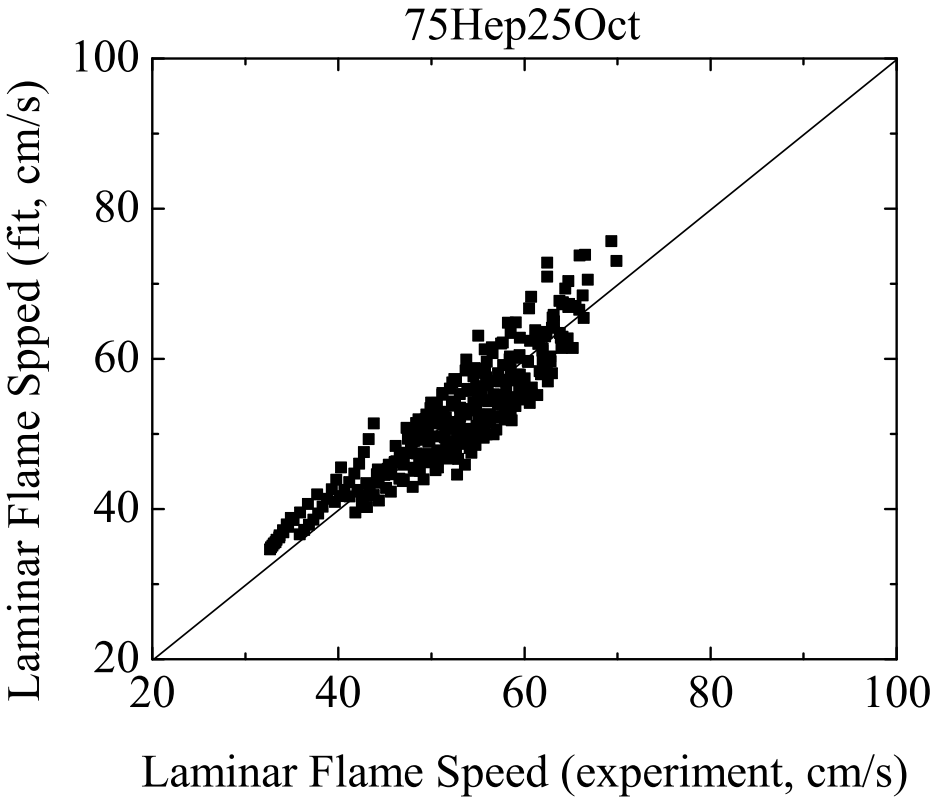

Figure 5.10: Fitting result of 25 *iso*-octane and 75 *n*-heptane blend.

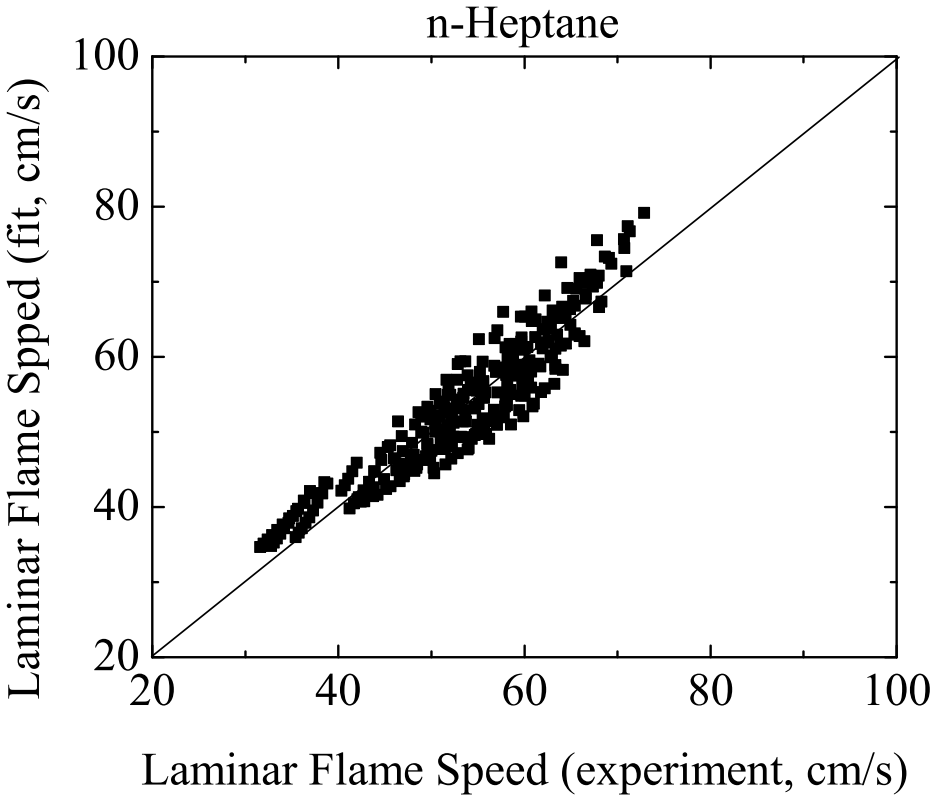

Figure 5.11: Fitting result of n-heptane.

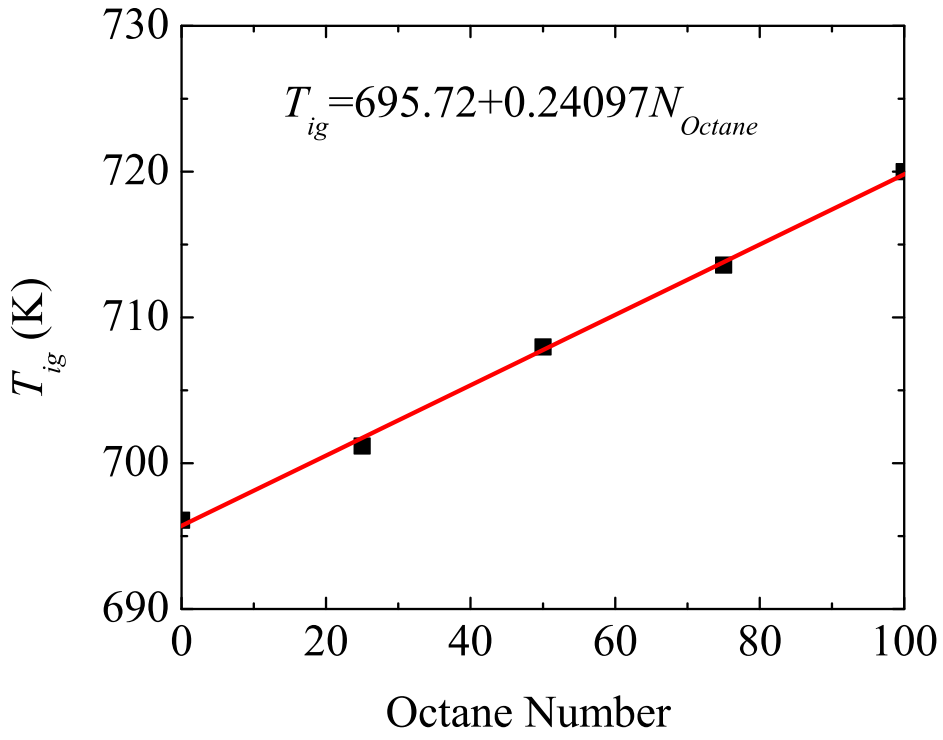

Figure 5.12: Ignition temperature versus octane number for *iso*-octane, *n*-heptane and blends.

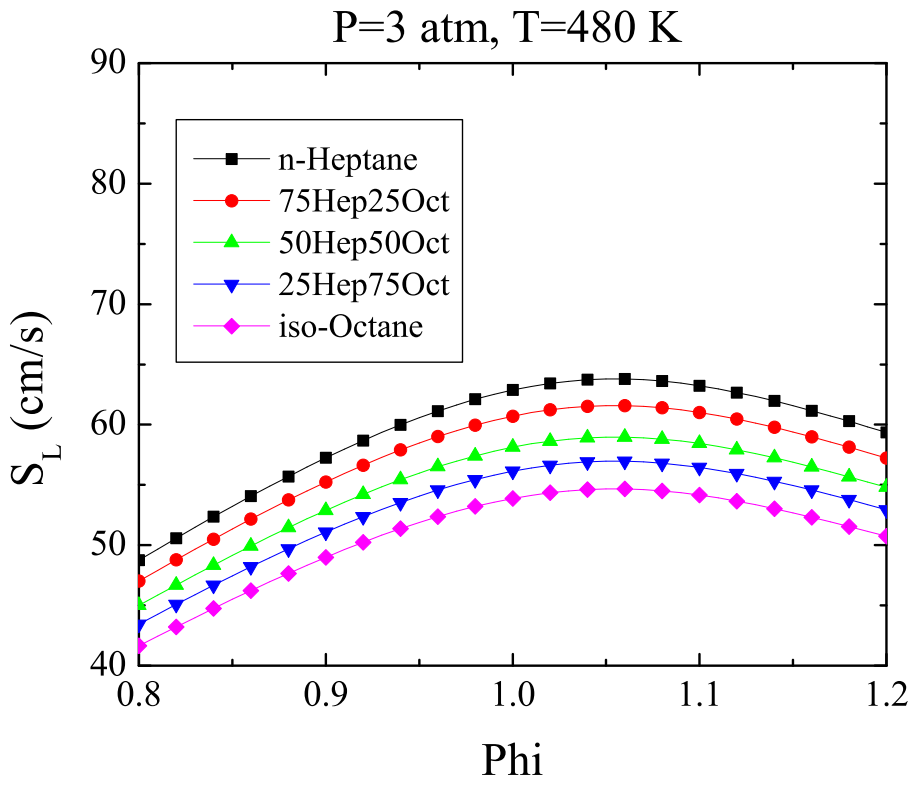

Figure 5.13: Laminar flame speeds of *iso*-octane, *n*-heptane and blends with 3 atm and 480 K.

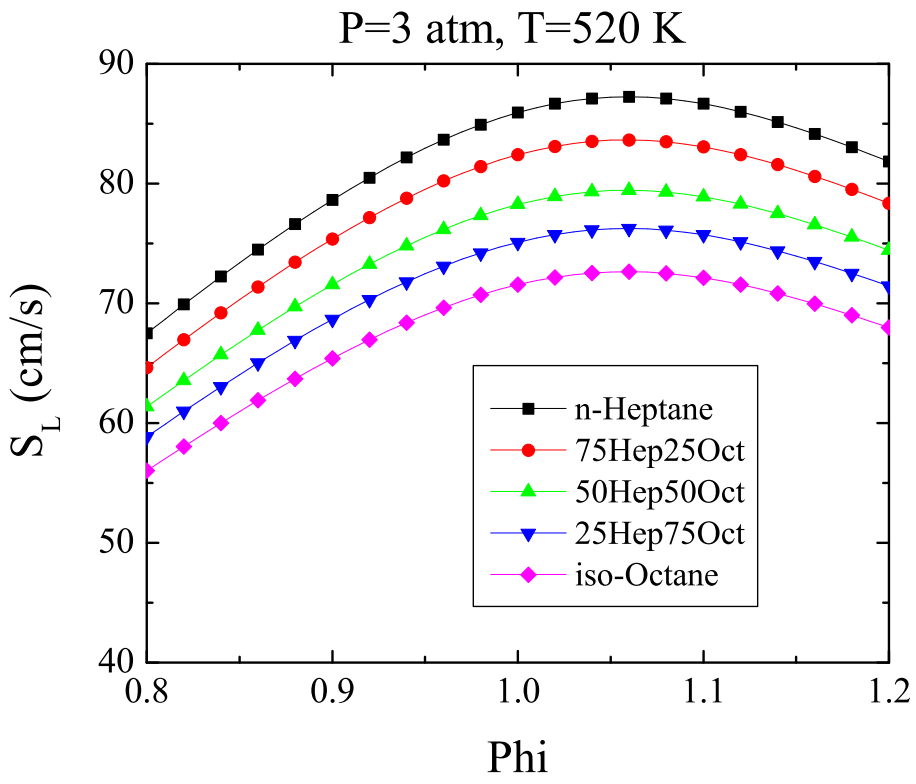

Figure 5.14: Laminar flame speeds of *iso*-octane, *n*-heptane and blends at 3 atm and 520 K.

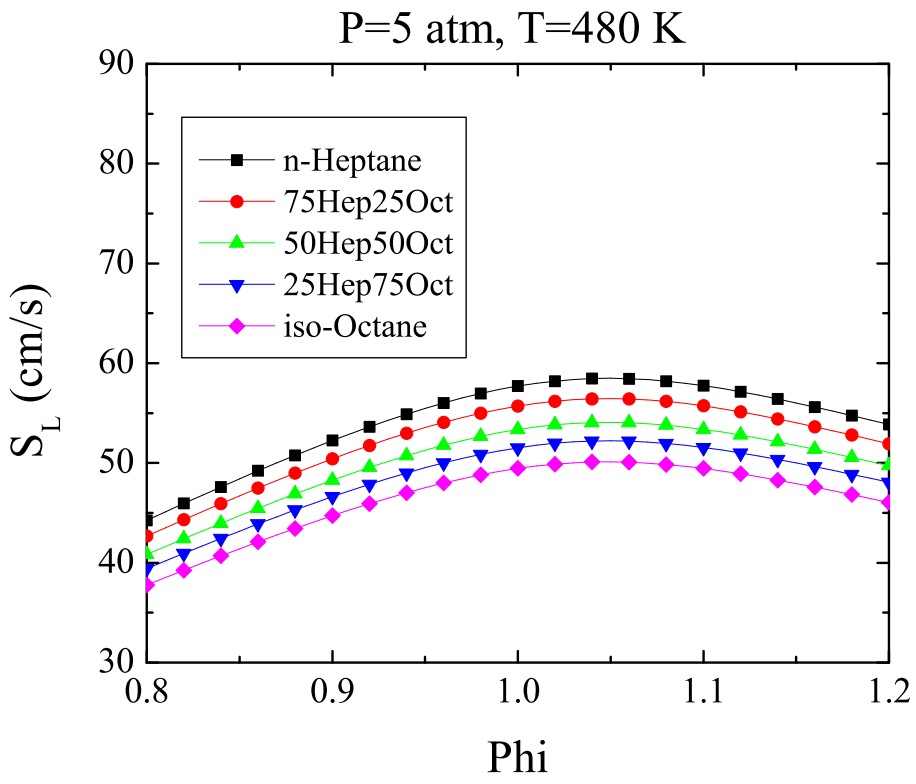

Figure 5.15: Laminar flame speeds of *iso*-octane, *n*-heptane and blends at 5 atm and 480 K.

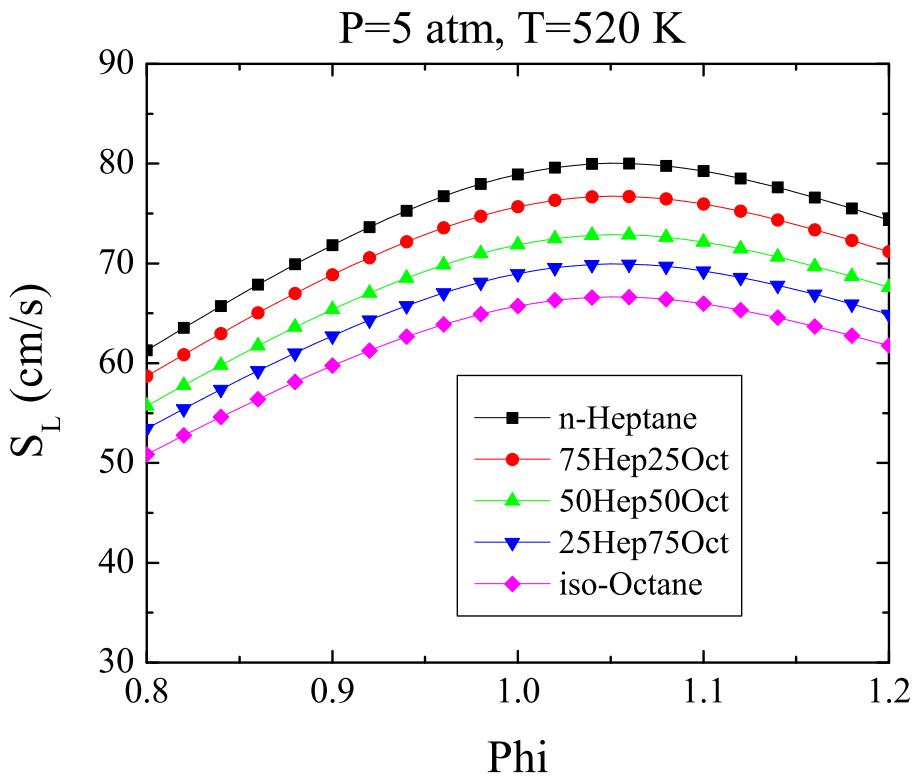

Figure 5.16: Laminar flame speeds of *iso*-octane, *n*-heptane and blends at 5 atm and 520 K.

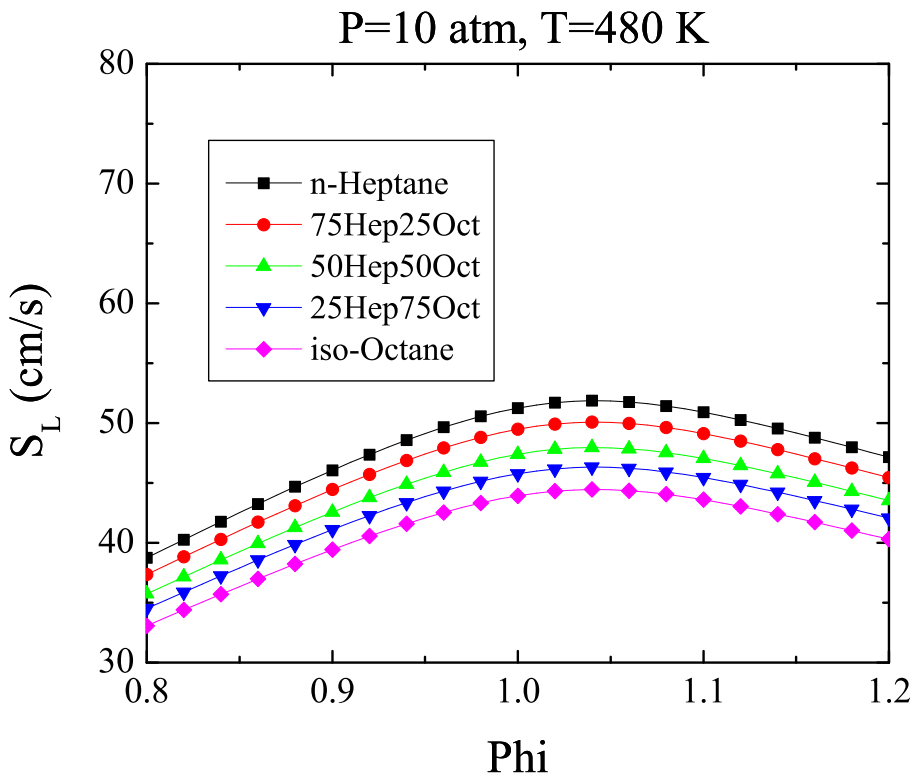

Figure 5.17: Laminar flame speeds of *iso*-octane, *n*-heptane and blends at 10 atm and 480 K.

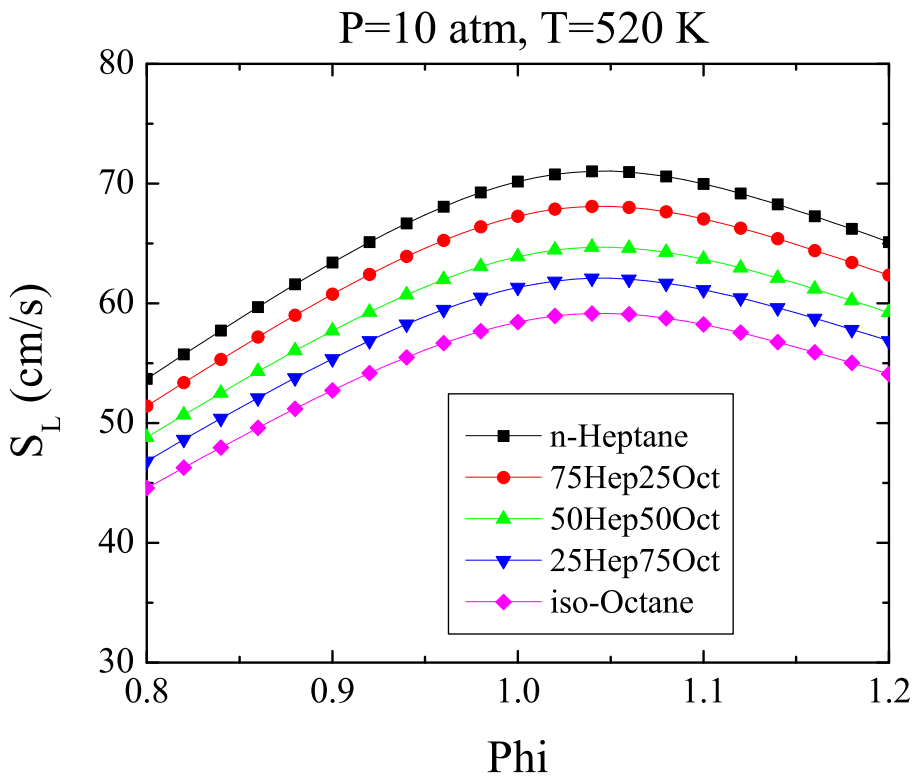

Figure 5.18: Laminar flame speeds of *iso*-octane, *n*-heptane and blends at 10 atm and 520 K.

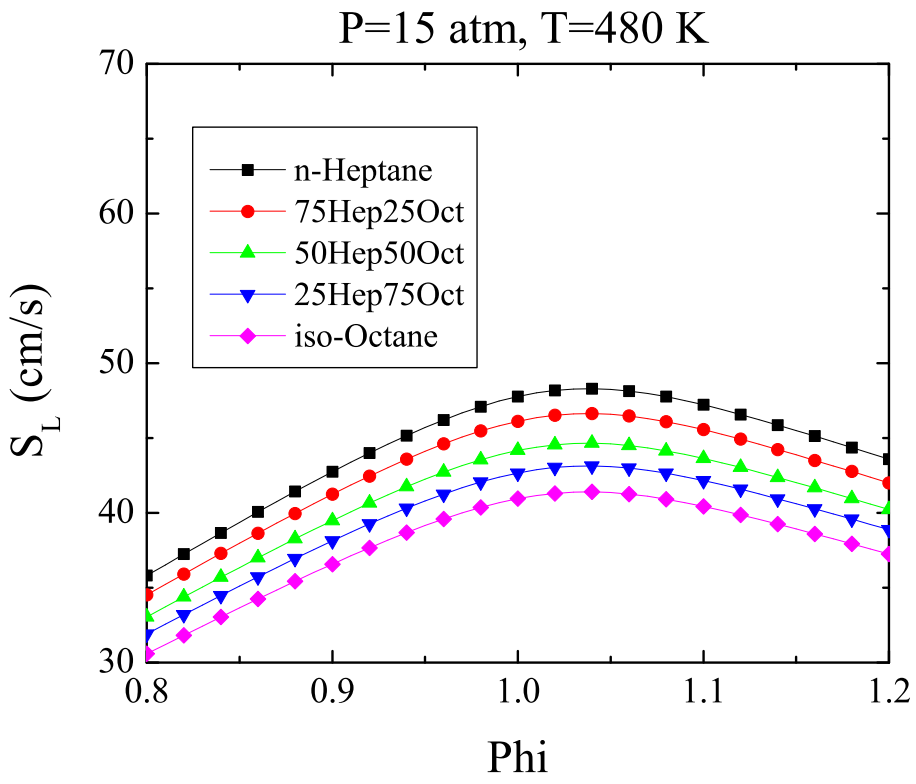

Figure 5.19: Laminar flame speeds of *iso*-octane, *n*-heptane and blends at 15 atm and 480 K.

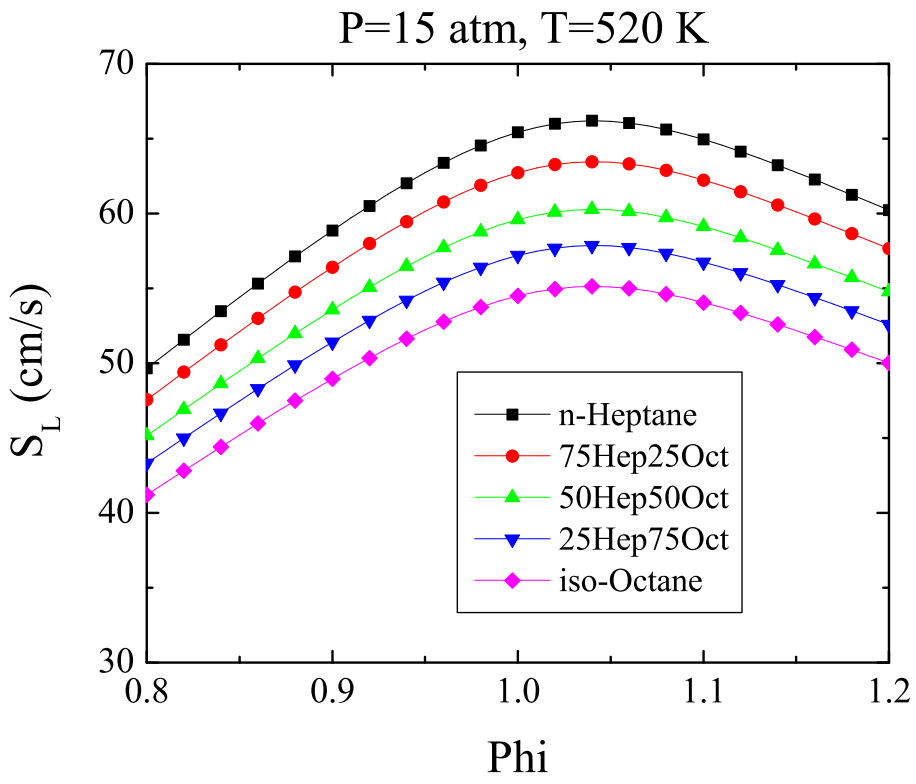

Figure 5.20: Laminar flame speeds of *iso*-octane, *n*-heptane and blends at 15 atm and 520 K.

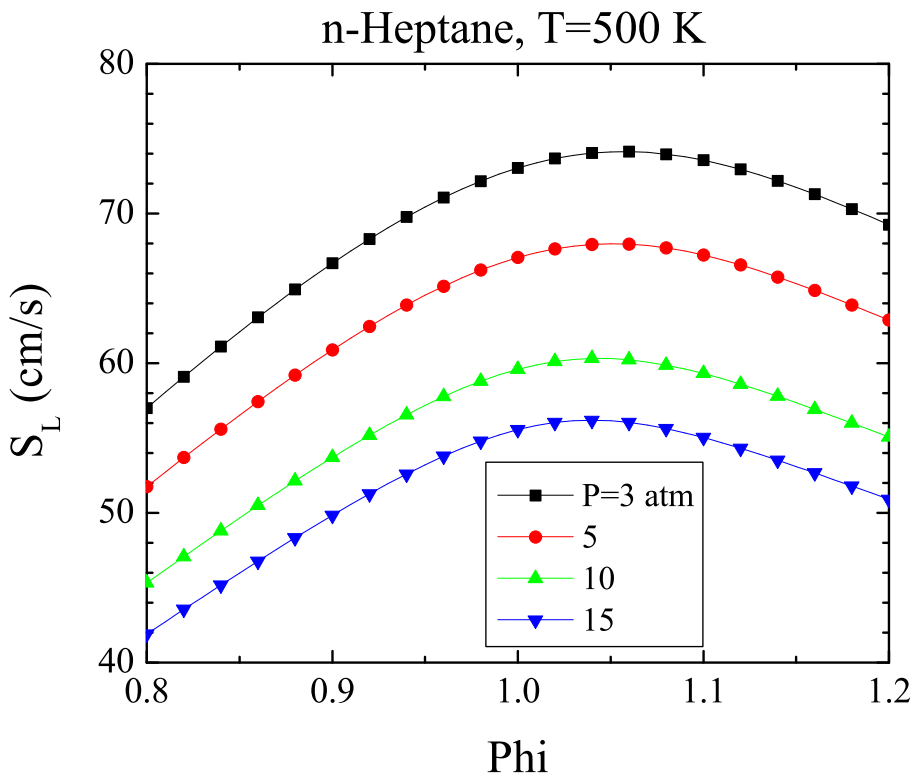

Figure 5.21: Laminar flame speeds of *n*-heptane at 500 K and various pressures.

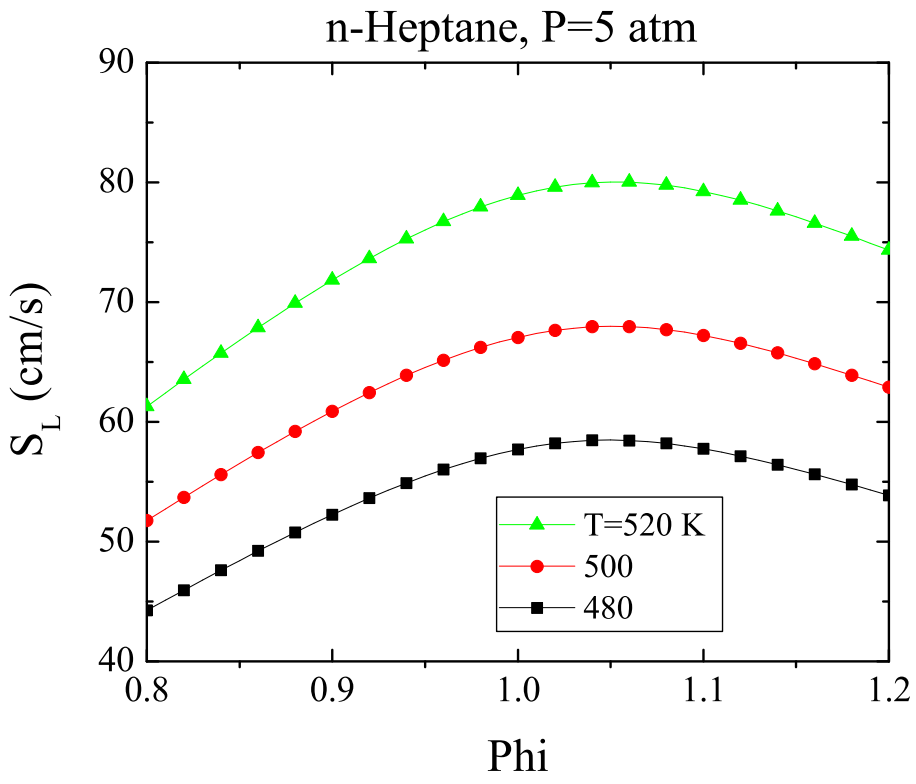

Figure 5.22: Laminar flame speeds of n-heptane at 5 atm and various unburned air-fuel mixture temperatures.

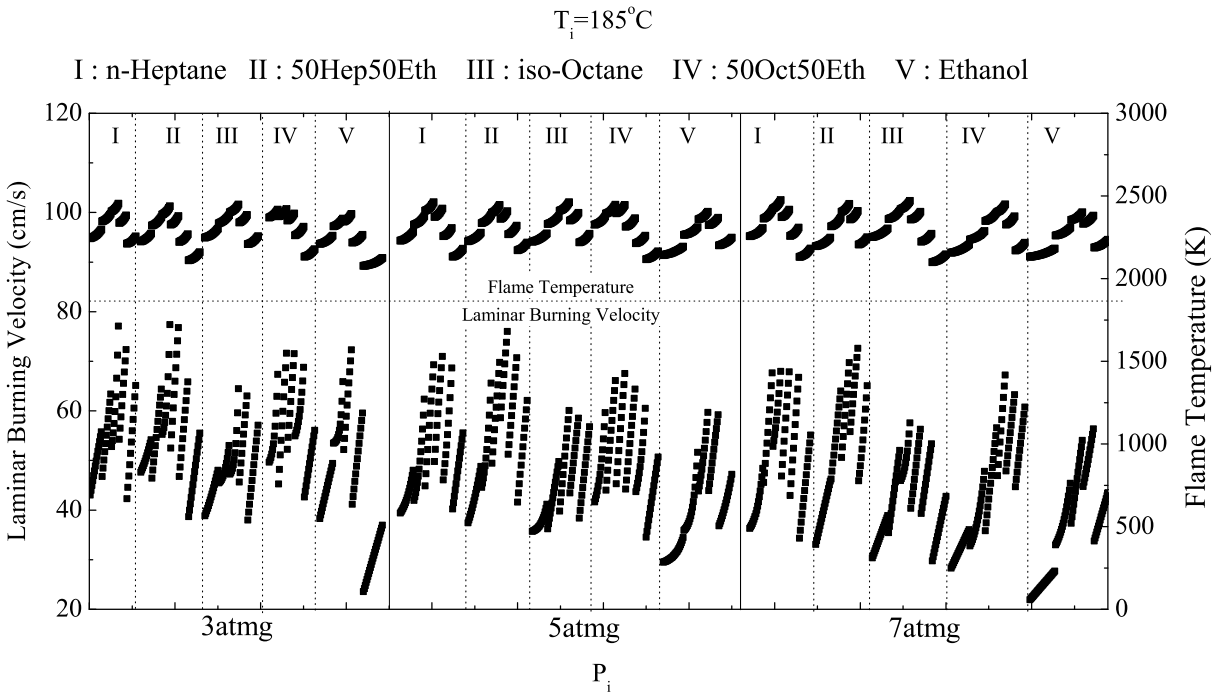

Figure 5.23: Laminar burning velocity and flame temperature of *iso*-octane, *n*-heptane, ethanol and blends (Ti=185 °C, Pi=3,5,7 atmg).

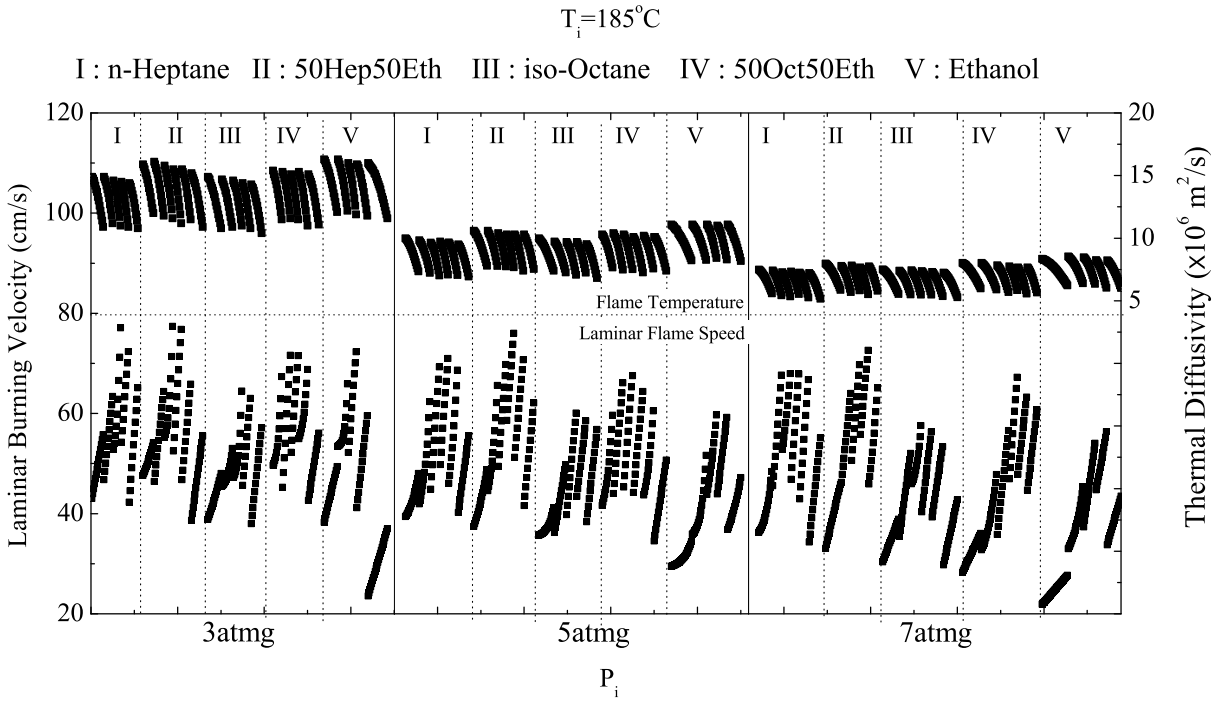

Figure 5.24: Laminar burning velocity and thermal diffusivity of *iso*-octane, *n*-heptane, ethanol and blends (Ti=185 °C, Pi=3,5,7 atmg).

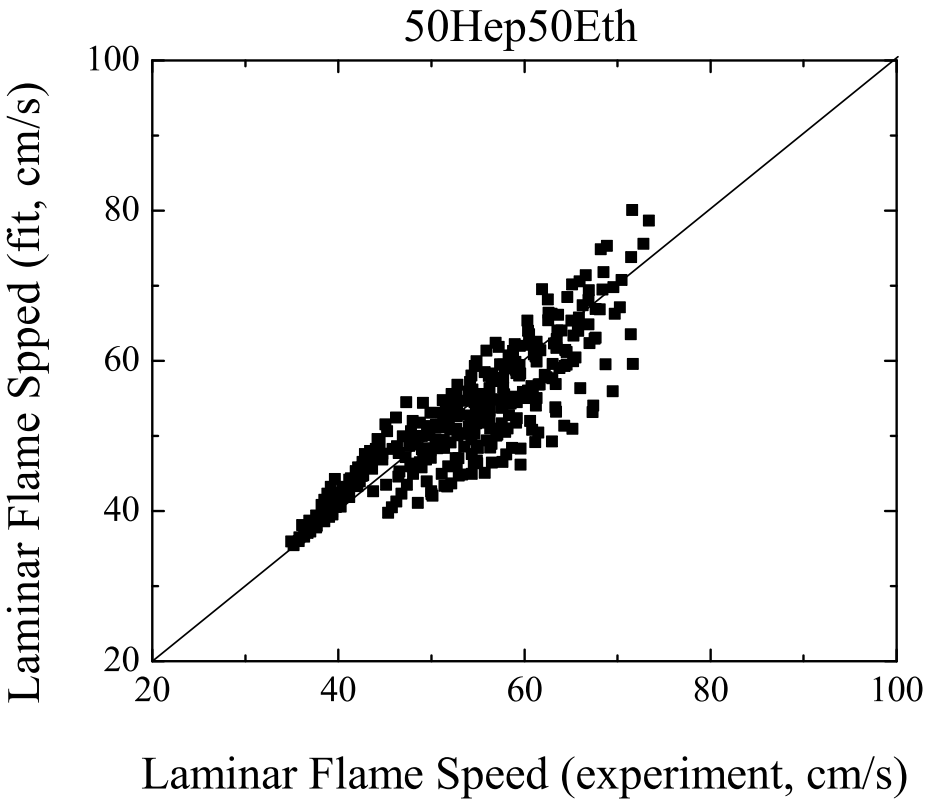

Figure 5.25: Fitting result of 50 n-heptane and 50 ethanol blend.

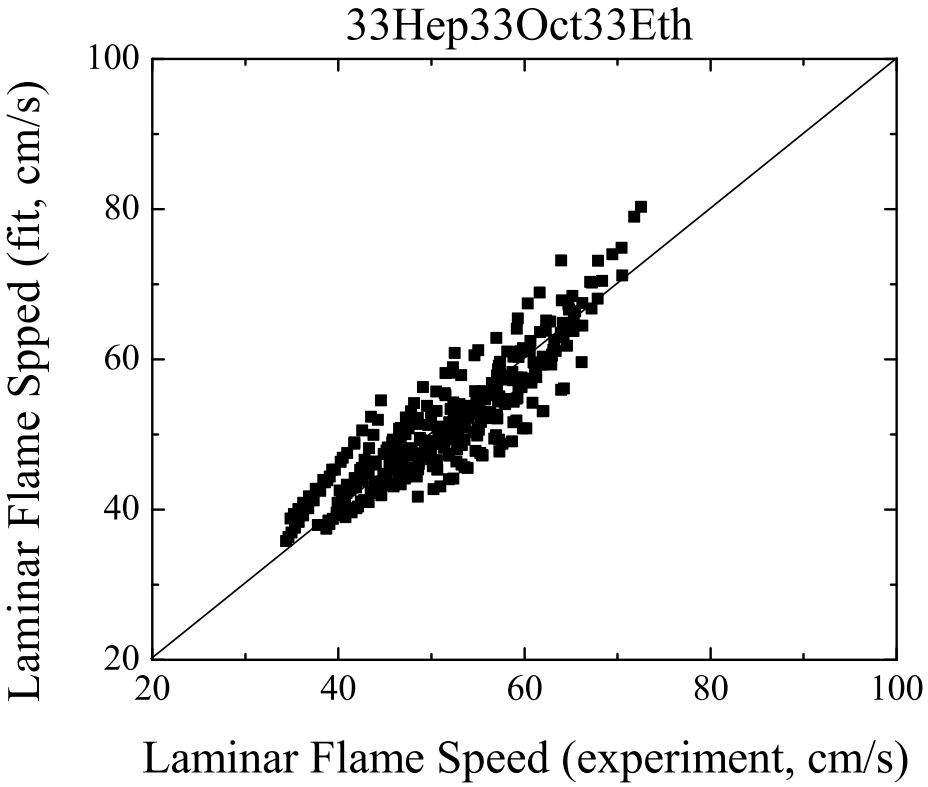

Figure 5.26: Fitting result of 33 *n*-heptane, 33 *iso*-octane and 33 ethanol blend.

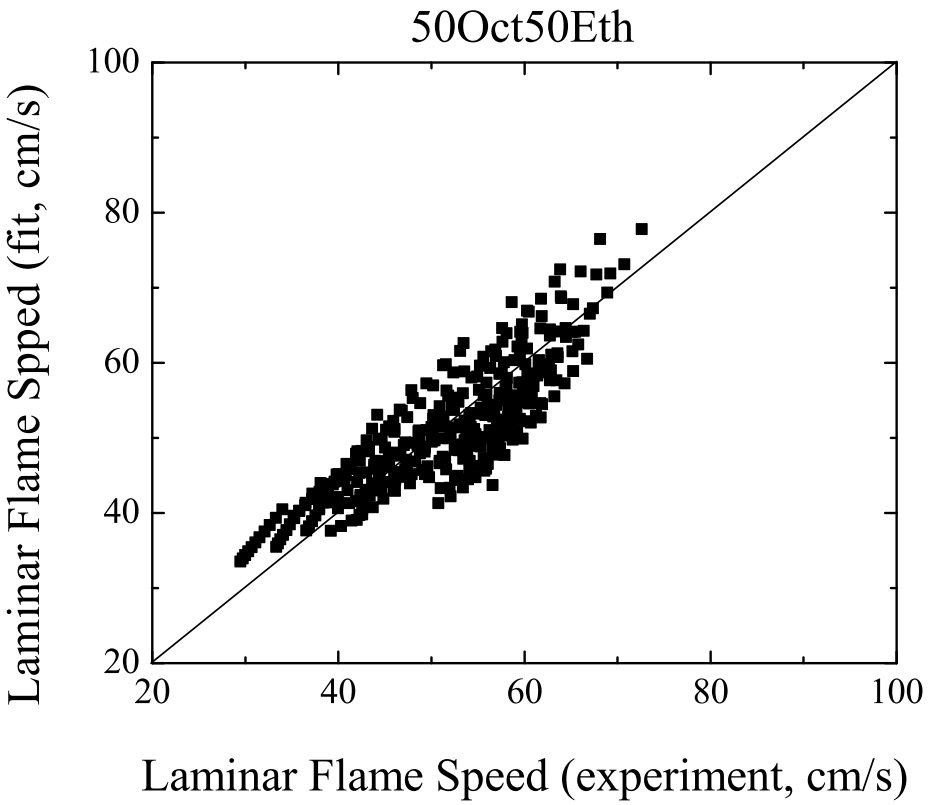

Figure 5.27: Fitting result of 50 *iso*-octane and 50 ethanol blend.

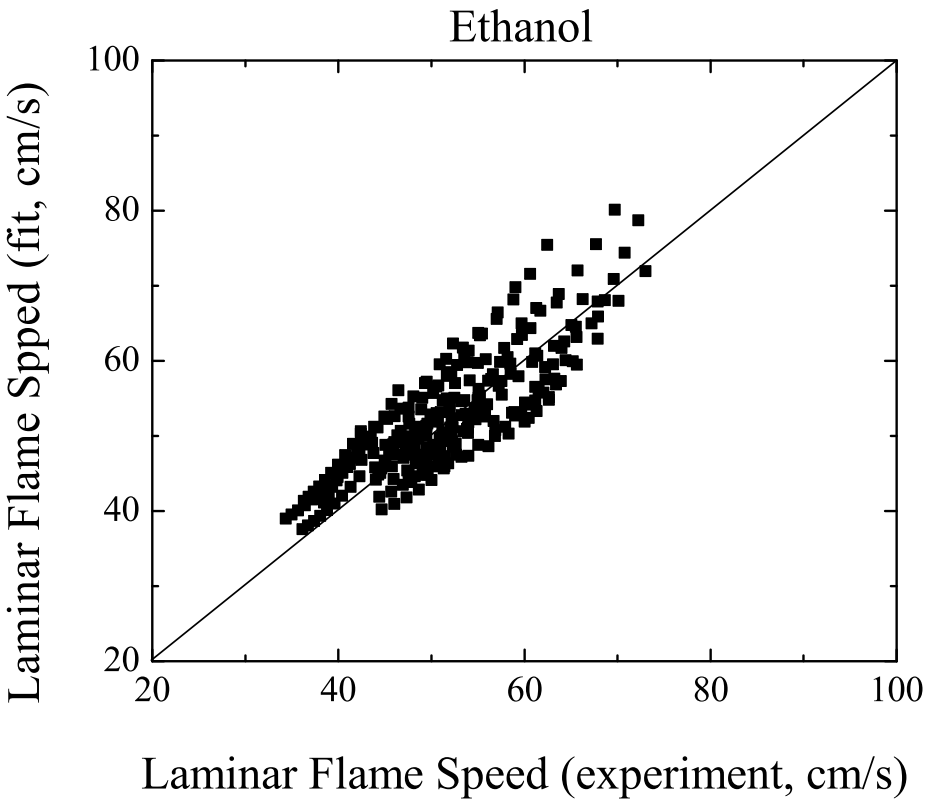

Figure 5.28: Fitting result of ethanol.

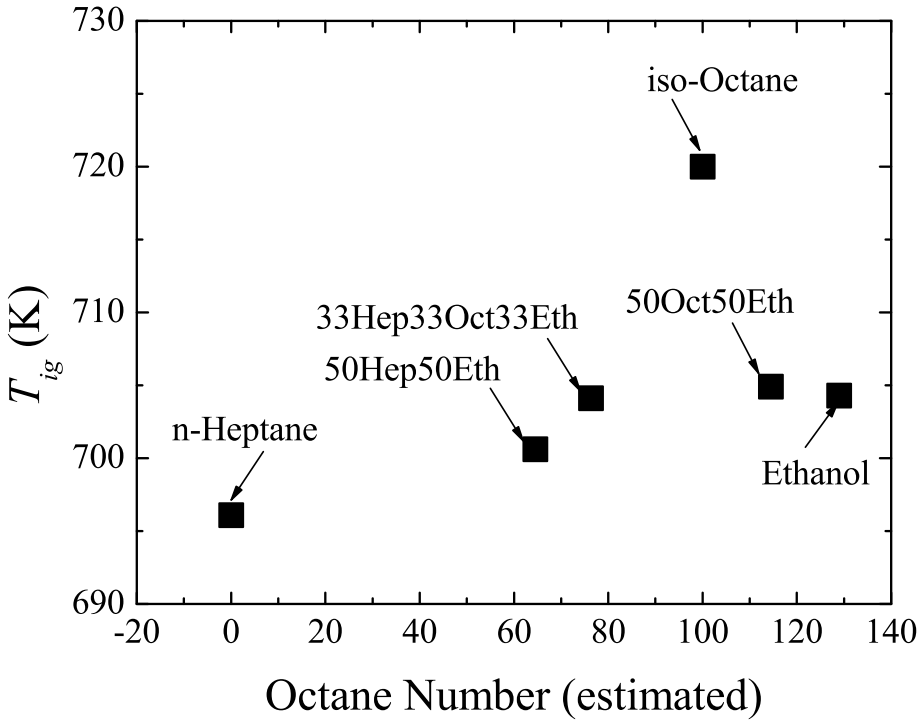

Figure 5.29: Ignition temperature versus octane number for *iso*-octane, *n*-heptane, ethanol and blends.

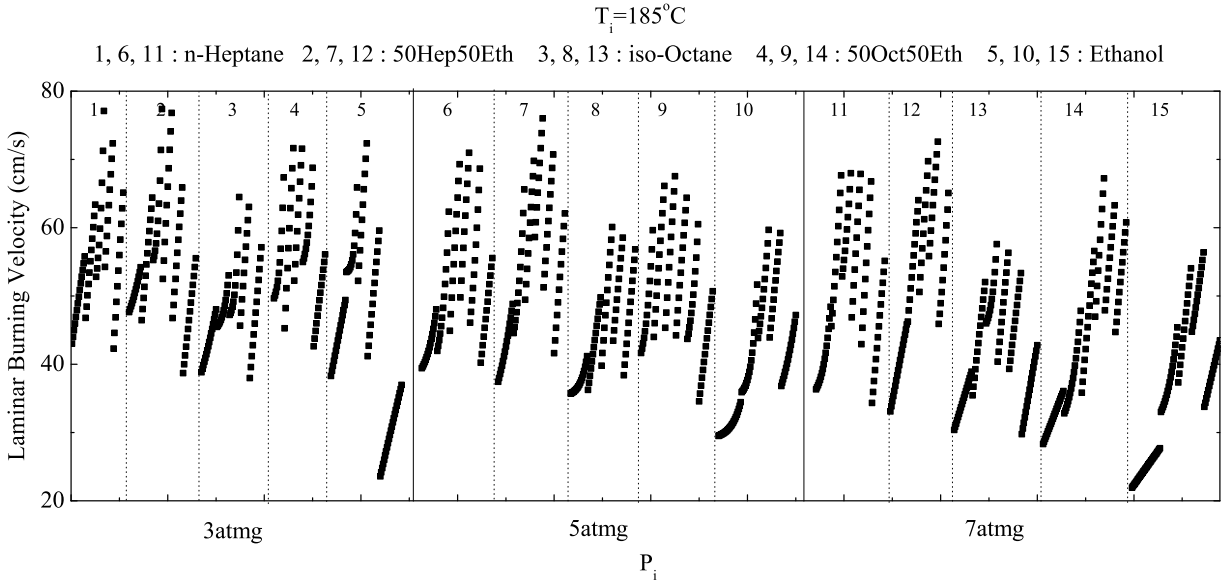

Figure 5.30: Laminar burning velocity of *iso*-octane, *n*-heptane, ethanol and binary blends (Ti=185 °C, Pi=3,5,7 atmg).

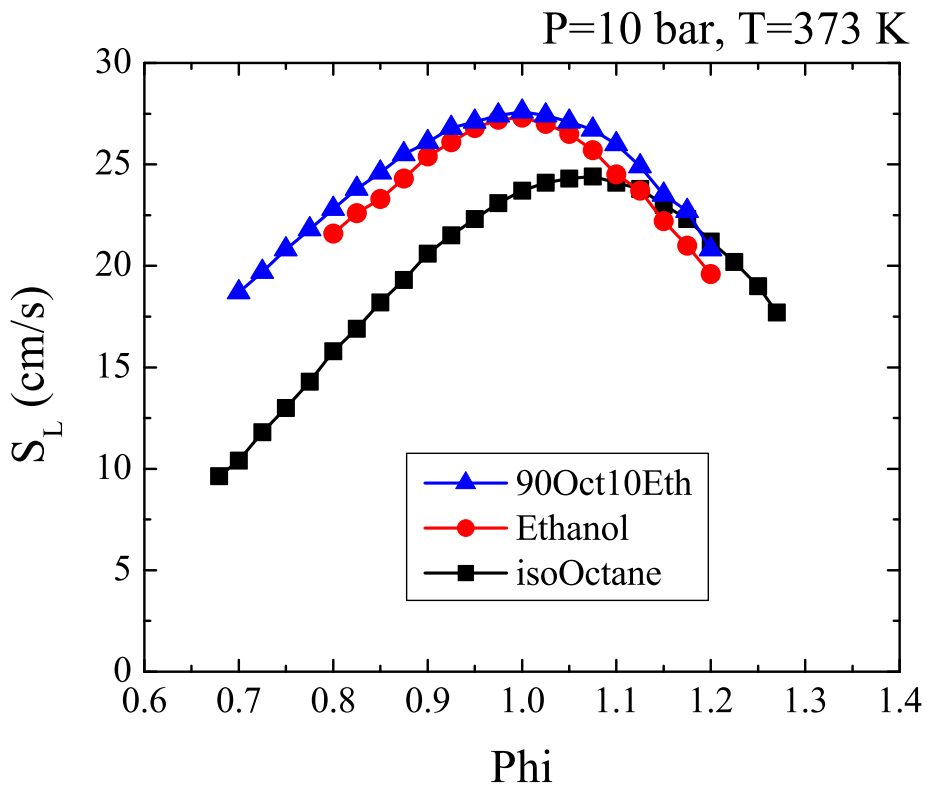

Figure 5.31: Laminar flame speeds of *iso*-octane and ethanol and blend [3].

Chapter 6

Conclusions and Recommendations

An automatically controlled experimental apparatus was built and used to measure the pressure trace data during combustion in a spherical chamber. The number of tests and accuracy was improved with this new experimental set up, compared to previous efforts. These devices are expected to be used for other fuels to measure the laminar flame speeds.

In this research, ten fuels including four pure fuels, methane, *iso*-octane, n-heptane and ethanol, and six blended fuels were tested over a wide range of equivalence ratios at the elevated temperatures and pressures. Oxygen sensor calibration was conducted for each fuel before measuring the pressure trace. Laminar burning velocities were calculated using measured pressure traces by an analysis code that had been updated to improve efficiency and accuracy. Methane was used as a fuel to verify the experimental and computational method. For each fuel, more than 2,000 data points were collected, and a large database of the laminar burning velocity was established. This database is expected to be used in the research of not only the laminar flame speed but also the effect of ignition, stretch and chamber wall interactions on the flame and cellularity generation.

From this large laminar burning velocity database, laminar flame speeds were extracted with reasonable criteria. Laminar flame speeds of *n*-heptane, *iso*-octane and their various blends were examined to derive a new laminar flame speed correlation. With this new correlation, the laminar flame speed of *n*-heptane and *iso*-octane blends with any blending ratio can be predicted within the applicable range. From this analysis, it has been proved that Mallard and Le Chatelier's conduction theory can be used in developing a new physically-based flame-speed blending model that can predict the laminar flame speed of *n*-heptane and *iso*-octane blends.

The form of the new blending model is as follows.

$$S_L = S_{L0}\alpha^{k_1}\left(\frac{T_f - T_{ig}}{T_{ig} - T_0}\right)^{k_2} k_3 e^{-\frac{E_a}{R_u T_f}} P^{k_4}$$

From the data-fit process with laminar flame speeds for each fuel, the final form of the new blending model for laminar flame speed of *n*-heptane and *iso*-octane blends was derived as

$$S_L(cm/s) = 24\alpha^{0.20008}\left(\frac{T_f - T_{ig}}{T_{ig} - T_0}\right)^{1.27777} 3.7173 e^{-\frac{16816.95963}{R_u T_f}} P^{-8.2234E-26}$$

where T_{ig} was obtained with octane number with following equation.

$$T_{ig}(K) = 695.72 + 0.24097 N_{Octane}$$

The laminar flame speeds of ethanol and blends with *n*-heptane and *iso*-octane were also extracted from the laminar burning velocity database.

The same method was used to find the blending model for these fuels. This attempt was not successful due to the non-linear behavior of ethanol in blends as shown in the following table.

Fuel	*n*-Heptane	50Hep50Eth	33Hep33Oct33Eth	*iso*-Octane	50Oct50Eth	Ethanol
T_{ig} (K)	696.09	700.60	704.12	720.00	704.90	704.31

It was shown that this non-linearity was due to the role of ethanol as an accelerator in blends.

For future work, tests with a wider range of temperature and pressure need to be conducted to have a more practical blending model of *n*-heptane and *iso*-octane fuel blends. Also, tests with more research fuels will be required to verify the feasibility of using the Mallard and Le Chatelier's conduction theory to develop a general blending model. Also more tests and analysis are required for the blends with alcohol fuel to investigate the behavior of it in fuel blends and to derive a blending model.

Appendices

Appendix A

Laminar Burning Velocity and Laminar Flame Speed of Methane

phi	P (atm)	T (K)	LBV(experments) (cm/s)	LFS(CHEMKIN) (cm/s)	% error, abs (%)
0.888	5.37	382.89	23.91	25.39	5.82
0.888	5.43	384.09	23.96	25.33	5.40
0.888	5.51	385.54	24.02	25.36	5.30
0.888	5.58	386.94	24.08	25.41	5.24
0.888	5.67	388.65	24.15	25.47	5.20
0.888	5.76	390.31	24.22	25.45	4.82
0.888	5.87	392.30	24.31	25.52	4.75
0.888	5.98	394.44	24.40	25.47	4.20
0.888	6.12	396.83	24.51	25.54	4.05
0.888	6.26	399.30	24.62	25.60	3.82
0.888	6.40	401.83	24.75	25.60	3.31
0.888	6.57	404.59	24.90	25.57	2.63
0.888	6.75	407.68	25.06	25.57	2.00
0.888	6.94	410.77	25.24	25.64	1.57
0.888	7.15	414.14	25.44	25.69	0.99
0.888	7.38	417.67	25.66	25.71	0.20
0.888	7.62	421.35	25.91	25.81	0.37
0.888	7.88	425.23	26.18	25.85	1.28
0.888	8.15	429.17	26.49	26.03	1.75
0.888	8.46	433.47	26.83	26.21	2.35
0.888	8.79	437.96	27.20	26.27	3.56
0.888	9.14	442.71	27.63	26.38	4.72
0.888	9.53	447.75	28.10	26.48	6.10
0.888	9.95	452.91	28.62	26.49	8.03
0.888	10.40	458.45	29.20	26.63	9.64
0.888	10.90	464.24	29.85	26.49	11.49
0.888	11.44	470.30	30.56	26.49	13.66
0.888	12.02	476.55	31.37	26.49	15.91

phi	P (atm)	T (K)	LBV(experments) (cm/s)	LFS(CHEMKIN) (cm/s)	error, abs (%)
0.948	5.47	382.69	26.85	27.86	3.61
0.948	5.52	383.78	26.91	27.86	3.43
0.948	5.61	385.48	26.96	27.88	3.29
0.948	5.71	387.26	27.03	27.88	3.05
0.948	5.81	389.10	27.11	27.92	2.91
0.948	5.94	391.40	27.19	27.87	2.42
0.948	6.06	393.70	27.29	27.90	2.17
0.948	6.22	396.40	27.41	27.92	1.83
0.948	6.38	399.14	27.54	27.92	1.36
0.948	6.55	402.14	27.69	27.98	1.04
0.948	6.76	405.54	27.86	27.99	0.47
0.948	6.97	408.97	28.05	28.00	0.19
0.948	7.21	412.75	28.28	28.09	0.66
0.948	7.46	416.67	28.53	28.13	1.42
0.948	7.74	420.81	28.82	28.17	2.31
0.948	8.05	425.31	29.15	28.25	3.19
0.948	8.38	429.99	29.53	28.33	4.24
0.948	8.74	434.90	29.96	28.41	5.47
0.948	9.13	440.06	30.46	28.38	7.32
0.948	9.56	445.54	31.02	28.71	8.06
0.948	10.03	451.38	31.67	28.90	9.58
0.948	10.56	457.69	32.41	28.89	12.18
0.948	11.15	464.36	33.25	29.02	14.58
0.948	11.79	471.44	34.22	29.21	17.13
0.948	12.50	478.79	35.32	29.46	19.88

phi	P (atm)	T (K)	LBV(experments) (cm/s)	LFS(CHEMKIN) (cm/s)	error, abs (%)
1.025	5.38	382.94	26.56	29.99	11.43
1.025	5.46	384.46	26.73	30.02	10.96
1.025	5.54	386.00	26.90	30.01	10.37
1.025	5.64	388.01	27.06	30.11	10.11
1.025	5.75	389.95	27.23	30.08	9.47
1.025	5.88	392.37	27.40	30.09	8.94
1.025	6.02	394.94	27.57	30.04	8.23
1.025	6.17	397.59	27.74	30.03	7.64
1.025	6.35	400.75	27.90	30.10	7.30
1.025	6.54	403.88	28.07	30.13	6.84
1.025	6.75	407.47	28.24	30.13	6.28
1.025	6.98	411.22	28.41	30.24	6.07
1.025	7.24	415.26	28.57	30.26	5.58
1.025	7.51	419.37	28.74	30.25	4.99
1.025	7.81	423.90	28.91	30.26	4.47
1.025	8.13	428.49	29.08	30.37	4.26
1.025	8.47	433.30	29.24	30.44	3.93
1.025	8.85	438.47	29.41	30.49	3.54
1.025	9.27	443.88	29.58	30.59	3.31
1.025	9.71	449.50	29.75	31.05	4.20
1.025	10.19	455.32	29.91	31.18	4.06
1.025	10.71	461.54	30.08	31.33	3.99
1.025	11.27	467.87	30.25	31.47	3.88
1.025	11.89	474.52	30.42	31.66	3.93
1.025	12.54	481.36	30.58	31.73	3.62

phi	P (atm)	T (K)	LBV(experments) (cm/s)	LFS(CHEMKIN) (cm/s)	error, abs (%)
1.123	5.43	383.02	26.66	28.74	7.24
1.123	5.50	384.42	26.91	28.81	6.60
1.123	5.59	386.02	27.15	28.72	5.48
1.123	5.69	387.92	27.37	28.74	4.76
1.123	5.80	389.89	27.58	28.76	4.09
1.123	5.92	392.18	27.79	28.79	3.48
1.123	6.07	394.75	27.98	28.57	2.05
1.123	6.22	397.47	28.17	28.80	2.19
1.123	6.41	400.64	28.34	28.76	1.45
1.123	6.60	403.98	28.51	28.76	0.86
1.123	6.82	407.49	28.67	28.78	0.38
1.123	7.05	411.17	28.82	28.84	0.06
1.123	7.30	415.13	28.97	28.84	0.44
1.123	7.57	419.27	29.10	28.82	0.99
1.123	7.88	423.72	29.24	28.86	1.30
1.123	8.20	428.32	29.36	28.93	1.48
1.123	8.56	433.27	29.48	28.95	1.82
1.123	8.93	438.31	29.59	29.01	2.00
1.123	9.35	443.73	29.70	29.36	1.15
1.123	9.79	449.25	29.80	29.55	0.85
1.123	10.27	455.01	29.90	29.62	0.94
1.123	10.78	460.92	29.99	29.13	2.95
1.123	11.32	467.04	30.08	29.85	0.76
1.123	11.92	473.47	30.16	29.84	1.08
1.123	12.55	479.92	30.24	29.65	2.00

phi	P (atm)	T (K)	LBV(experments) (cm/s)	LFS(CHEMKIN) (cm/s)	error, abs (%)
1.206	5.43	382.88	21.42	22.91	6.49
1.206	5.48	383.98	21.48	22.94	6.37
1.206	5.55	385.27	21.53	22.92	6.05
1.206	5.61	386.39	21.59	22.93	5.84
1.206	5.69	387.87	21.65	22.96	5.72
1.206	5.77	389.37	21.70	22.92	5.31
1.206	5.87	391.09	21.76	22.89	4.94
1.206	5.98	393.20	21.81	22.93	4.87
1.206	6.10	395.30	21.87	22.91	4.54
1.206	6.21	397.25	21.93	22.90	4.25
1.206	6.35	399.62	21.98	22.88	3.92
1.206	6.49	401.94	22.04	22.86	3.60
1.206	6.65	404.64	22.09	22.86	3.35
1.206	6.81	407.20	22.15	23.22	4.61
1.206	6.98	409.95	22.21	23.22	4.37
1.206	7.16	412.81	22.26	23.19	4.00
1.206	7.36	415.86	22.32	23.22	3.88
1.206	7.57	419.12	22.37	23.29	3.93
1.206	7.79	422.36	22.43	23.21	3.36
1.206	8.04	425.89	22.49	23.28	3.41
1.206	8.28	429.29	22.54	23.37	3.54
1.206	8.55	432.95	22.60	23.42	3.51
1.206	8.84	436.82	22.65	23.51	3.64
1.206	9.13	440.63	22.71	23.58	3.69
1.206	9.45	444.72	22.77	23.54	3.29
1.206	9.78	448.84	22.82	23.66	3.54
1.206	10.14	453.23	22.88	23.77	3.75
1.206	10.52	457.65	22.93	23.93	4.16
1.206	10.91	462.16	22.99	24.04	4.37
1.206	11.34	466.87	23.05	24.31	5.20
1.206	11.79	471.75	23.10	24.47	5.59
1.206	12.24	476.43	23.16	24.61	5.90
1.206	12.73	481.43	23.21	24.80	6.40

Appendix B

Laminar Flame Speed from Experiments and Fitting with New Correlation for *iso*-Octane

phi	P (atm)	T (K)	LFS(experments) (cm/s)	LFS(fit) (cm/s)	% error, abs (%)
0.94	9.23	488.58	42.13	44.19	4.88
0.94	9.49	492.05	43.50	45.03	3.52
0.94	9.80	495.85	44.87	46.00	2.51
0.94	10.16	500.30	46.24	47.18	2.03
0.94	10.60	505.53	47.61	48.64	2.15
0.94	11.14	511.71	48.98	50.47	3.04
0.94	11.76	518.50	50.35	52.63	4.53
0.94	12.49	526.20	51.72	55.29	6.91
1.05	9.40	491.78	49.11	48.24	1.76
1.05	9.79	496.64	50.61	49.56	2.08
1.05	10.26	502.35	52.10	51.19	1.75
1.05	10.82	508.79	53.60	53.14	0.85
1.05	11.46	515.94	55.09	55.49	0.73
1.05	12.26	524.33	56.59	58.52	3.41
1.19	9.36	490.29	48.12	43.81	8.95
1.19	9.69	494.45	49.27	44.84	8.99
1.19	10.13	499.64	50.54	46.17	8.65
1.19	10.65	505.60	51.94	47.78	8.00
1.19	11.26	512.40	53.47	49.77	6.91
1.19	11.98	519.91	55.16	52.14	5.47
0.94	11.58	490.10	42.10	42.92	1.95
0.94	11.91	493.55	43.28	43.76	1.10
0.94	12.33	497.74	44.47	44.80	0.75
0.94	12.84	502.70	45.66	46.09	0.95
0.94	13.43	508.32	46.85	47.65	1.71
0.94	14.12	514.53	48.03	49.48	3.02
0.94	14.91	521.38	49.22	51.65	4.94
1.06	11.46	491.03	47.68	46.28	2.93
1.06	11.87	495.20	48.54	47.37	2.41
1.06	12.37	500.27	49.52	48.74	1.58
1.06	13.00	506.24	50.63	50.45	0.36
1.06	13.73	512.98	51.89	52.52	1.21
1.06	14.59	520.51	53.31	55.01	3.19
0.84	2.62	474.72	46.34	43.97	5.11
0.84	2.70	478.36	46.78	44.79	4.26
0.84	2.79	482.41	47.32	45.79	3.23
0.84	2.89	486.70	47.98	46.86	2.34
0.84	3.03	492.21	48.78	48.31	0.97
0.84	3.18	498.44	49.77	50.07	0.61
0.84	3.37	505.55	50.97	52.22	2.44
0.92	2.48	475.36	52.91	49.69	6.09
0.92	2.57	479.87	54.32	50.85	6.40
0.92	2.70	485.64	55.73	52.43	5.92
0.92	2.86	492.56	57.14	54.45	4.71
0.92	3.04	500.16	58.55	56.86	2.89
0.92	3.26	508.57	59.95	59.73	0.36
1.03	2.59	476.26	55.57	53.98	2.87
1.03	2.71	481.52	57.00	55.48	2.67
1.03	2.87	488.09	58.68	57.43	2.12
1.03	3.06	495.80	60.65	59.94	1.17
1.03	3.28	504.42	62.94	62.97	0.04
1.10	2.39	474.27	53.70	53.82	0.23
1.10	2.50	479.48	55.20	55.27	0.12

1.10	2.63	485.08	56.79	56.92	0.24
1.10	2.78	491.92	58.46	59.03	0.98
1.10	2.98	500.04	60.21	61.80	2.63
1.10	3.21	509.29	62.06	65.22	5.10
0.86	4.65	475.40	40.92	40.82	0.25
0.86	4.78	478.72	41.48	41.54	0.15
0.86	4.93	482.45	42.05	42.40	0.83
0.86	5.10	486.54	42.64	43.32	1.59
0.86	5.30	491.25	43.25	44.52	2.93
0.86	5.54	496.55	43.88	45.81	4.40
0.86	5.80	502.20	44.52	47.35	6.36
0.86	6.10	508.57	45.18	49.22	8.95
0.93	4.65	473.44	46.16	44.66	3.24
0.93	4.81	477.42	46.48	45.56	1.97
0.93	4.98	481.54	46.87	46.60	0.58
0.93	5.21	486.90	47.34	47.90	1.19
0.93	5.47	492.73	47.90	49.50	3.33
0.93	5.75	498.83	48.59	51.19	5.35
0.93	6.11	506.21	49.41	53.44	8.16
1.04	4.69	474.83	48.44	48.51	0.15
1.04	4.88	479.51	49.17	49.70	1.08
1.04	5.11	484.87	50.18	51.07	1.78
1.04	5.39	491.25	51.55	52.86	2.53
1.04	5.71	498.20	53.44	54.95	2.82
1.04	6.12	506.46	56.04	57.69	2.95
1.19	4.69	474.17	49.51	44.81	9.49
1.19	4.88	478.77	51.44	45.89	10.79
1.19	5.12	484.21	53.38	47.26	11.47
1.19	5.42	490.80	55.31	48.98	11.44
1.19	5.78	498.39	57.24	51.06	10.79
1.19	6.19	506.74	59.17	53.57	9.46
0.84	6.83	473.50	36.09	36.18	0.25
0.84	6.99	476.13	36.22	36.69	1.29
0.84	7.16	479.13	36.38	37.27	2.45
0.84	7.36	482.42	36.56	37.93	3.75
0.84	7.59	486.08	36.77	38.70	5.24
0.84	7.84	490.01	37.02	39.55	6.82
0.84	8.12	494.28	37.31	40.51	8.57
0.84	8.42	498.81	37.64	41.57	10.45
0.84	8.75	503.62	38.03	42.77	12.45
0.84	9.12	508.78	38.49	44.12	14.63
0.92	6.97	473.63	39.37	40.99	4.10
0.92	7.18	477.04	40.42	41.71	3.19
0.92	7.42	480.97	41.46	42.57	2.69
0.92	7.70	485.39	42.50	43.59	2.57
0.92	8.00	490.05	43.54	44.71	2.68
0.92	8.36	495.38	44.58	46.05	3.30
0.92	8.78	501.32	45.63	47.65	4.42
0.92	9.23	507.61	46.67	49.44	5.94
1.02	7.09	475.86	45.34	45.35	0.03
1.02	7.35	480.09	47.18	46.36	1.75
1.02	7.67	485.06	49.03	47.57	2.97
1.02	8.05	490.94	50.87	49.11	3.47
1.02	8.54	497.94	52.72	51.06	3.15
1.02	9.12	506.00	54.56	53.48	1.99
1.17	6.86	472.66	46.47	41.74	10.18
1.17	7.11	476.66	47.98	42.60	11.21
1.17	7.40	481.31	49.49	43.64	11.83
1.17	7.75	486.71	51.00	44.91	11.94
1.17	8.19	493.10	52.51	46.50	11.45
1.17	8.71	500.44	54.02	48.46	10.29
1.17	9.30	508.39	55.53	50.77	8.58
0.85	9.23	475.73	32.75	35.82	9.38
0.85	9.45	478.47	33.23	36.35	9.39
0.85	9.69	481.59	33.70	36.95	9.64
0.85	9.96	484.79	34.17	37.59	10.02
0.85	10.24	488.21	34.65	38.31	10.56
0.85	10.57	492.02	35.12	39.13	11.41
0.85	10.92	496.04	35.59	40.03	12.46
0.85	11.32	500.54	36.07	41.08	13.89
0.85	11.77	505.33	36.54	42.26	15.65
0.85	12.26	510.49	37.01	43.60	17.81
0.94	9.38	476.17	40.56	40.69	0.32
0.94	9.67	479.75	41.83	41.45	0.90
0.94	9.98	483.58	43.11	42.30	1.88
0.94	10.36	488.04	44.38	43.32	2.38

0.94	10.82	493.30	45.65	44.59	2.32
0.94	11.37	499.29	46.93	46.12	1.73
0.94	12.03	506.22	48.20	48.02	0.37
1.04	9.23	475.61	47.29	43.40	8.22
1.04	9.58	479.93	47.91	44.37	7.39
1.04	10.00	485.00	48.65	45.57	6.32
1.04	10.50	490.76	49.55	47.01	5.13
1.04	11.08	497.26	50.62	48.73	3.74
1.04	11.76	504.49	51.92	50.79	2.18
1.04	12.58	512.72	53.48	53.33	0.28
1.17	9.19	474.44	44.73	40.12	10.30
1.17	9.51	478.36	46.18	40.94	11.34
1.17	9.89	482.91	47.63	41.92	11.99
1.17	10.36	488.39	49.08	43.17	12.04
1.17	10.91	494.40	50.53	44.62	11.70
1.17	11.57	501.35	51.98	46.41	10.72
1.17	12.35	509.24	53.43	48.60	9.04
0.85	11.46	475.22	31.01	33.86	9.17
0.85	11.69	477.57	31.20	34.28	9.86
0.85	11.95	480.25	31.42	34.77	10.65
0.85	12.24	483.11	31.67	35.29	11.44
0.85	12.57	486.28	31.96	35.91	12.35
0.85	12.91	489.60	32.29	36.57	13.27
0.85	13.32	493.36	32.67	37.35	14.33
0.85	13.76	497.35	33.11	38.22	15.43
0.85	14.23	501.56	33.60	39.16	16.54
0.85	14.75	506.04	34.17	40.22	17.69
0.85	15.32	510.80	34.83	41.40	18.86
0.94	11.44	474.27	38.97	38.77	0.51
0.94	11.75	477.35	40.03	39.39	1.59
0.94	12.11	480.94	41.10	40.14	2.33
0.94	12.54	485.16	42.17	41.05	2.66
0.94	13.06	490.04	43.23	42.15	2.50
0.94	13.68	495.62	44.30	43.47	1.88
0.94	14.37	501.67	45.36	44.99	0.81
0.94	15.16	508.23	46.43	46.75	0.70
1.05	11.40	474.27	44.45	41.45	6.75
1.05	11.77	477.97	45.51	42.23	7.22
1.05	12.21	482.35	46.58	43.21	7.24
1.05	12.76	487.49	47.64	44.40	6.79
1.05	13.40	493.34	48.70	45.83	5.89
1.05	14.17	500.04	49.77	47.59	4.39
1.05	15.05	507.39	50.83	49.66	2.31
1.19	11.73	476.27	44.80	38.22	14.69
1.19	12.17	480.50	46.12	39.07	15.29
1.19	12.69	485.31	47.44	40.07	15.53
1.19	13.31	490.87	48.75	41.30	15.29
1.19	14.01	496.97	50.07	42.72	14.68
1.19	14.86	503.95	51.39	44.45	13.50
1.19	15.86	511.79	52.71	46.59	11.62
0.85	2.35	456.58	45.95	40.38	12.11
0.85	2.42	460.18	46.42	41.11	11.44
0.85	2.52	464.70	46.97	42.02	10.54
0.85	2.63	469.80	47.59	43.11	9.42
0.85	2.77	475.89	48.31	44.52	7.85
0.85	2.91	481.85	49.14	45.92	6.55
0.85	3.08	488.57	50.08	47.63	4.89
0.94	2.33	456.78	49.44	45.88	7.20
0.94	2.44	461.89	51.18	47.00	8.17
0.94	2.57	467.71	52.92	48.36	8.61
0.94	2.72	474.35	54.66	50.04	8.46
0.94	2.90	481.91	56.41	52.02	7.79
0.94	3.11	490.18	58.15	54.42	6.41
1.06	2.35	456.96	51.66	48.65	5.83
1.06	2.46	461.80	53.31	49.79	6.60
1.06	2.59	467.75	54.95	51.27	6.70
1.06	2.75	474.59	56.60	53.05	6.27
1.06	2.95	482.83	58.24	55.37	4.93
1.06	3.19	492.26	59.88	58.25	2.73
1.20	2.33	454.61	43.75	44.53	1.79
1.20	2.42	458.70	46.29	45.41	1.90
1.20	2.52	463.28	48.83	46.41	4.95
1.20	2.63	468.04	51.37	47.50	7.53
1.20	2.79	474.96	53.92	49.19	8.77
1.20	3.00	483.09	56.46	51.32	9.11
0.85	4.68	457.16	35.74	35.62	0.33

0.85	4.81	460.28	36.20	36.16	0.10
0.85	4.94	463.44	36.67	36.73	0.15
0.85	5.09	466.87	37.13	37.36	0.63
0.85	5.27	470.86	37.60	38.15	1.45
0.85	5.46	475.23	38.06	38.98	2.42
0.85	5.68	479.94	38.53	40.00	3.82
0.85	5.93	484.98	38.99	41.08	5.36
0.85	6.21	490.56	39.46	42.36	7.34
0.92	4.68	457.75	41.85	40.08	4.23
0.92	4.83	461.30	42.53	40.72	4.25
0.92	5.00	465.48	43.20	41.60	3.71
0.92	5.21	470.08	43.88	42.54	3.04
0.92	5.45	475.35	44.56	43.70	1.92
0.92	5.72	481.13	45.23	45.05	0.39
0.92	6.03	487.52	45.91	46.65	1.62
1.03	4.58	455.76	45.02	43.04	4.40
1.03	4.73	459.44	46.13	43.82	5.01
1.03	4.92	463.86	47.25	44.75	5.30
1.03	5.14	469.06	48.37	45.91	5.08
1.03	5.41	474.91	49.49	47.24	4.54
1.03	5.72	481.52	50.61	48.86	3.47
1.03	6.10	488.96	51.72	50.83	1.72
1.17	4.60	455.79	44.49	40.49	8.99
1.17	4.78	460.05	46.53	41.30	11.23
1.17	5.00	465.21	48.57	42.30	12.92
1.17	5.29	471.47	50.61	43.69	13.68
1.17	5.61	478.22	52.65	45.21	14.12
1.17	5.99	485.78	54.69	46.98	14.09
0.83	6.83	457.84	29.79	32.13	7.86
0.83	6.97	460.19	30.11	32.50	7.95
0.83	7.12	462.69	30.43	32.90	8.13
0.83	7.30	465.56	30.74	33.38	8.60
0.83	7.50	468.80	31.06	33.94	9.26
0.83	7.71	472.02	31.38	34.50	9.94
0.83	7.94	475.50	31.70	35.13	10.84
0.83	8.18	479.14	32.02	35.82	11.85
0.83	8.45	483.06	32.33	36.58	13.15
0.83	8.76	487.34	32.65	37.44	14.68
0.83	9.08	491.78	32.97	38.39	16.44
0.91	6.87	458.43	36.98	36.97	0.02
0.91	7.05	461.46	37.30	37.52	0.60
0.91	7.27	465.07	37.67	38.19	1.39
0.91	7.52	468.97	38.08	38.94	2.26
0.91	7.81	473.30	38.53	39.81	3.31
0.91	8.14	478.19	39.03	40.82	4.59
0.91	8.50	483.48	39.60	41.97	5.99
0.91	8.91	489.08	40.23	43.27	7.55
0.91	9.37	495.21	40.92	44.76	9.38
1.01	6.76	456.41	40.26	40.24	0.04
1.01	6.96	459.74	41.04	40.89	0.37
1.01	7.20	463.59	41.98	41.64	0.80
1.01	7.49	468.03	43.09	42.56	1.22
1.01	7.81	472.89	44.42	43.60	1.84
1.01	8.21	478.79	45.99	44.94	2.29
1.01	8.71	485.80	47.86	46.63	2.57
1.01	9.31	493.69	50.09	48.68	2.82
1.18	6.86	458.72	45.17	37.94	16.00
1.18	7.12	462.89	46.49	38.71	16.73
1.18	7.44	467.75	47.82	39.64	17.10
1.18	7.81	473.32	49.14	40.76	17.04
1.18	8.25	479.61	50.46	42.09	16.58
1.18	8.80	487.04	51.79	43.79	15.45
0.91	9.19	459.12	33.60	35.23	4.84
0.91	9.41	461.86	33.98	35.69	5.04
0.91	9.69	465.17	34.42	36.27	5.37
0.91	9.99	468.76	34.94	36.93	5.70
0.91	10.32	472.57	35.55	37.64	5.89
0.91	10.71	476.89	36.26	38.50	6.17
0.91	11.12	481.38	37.11	39.41	6.20
0.91	11.59	486.40	38.10	40.48	6.25
0.91	12.13	491.82	39.26	41.69	6.20
1.02	9.13	458.56	39.06	38.84	0.55
1.02	9.42	462.07	40.47	39.51	2.38
1.02	9.78	466.38	41.89	40.34	3.71
1.02	10.21	471.37	43.31	41.35	4.53
1.02	10.73	477.09	44.73	42.56	4.84

1.02	11.31	483.35	46.15	43.97	4.71
1.02	11.99	490.24	47.57	45.63	4.08
1.16	9.07	458.62	43.17	36.54	15.37
1.16	9.40	462.59	44.30	37.24	15.94
1.16	9.79	467.18	45.49	38.08	16.29
1.16	10.25	472.37	46.74	39.08	16.39
1.16	10.78	478.15	48.05	40.24	16.25
1.16	11.41	484.69	49.42	41.65	15.73
1.16	12.16	492.13	50.87	43.35	14.77
0.93	11.55	459.72	32.58	34.54	6.01
0.93	11.82	462.36	33.08	34.98	5.73
0.93	12.12	465.33	33.63	35.49	5.55
0.93	12.48	468.71	34.25	36.08	5.36
0.93	12.88	472.38	34.93	36.77	5.27
0.93	13.34	476.49	35.69	37.55	5.20
0.93	13.86	481.00	36.54	38.44	5.21
0.93	14.43	485.88	37.47	39.45	5.30
0.93	15.11	491.42	38.51	40.66	5.59
0.93	15.88	497.48	39.67	42.06	6.02
1.03	11.70	462.66	40.57	38.25	5.72
1.03	12.12	466.65	41.55	39.00	6.14
1.03	12.60	471.13	42.53	39.88	6.24
1.03	13.17	476.25	43.51	40.93	5.93
1.03	13.83	481.99	44.49	42.15	5.26
1.03	14.58	488.25	45.47	43.58	4.16
1.03	15.45	495.12	46.45	45.25	2.59
0.94	2.65	489.17	56.14	55.61	0.95
0.94	2.77	494.44	58.14	57.22	1.58
0.94	2.92	500.83	60.13	59.35	1.30
0.94	3.11	508.38	62.13	62.05	0.12
0.94	3.32	516.59	64.13	65.22	1.70
0.94	3.58	526.15	66.13	69.36	4.88
1.07	2.61	489.08	55.09	58.85	6.83
1.07	2.73	494.37	57.49	60.61	5.43
1.07	2.88	500.84	59.88	62.84	4.95
1.07	3.07	508.58	62.28	65.73	5.55
1.07	3.31	517.69	64.67	69.47	7.42
0.85	4.63	487.67	44.09	44.13	0.09
0.85	4.75	490.76	44.65	44.89	0.55
0.85	4.90	494.53	45.20	45.82	1.38
0.85	5.08	499.06	45.76	47.02	2.76
0.85	5.28	503.76	46.31	48.33	4.37
0.85	5.51	508.97	46.86	49.88	6.44
0.85	5.77	514.91	47.42	51.77	9.18
0.85	6.07	521.46	47.97	53.95	12.47
0.93	4.76	487.49	47.05	49.17	4.50
0.93	4.92	491.50	48.24	50.23	4.13
0.93	5.12	496.32	49.43	51.61	4.40
0.93	5.34	501.48	50.62	53.17	5.03
0.93	5.62	507.69	51.81	55.12	6.39
0.93	5.93	514.44	53.00	57.42	8.33
0.93	6.31	522.35	54.19	60.38	11.43
1.05	4.61	488.22	51.78	53.20	2.75
1.05	4.80	492.81	53.83	54.57	1.37
1.05	5.01	498.13	55.89	56.25	0.65
1.05	5.28	504.54	57.95	58.29	0.59
1.05	5.62	512.07	60.01	61.02	1.68
1.05	6.03	520.80	62.07	64.42	3.78
1.20	4.75	490.19	54.56	49.59	9.12
1.20	4.98	495.52	55.51	51.05	8.04
1.20	5.24	501.64	56.67	52.86	6.73
1.20	5.56	508.73	58.11	55.15	5.10
1.20	5.94	516.88	59.87	57.95	3.20
0.93	7.12	490.75	43.71	46.46	6.29
0.93	7.36	494.76	44.29	47.50	7.26
0.93	7.65	499.50	45.03	48.80	8.38
0.93	7.96	504.33	45.97	50.19	9.19
0.93	8.32	509.89	47.16	51.88	10.01
0.93	8.75	516.20	48.66	53.92	10.81
0.93	9.26	523.31	50.57	56.41	11.54
1.03	6.97	488.85	48.44	49.77	2.74
1.03	7.23	493.26	50.36	50.98	1.24
1.03	7.57	498.68	52.29	52.55	0.51
1.03	7.96	504.83	54.21	54.44	0.42
1.03	8.45	512.16	56.13	56.86	1.31

1.03	9.05	520.70	58.05	59.94	3.26
1.20	6.87	487.31	49.79	45.33	8.96
1.20	7.13	491.61	50.67	46.40	8.43
1.20	7.43	496.52	51.70	47.69	7.75
1.20	7.79	502.11	52.91	49.24	6.94
1.20	8.24	508.88	54.36	51.22	5.77
1.20	8.77	516.38	56.06	53.62	4.36
1.20	9.39	524.76	58.08	56.54	2.65

Appendix C

Laminar Flame Speed from Experiments and Fitting with New Correlation for 75 *iso*-Octane and 25 *n*-Heptane blend

phi	P (atm)	T (K)	LFS(experments) (cm/s)	LFS(fit) (cm/s)	% error, abs (%)
0.87	2.43	486.51	52.41	52.94	1.01
0.87	2.53	491.32	53.83	54.41	1.07
0.87	2.63	496.17	55.26	55.96	1.26
0.87	2.75	501.68	56.68	57.80	1.98
0.87	2.91	508.41	58.11	60.22	3.64
0.87	3.08	515.79	59.53	63.12	6.03
0.87	3.29	524.24	60.96	66.74	9.48
0.98	2.45	487.32	58.78	59.75	1.66
0.98	2.56	492.54	60.78	61.52	1.22
0.98	2.70	498.63	62.79	63.70	1.45
0.98	2.86	505.93	64.79	66.57	2.74
0.98	3.08	515.15	66.80	70.46	5.48
1.11	2.43	485.41	58.32	60.01	2.90
1.11	2.53	490.06	59.91	61.58	2.79
1.11	2.65	495.70	61.51	63.59	3.39
1.11	2.82	502.88	63.10	66.31	5.09
1.11	3.01	510.93	64.69	69.66	7.69
1.11	3.26	520.72	66.28	74.14	11.85
0.86	4.60	486.38	45.71	46.24	1.15
0.86	4.73	489.79	46.08	47.15	2.33
0.86	4.90	494.14	46.52	48.34	3.92
0.86	5.09	498.85	47.02	49.70	5.70
0.86	5.31	503.90	47.61	51.25	7.64
0.86	5.55	509.43	48.29	52.98	9.70
0.86	5.82	515.44	49.08	55.08	12.23
0.86	6.14	522.35	50.00	57.64	15.27
0.94	4.66	486.27	48.96	51.38	4.94
0.94	4.81	490.05	50.39	52.44	4.08
0.94	5.01	495.21	51.82	54.04	4.28
0.94	5.26	501.03	53.25	55.89	4.96
0.94	5.55	507.63	54.68	58.17	6.37
0.94	5.87	514.70	56.12	60.81	8.35
0.94	6.26	522.88	57.55	64.09	11.36
1.05	4.82	489.42	54.05	55.57	2.81
1.05	5.03	494.48	55.48	57.13	2.97
1.05	5.30	500.79	57.23	59.26	3.55
1.05	5.62	507.98	59.37	61.91	4.28
1.05	6.02	516.42	62.00	65.26	5.26
1.20	4.81	487.20	54.60	50.58	7.36
1.20	5.04	492.53	56.42	52.09	7.68
1.20	5.31	498.78	58.24	54.00	7.27
1.20	5.64	505.95	60.05	56.32	6.22
1.20	6.02	513.77	61.87	59.17	4.36
1.20	6.48	522.88	63.68	62.79	1.40
0.92	6.97	486.92	45.59	46.62	2.25
0.92	7.17	490.36	45.89	47.53	3.58
0.92	7.43	494.61	46.29	48.70	5.20
0.92	7.71	499.20	46.80	50.03	6.90
0.92	8.04	504.37	47.47	51.59	8.68
0.92	8.44	510.38	48.35	53.54	10.73

1.02	7.04	489.89	50.22	51.92	3.39
1.02	7.34	494.92	52.25	53.42	2.24
1.02	7.69	500.62	54.28	55.22	1.72
1.02	8.13	507.39	56.31	57.51	2.13
1.02	8.67	515.35	58.34	60.43	3.58
1.02	9.31	524.25	60.37	64.04	6.07
1.17	7.02	489.27	53.43	48.71	8.83
1.17	7.34	494.49	55.07	50.17	8.89
1.17	7.73	500.60	56.70	51.99	8.30
1.17	8.18	507.36	58.34	54.15	7.18
1.17	8.73	515.38	59.97	56.93	5.08
1.17	9.40	524.48	61.61	60.40	1.96
0.94	9.33	489.83	44.50	46.54	4.58
0.94	9.65	493.95	46.27	47.65	2.98
0.94	10.01	498.40	48.04	48.89	1.77
0.94	10.47	503.85	49.80	50.49	1.39
0.94	11.03	510.41	51.57	52.57	1.93
0.94	11.72	518.03	53.34	55.18	3.45
0.94	12.49	526.11	55.11	58.21	5.63
1.06	9.32	489.00	50.85	49.37	2.92
1.06	9.71	493.87	52.40	50.73	3.18
1.06	10.16	499.39	53.96	52.38	2.93
1.06	10.71	505.77	55.51	54.39	2.01
1.06	11.37	513.10	57.07	56.91	0.28
1.06	12.16	521.44	58.62	60.03	2.40
0.94	11.46	488.29	42.46	44.43	4.63
0.94	11.79	491.79	43.87	45.32	3.31
0.94	12.21	496.03	45.28	46.43	2.54
0.94	12.73	501.09	46.70	47.83	2.42
0.94	13.34	506.88	48.11	49.54	2.97
0.94	14.06	513.48	49.52	51.62	4.24
0.94	14.87	520.51	50.93	54.00	6.02
1.06	11.44	488.02	47.42	47.22	0.42
1.06	11.83	492.00	49.00	48.29	1.46
1.06	12.33	496.97	50.59	49.69	1.79
1.06	12.93	502.74	52.17	51.40	1.48
1.06	13.67	509.55	53.76	53.54	0.40
1.06	14.54	517.15	55.34	56.17	1.50
1.06	15.56	525.60	56.92	59.36	4.28
1.20	11.65	489.05	48.37	43.16	10.78
1.20	12.08	493.37	49.93	44.22	11.43
1.20	12.63	498.56	51.50	45.57	11.51
1.20	13.25	504.31	53.07	47.16	11.14
1.20	14.02	511.10	54.64	49.15	10.05
1.20	14.93	518.77	56.20	51.62	8.15
0.83	2.86	475.85	45.82	44.67	2.51
0.83	2.96	479.75	46.90	45.63	2.71
0.83	3.07	484.42	48.02	46.81	2.51
0.83	3.20	489.38	49.20	48.14	2.15
0.83	3.35	494.94	50.42	49.74	1.36
0.83	3.52	501.23	51.70	51.63	0.14
0.83	3.73	508.37	53.03	53.97	1.77
0.92	2.82	476.53	52.45	51.35	2.10
0.92	2.93	481.34	54.14	52.70	2.65
0.92	3.08	487.05	55.83	54.38	2.59
0.92	3.26	494.10	57.52	56.60	1.59
0.92	3.47	501.88	59.22	59.28	0.10
0.92	3.74	510.97	60.91	62.63	2.82
1.04	2.66	474.58	50.06	55.41	10.69
1.04	2.77	479.52	52.70	56.91	7.98
1.04	2.91	485.12	55.34	58.62	5.93
1.04	3.08	491.90	57.97	60.89	5.04
1.04	3.29	500.11	60.61	63.87	5.38
1.04	3.57	509.95	63.25	67.75	7.11
1.17	2.74	476.23	53.27	53.19	0.15
1.17	2.88	481.75	54.66	54.80	0.25
1.17	3.04	488.35	56.43	56.78	0.62
1.17	3.23	495.44	58.69	59.13	0.75
1.17	3.46	503.59	61.56	61.99	0.69
0.85	4.72	472.89	39.09	41.40	5.91
0.85	4.87	476.47	39.96	42.21	5.64
0.85	5.01	479.99	40.84	42.97	5.23
0.85	5.18	483.85	41.71	43.92	5.30
0.85	5.37	488.25	42.58	44.99	5.66
0.85	5.58	493.05	43.45	46.30	6.56

0.85	5.83	498.34	44.33	47.76	7.73
0.85	6.11	504.17	45.20	49.48	9.47
0.85	6.43	510.67	46.07	51.46	11.71
0.94	4.63	473.97	45.91	47.00	2.38
0.94	4.80	478.12	47.22	48.03	1.71
0.94	4.99	482.70	48.52	49.22	1.45
0.94	5.24	488.52	49.83	50.80	1.95
0.94	5.52	494.87	51.14	52.73	3.11
0.94	5.84	501.83	52.45	54.93	4.73
0.94	6.21	509.34	53.75	57.51	6.99
1.04	4.70	474.27	48.13	50.26	4.42
1.04	4.89	478.79	49.36	51.46	4.26
1.04	5.11	484.02	50.94	52.96	3.96
1.04	5.39	490.25	52.96	54.80	3.47
1.04	5.71	497.26	55.56	57.04	2.67
1.04	6.12	505.53	58.90	59.87	1.65
1.19	4.68	472.09	49.80	45.90	7.83
1.19	4.86	476.42	51.77	46.95	9.32
1.19	5.10	481.92	53.74	48.31	10.10
1.19	5.38	488.08	55.71	49.96	10.32
1.19	5.72	495.26	57.68	52.06	9.74
1.19	6.12	503.46	59.65	54.60	8.46
0.84	6.82	472.65	35.77	37.52	4.90
0.84	6.97	475.35	36.07	38.07	5.53
0.84	7.14	478.24	36.41	38.66	6.18
0.84	7.34	481.50	36.77	39.36	7.05
0.84	7.57	485.25	37.16	40.19	8.15
0.84	7.82	489.22	37.59	41.10	9.35
0.84	8.11	493.59	38.05	42.16	10.79
0.84	8.41	498.07	38.56	43.29	12.26
0.84	8.76	503.14	39.11	44.63	14.11
0.84	9.13	508.36	39.70	46.09	16.10
0.92	6.78	472.92	41.47	43.02	3.74
0.92	6.99	476.47	42.06	43.84	4.24
0.92	7.23	480.44	42.75	44.78	4.74
0.92	7.50	484.89	43.55	45.89	5.37
0.92	7.79	489.37	44.50	47.04	5.71
0.92	8.16	495.07	45.60	48.60	6.57
0.92	8.58	501.11	46.89	50.35	7.39
0.92	9.06	507.85	48.39	52.45	8.40
1.03	6.81	474.31	45.48	47.08	3.52
1.03	7.05	478.36	47.62	48.10	1.00
1.03	7.36	483.53	49.76	49.45	0.63
1.03	7.74	489.46	51.90	51.09	1.56
1.03	8.22	496.61	54.04	53.21	1.54
1.03	8.79	504.81	56.18	55.84	0.60
1.18	6.87	474.90	50.18	43.87	12.58
1.18	7.15	479.44	51.39	44.93	12.57
1.18	7.50	484.99	52.70	46.31	12.13
1.18	7.92	491.35	54.13	47.98	11.37
1.18	8.43	498.77	55.68	50.06	10.09
1.18	9.03	506.89	57.35	52.55	8.38
0.94	9.19	474.78	41.68	41.98	0.72
0.94	9.48	478.40	43.09	42.79	0.69
0.94	9.80	482.33	44.51	43.72	1.78
0.94	10.18	486.92	45.92	44.83	2.38
0.94	10.65	492.34	47.33	46.22	2.34
0.94	11.22	498.66	48.74	47.94	1.64
0.94	11.89	505.76	50.16	50.02	0.28
1.05	9.25	474.29	51.34	44.73	12.87
1.05	9.65	479.28	53.17	45.92	13.64
1.05	10.14	485.08	54.99	47.37	13.86
1.05	10.73	491.80	56.82	49.17	13.47
1.05	11.45	499.59	58.65	51.42	12.33
1.05	12.31	508.41	60.48	54.22	10.35
0.95	11.27	473.72	40.27	40.77	1.23
0.95	11.58	476.88	41.52	41.44	0.19
0.95	11.95	480.62	42.77	42.28	1.15
0.95	12.41	485.11	44.02	43.33	1.56
0.95	12.98	490.44	45.27	44.64	1.38
0.95	13.63	496.42	46.52	46.19	0.72
0.95	14.38	502.96	47.77	48.01	0.50
0.95	15.23	510.06	49.02	50.13	2.26
1.05	11.53	476.78	47.26	43.72	7.50
1.05	11.98	481.19	48.19	44.75	7.14
1.05	12.52	486.46	49.23	46.05	6.47

1.05	13.18	492.49	50.40	47.62	5.51
1.05	13.96	499.42	51.72	49.56	4.18
1.05	14.88	507.20	53.19	51.91	2.41
1.20	11.47	475.13	45.10	39.14	13.22
1.20	11.88	479.09	46.64	39.98	14.28
1.20	12.39	483.94	48.18	41.03	14.85
1.20	12.98	489.37	49.72	42.28	14.96
1.20	13.68	495.57	51.26	43.81	14.54
1.20	14.53	502.69	52.81	45.68	13.51
1.20	15.55	510.82	54.35	47.99	11.69
0.86	2.41	459.84	46.97	43.18	8.06
0.86	2.49	463.46	48.22	43.95	8.85
0.86	2.59	467.98	49.47	45.00	9.05
0.86	2.69	472.45	50.72	46.06	9.18
0.86	2.82	478.18	51.97	47.51	8.59
0.86	2.98	484.60	53.22	49.20	7.54
0.86	3.16	491.69	54.46	51.23	5.93
0.95	2.39	462.57	53.54	49.36	7.81
0.95	2.51	468.10	55.11	50.75	7.92
0.95	2.65	474.19	56.68	52.38	7.58
0.95	2.81	481.16	58.25	54.36	6.68
0.95	2.99	488.67	59.82	56.66	5.28
0.95	3.22	497.54	61.39	59.62	2.88
1.06	2.37	462.03	54.00	52.08	3.55
1.06	2.49	467.37	55.93	53.48	4.38
1.06	2.62	473.30	57.86	55.14	4.71
1.06	2.80	480.91	59.78	57.39	4.00
1.06	3.01	489.52	61.71	60.19	2.47
1.20	2.47	462.33	47.95	48.16	0.43
1.20	2.57	466.82	51.23	49.24	3.89
1.20	2.70	472.20	54.51	50.63	7.12
1.20	2.86	478.93	57.79	52.44	9.25
1.20	3.08	487.35	61.07	54.91	10.08
0.85	4.73	459.55	38.01	37.59	1.12
0.85	4.84	462.22	38.77	38.07	1.80
0.85	4.98	465.65	39.52	38.75	1.95
0.85	5.14	469.18	40.28	39.47	2.02
0.85	5.33	473.50	41.03	40.34	1.68
0.85	5.55	478.45	41.78	41.48	0.72
0.85	5.80	483.61	42.54	42.66	0.28
0.85	6.06	489.08	43.29	43.98	1.60
0.85	6.37	495.18	44.05	45.57	3.45
0.93	4.90	462.93	44.01	42.86	2.62
0.93	5.07	466.86	45.32	43.74	3.49
0.93	5.29	471.71	46.62	44.83	3.84
0.93	5.54	477.21	47.93	46.16	3.70
0.93	5.84	483.50	49.24	47.71	3.12
0.93	6.19	490.56	50.55	49.68	1.72
0.93	6.59	498.15	51.86	51.88	0.05
1.03	4.84	463.69	48.33	46.64	3.50
1.03	5.05	468.52	49.68	47.78	3.82
1.03	5.31	474.32	51.27	49.19	4.06
1.03	5.63	481.14	53.13	50.99	4.03
1.03	5.98	488.46	55.30	53.07	4.03
1.03	6.43	497.14	57.85	55.80	3.54
1.19	4.67	459.74	45.89	42.32	7.79
1.19	4.83	463.54	47.93	43.15	9.97
1.19	5.05	468.36	49.98	44.21	11.54
1.19	5.31	474.12	52.02	45.51	12.51
1.19	5.64	481.05	54.06	47.22	12.65
1.19	6.02	488.54	56.11	49.22	12.29
1.19	6.48	497.24	58.15	51.68	11.12
0.84	6.87	462.50	34.85	34.83	0.04
0.84	7.03	465.17	35.25	35.31	0.17
0.84	7.22	468.28	35.65	35.88	0.65
0.84	7.43	471.69	36.05	36.54	1.35
0.84	7.66	475.24	36.44	37.23	2.16
0.84	7.94	479.50	36.84	38.10	3.43
0.84	8.24	483.96	37.24	39.05	4.87
0.84	8.56	488.65	37.63	40.10	6.57
0.84	8.91	493.60	38.03	41.26	8.50
0.84	9.32	499.08	38.43	42.62	10.91
0.92	6.91	461.92	42.48	39.70	6.53
0.92	7.13	465.53	42.59	40.43	5.06
0.92	7.37	469.48	42.76	41.26	3.50
0.92	7.65	473.81	43.01	42.20	1.89

0.92	7.98	478.77	43.37	43.33	0.10
0.92	8.35	484.27	43.92	44.64	1.64
0.92	8.80	490.56	44.74	46.24	3.35
0.92	9.29	497.15	45.95	48.02	4.50
1.03	7.05	464.15	46.89	43.78	6.63
1.03	7.31	468.43	48.63	44.74	8.01
1.03	7.67	473.90	50.37	46.01	8.67
1.03	8.11	480.47	52.12	47.63	8.62
1.03	8.64	487.95	53.86	49.62	7.88
1.03	9.28	496.46	55.60	52.06	6.37
1.18	6.76	460.61	46.20	39.89	13.67
1.18	7.01	464.74	47.71	40.71	14.68
1.18	7.33	469.80	49.21	41.76	15.13
1.18	7.71	475.48	50.71	43.01	15.18
1.18	8.15	481.86	52.21	44.50	14.77
1.18	8.67	489.10	53.72	46.30	13.80
1.18	9.29	497.19	55.22	48.49	12.19
0.98	9.28	462.65	40.32	40.50	0.45
0.98	9.58	466.37	41.79	41.26	1.26
0.98	9.93	470.52	43.26	42.14	2.58
0.98	10.39	475.69	44.73	43.28	3.23
0.98	10.92	481.59	46.20	44.67	3.31
0.98	11.55	488.23	47.67	46.32	2.83
0.98	12.27	495.53	49.14	48.27	1.77
1.09	9.40	464.33	47.12	41.06	12.87
1.09	9.78	468.83	48.06	42.00	12.61
1.09	10.25	474.22	49.12	43.18	12.10
1.09	10.81	480.37	50.32	44.59	11.38
1.09	11.48	487.44	51.67	46.35	10.30
1.09	12.28	495.43	53.20	48.48	8.87
1.04	11.35	460.87	44.37	39.51	10.96
1.04	11.75	464.75	44.94	40.28	10.38
1.04	12.22	469.24	45.59	41.21	9.62
1.04	12.76	474.26	46.33	42.27	8.75
1.04	13.40	479.93	47.18	43.57	7.66
1.04	14.13	486.21	48.16	45.06	6.43
1.04	15.01	493.44	49.28	46.92	4.79
0.94	11.64	463.24	36.46	37.54	2.96
0.94	11.97	466.53	37.56	38.17	1.62
0.94	12.36	470.23	38.66	38.90	0.62
0.94	12.83	474.55	39.77	39.78	0.02
0.94	13.35	479.23	40.87	40.78	0.23
0.94	13.97	484.66	41.97	42.00	0.08
0.94	14.68	490.58	43.08	43.41	0.77
0.94	15.49	497.16	44.18	45.08	2.04

Appendix D

Laminar Flame Speed from Experiments and Fitting with New Correlation for 50 *iso*-Octane and 50 *n*-Heptane blend

phi	P (atm)	T (K)	LFS(experments) (cm/s)	LFS(fit) (cm/s)	% error (%)
0.85	4.73	488.60	44.33	47.98	8.23
0.85	4.88	492.38	45.53	49.09	7.81
0.85	5.05	496.59	46.73	50.32	7.68
0.85	5.26	501.61	47.93	51.90	8.28
0.85	5.50	507.20	49.13	53.71	9.31
0.85	5.78	513.35	50.33	55.94	11.14
0.85	6.10	520.28	51.53	58.59	13.70
0.93	4.61	487.89	51.11	53.65	4.97
0.93	4.79	492.56	52.79	55.13	4.44
0.93	5.00	497.82	54.48	56.84	4.33
0.93	5.27	504.19	56.16	59.10	5.23
0.93	5.59	511.45	57.85	61.91	7.02
0.93	5.96	519.64	59.53	65.32	9.73
1.05	4.68	487.28	54.86	57.08	4.05
1.05	4.88	492.37	56.98	58.73	3.07
1.05	5.16	498.88	59.30	61.05	2.96
1.05	5.47	506.14	61.86	63.78	3.10
1.05	5.85	514.38	64.68	67.20	3.90
1.05	6.35	524.52	67.77	72.00	6.24
1.20	4.69	489.78	56.46	53.60	5.07
1.20	4.92	495.30	58.74	55.34	5.78
1.20	5.23	502.59	61.03	57.82	5.27
1.20	5.59	510.63	63.31	60.81	3.94
1.20	6.03	519.74	65.59	64.51	1.65
0.92	6.96	489.03	47.87	49.14	2.65
0.92	7.21	493.18	48.28	50.34	4.27
0.92	7.50	498.05	48.85	51.83	6.09
0.92	7.84	503.46	49.64	53.57	7.91
0.92	8.23	509.59	50.73	55.68	9.75
0.92	8.69	516.42	52.25	58.21	11.40
0.92	9.24	524.20	54.35	61.36	12.91
1.02	6.87	486.79	51.41	52.97	3.03
1.02	7.11	490.96	53.22	54.25	1.93
1.02	7.43	496.11	55.15	55.91	1.37
1.02	7.82	502.42	57.19	58.07	1.54
1.02	8.34	510.24	59.36	60.98	2.73
1.02	8.94	519.01	61.66	64.56	4.70
1.16	6.96	488.15	52.17	50.59	3.04
1.16	7.25	492.91	54.52	51.99	4.63
1.16	7.63	499.01	56.87	53.90	5.22
1.16	8.09	506.05	59.21	56.28	4.95
1.16	8.65	514.09	61.56	59.24	3.77
1.16	9.33	523.40	63.91	63.03	1.38
0.93	9.18	488.39	46.50	47.67	2.51
0.93	9.50	492.51	48.22	48.82	1.24
0.93	9.87	497.22	49.94	50.21	0.54
0.93	10.31	502.55	51.66	51.86	0.39
0.93	10.87	509.06	53.38	54.01	1.18
0.93	11.53	516.50	55.10	56.68	2.87
0.93	12.31	524.74	56.82	59.94	5.50

1.05	9.43	491.21	53.27	51.97	2.45
1.05	9.85	496.49	55.11	53.59	2.75
1.05	10.39	502.88	56.94	55.71	2.16
1.05	11.04	510.29	58.78	58.33	0.76
1.05	11.83	518.88	60.61	61.70	1.79
0.88	2.49	489.64	51.04	56.52	10.74
0.88	2.59	494.29	53.43	58.08	8.70
0.88	2.71	499.83	55.81	60.04	7.58
0.88	2.86	506.42	58.20	62.59	7.54
0.88	3.05	514.46	60.58	65.92	8.82
0.88	3.27	523.35	62.97	69.97	11.12
1.12	2.46	486.95	57.76	62.54	8.27
1.12	2.58	492.78	60.37	64.65	7.09
1.12	2.72	498.96	62.98	67.09	6.53
1.12	2.92	507.53	65.58	70.68	7.77
1.12	3.15	516.80	68.19	75.05	10.06
0.94	11.57	490.10	45.42	46.42	2.19
0.94	11.98	494.27	46.97	47.57	1.27
0.94	12.49	499.41	48.51	49.04	1.10
0.94	13.10	505.28	50.06	50.84	1.57
0.94	13.82	511.87	51.61	53.02	2.73
0.94	14.63	519.09	53.15	55.60	4.61
0.94	15.57	527.02	54.70	58.71	7.33
1.06	11.68	490.25	50.16	49.68	0.95
1.06	12.17	495.09	52.01	51.09	1.77
1.06	12.75	500.78	53.86	52.85	1.87
1.06	13.48	507.53	55.70	55.10	1.08
1.06	14.36	515.28	57.55	57.90	0.60
1.06	15.39	523.92	59.39	61.34	3.28
1.20	11.63	489.13	49.62	44.86	9.59
1.20	12.08	493.54	51.20	46.03	10.10
1.20	12.63	498.88	52.89	47.51	10.18
1.20	13.32	505.19	54.69	49.39	9.70
1.20	14.13	512.29	56.62	51.66	8.77
1.20	15.11	520.49	58.69	54.52	7.10
0.84	2.51	474.09	47.60	47.25	0.74
0.84	2.60	478.14	48.97	48.31	1.36
0.84	2.71	482.93	50.35	49.65	1.40
0.84	2.83	488.47	51.73	51.26	0.90
0.84	2.98	494.54	53.11	53.12	0.02
0.84	3.14	501.27	54.49	55.35	1.58
0.84	3.33	508.67	55.86	58.02	3.87
0.94	2.56	474.53	58.00	54.46	6.10
0.94	2.68	479.96	59.39	56.11	5.52
0.94	2.83	486.43	60.78	58.15	4.32
0.94	3.01	493.77	62.17	60.68	2.40
0.94	3.22	501.99	63.56	63.78	0.35
1.05	2.49	475.51	57.75	58.47	1.25
1.05	2.61	481.04	59.84	60.25	0.68
1.05	2.76	487.50	61.93	62.50	0.92
1.05	2.95	495.41	64.02	65.43	2.20
1.05	3.20	505.35	66.11	69.47	5.07
1.18	2.57	475.06	49.45	55.00	11.21
1.18	2.68	479.98	51.48	56.48	9.72
1.18	2.81	485.60	53.86	58.26	8.17
1.18	2.98	492.51	56.66	60.61	6.97
1.18	3.19	500.37	59.95	63.54	5.98
0.90	4.64	472.71	46.19	45.85	0.74
0.90	4.80	476.77	47.00	46.84	0.34
0.90	4.98	481.06	47.82	48.01	0.40
0.90	5.19	486.00	48.64	49.37	1.51
0.90	5.43	491.57	49.46	50.94	2.98
0.90	5.72	497.85	50.27	52.93	5.28
0.90	6.03	504.54	51.09	55.12	7.89
0.99	4.64	474.43	48.72	51.15	4.99
0.99	4.83	479.08	50.02	52.46	4.88
0.99	5.06	484.69	51.47	54.16	5.23
0.99	5.34	491.00	53.07	56.14	5.78
0.99	5.66	498.11	54.84	58.46	6.61
0.99	6.03	505.89	56.79	61.35	8.02
1.06	9.38	476.35	51.27	46.79	8.73
1.06	9.79	481.26	52.74	48.06	8.87
1.06	10.26	486.88	54.21	49.59	8.52
1.06	10.86	493.64	55.68	51.55	7.42
1.06	11.59	501.38	57.15	53.99	5.52

1.06	12.47	510.33	58.63	57.08	2.64
0.85	6.91	473.44	37.36	40.10	7.32
0.85	7.08	476.31	38.00	40.73	7.19
0.85	7.28	479.66	38.64	41.50	7.40
0.85	7.51	483.40	39.28	42.38	7.89
0.85	7.77	487.54	39.92	43.41	8.73
0.85	8.07	492.13	40.56	44.59	9.94
0.85	8.40	497.03	41.20	45.92	11.45
0.85	8.77	502.41	41.84	47.46	13.43
0.85	9.18	508.10	42.49	49.19	15.78
0.93	7.05	474.66	43.35	45.35	4.61
0.93	7.27	478.38	44.41	46.27	4.19
0.93	7.56	482.90	45.63	47.46	4.00
0.93	7.89	487.99	47.04	48.84	3.82
0.93	8.27	493.75	48.67	50.50	3.76
0.93	8.72	500.25	50.54	52.51	3.90
0.93	9.26	507.69	52.71	54.99	4.33
1.03	7.08	476.02	49.65	49.07	1.17
1.03	7.37	480.82	51.92	50.38	2.97
1.03	7.76	486.85	54.18	52.09	3.85
1.03	8.24	494.08	56.45	54.31	3.80
1.03	8.83	502.42	58.71	57.09	2.77
1.03	9.54	511.85	60.98	60.56	0.68
1.19	7.10	476.31	51.40	45.36	11.74
1.19	7.42	481.46	53.40	46.67	12.61
1.19	7.80	487.20	55.41	48.19	13.03
1.19	8.28	494.28	57.42	50.21	12.57
1.19	8.87	502.31	59.42	52.68	11.34
0.87	9.07	473.63	37.40	39.13	4.62
0.87	9.30	476.57	37.60	39.76	5.74
0.87	9.56	479.84	37.85	40.48	6.94
0.87	9.84	483.28	38.16	41.27	8.14
0.87	10.16	487.21	38.54	42.21	9.51
0.87	10.53	491.49	39.02	43.27	10.90
0.87	10.94	496.17	39.60	44.51	12.39
0.87	11.41	501.35	40.32	45.93	13.92
0.87	11.94	507.03	41.22	47.59	15.46
0.96	9.19	474.44	43.99	44.38	0.88
0.96	9.49	478.15	45.71	45.27	0.97
0.96	9.84	482.51	47.44	46.37	2.26
0.96	10.30	487.98	49.16	47.82	2.72
0.96	10.85	494.25	50.89	49.59	2.55
0.96	11.53	501.58	52.61	51.83	1.49
0.96	12.30	509.65	54.34	54.51	0.31
1.06	9.38	476.35	51.27	46.79	8.73
1.06	9.79	481.26	52.74	48.06	8.87
1.06	10.26	486.88	54.21	49.59	8.52
1.06	10.86	493.64	55.68	51.55	7.42
1.06	11.59	501.38	57.15	53.99	5.52
1.06	12.47	510.33	58.63	57.08	2.64
0.86	11.40	474.21	34.66	37.32	7.67
0.86	11.65	476.74	34.99	37.83	8.12
0.86	11.93	479.62	35.39	38.45	8.64
0.86	12.26	482.81	35.85	39.14	9.19
0.86	12.63	486.44	36.38	39.96	9.85
0.86	13.04	490.33	37.00	40.88	10.49
0.86	13.52	494.76	37.72	41.96	11.25
0.86	14.05	499.47	38.56	43.17	11.97
0.86	14.65	504.69	39.53	44.59	12.80
0.86	15.34	510.40	40.67	46.25	13.73
0.96	11.71	476.70	43.99	43.23	1.73
0.96	12.13	480.81	45.35	44.21	2.52
0.96	12.64	485.73	46.71	45.45	2.70
0.96	13.25	491.40	48.07	46.95	2.34
0.96	13.96	497.74	49.43	48.73	1.41
0.96	14.79	504.81	50.79	50.88	0.18
0.96	15.73	512.47	52.15	53.41	2.41
1.06	11.50	475.33	48.32	44.80	7.29
1.06	11.95	479.80	49.90	45.89	8.03
1.06	12.48	484.93	51.48	47.22	8.27
1.06	13.15	491.15	53.06	48.91	7.81
1.06	13.95	498.22	54.64	50.99	6.68
1.06	14.92	506.34	56.22	53.57	4.71
0.84	2.47	460.20	48.57	43.17	11.12
0.84	2.55	463.71	49.64	43.93	11.51
0.84	2.65	468.23	50.70	44.99	11.26

0.84	2.75	472.80	51.77	46.12	10.92
0.84	2.88	478.47	52.83	47.58	9.94
0.84	3.04	485.00	53.90	49.40	8.34
0.84	3.24	492.46	54.96	51.58	6.15
0.84	2.47	460.20	49.22	43.17	12.30
0.84	2.55	463.71	49.87	43.93	11.91
0.84	2.65	468.23	50.61	44.99	11.10
0.84	2.75	472.80	51.45	46.12	10.37
0.84	2.88	478.47	52.40	47.58	9.20
0.84	3.04	485.00	53.48	49.40	7.62
0.84	3.24	492.46	54.70	51.58	5.71
0.93	2.43	458.08	55.23	48.44	12.29
0.93	2.56	464.05	56.60	49.94	11.77
0.93	2.69	469.80	57.97	51.48	11.19
0.93	2.85	476.69	59.34	53.40	10.01
0.93	3.03	483.86	60.70	55.59	8.42
0.93	3.27	493.11	62.07	58.59	5.60
1.18	2.44	461.38	57.47	50.27	12.53
1.18	2.55	466.45	59.39	51.60	13.11
1.18	2.67	471.56	61.31	53.00	13.55
1.18	2.83	478.23	63.23	54.92	13.14
1.18	3.04	486.55	65.15	57.53	11.69
1.18	3.31	496.56	67.08	60.94	9.15
0.87	4.64	462.64	43.04	41.44	3.71
0.87	4.79	466.37	43.90	42.21	3.84
0.87	4.97	470.59	44.75	43.21	3.45
0.87	5.16	475.15	45.60	44.26	2.93
0.87	5.40	480.56	46.45	45.61	1.80
0.87	5.67	486.34	47.31	47.15	0.34
0.87	5.97	492.66	48.16	48.87	1.48
0.95	4.62	463.36	48.35	46.20	4.45
0.95	4.80	467.73	49.31	47.24	4.20
0.95	5.02	472.92	50.41	48.57	3.66
0.95	5.29	479.09	51.65	50.19	2.83
0.95	5.61	486.09	53.07	52.19	1.66
0.95	5.97	493.50	54.68	54.48	0.37
1.06	4.67	463.18	51.03	48.38	5.19
1.06	4.89	468.22	53.56	49.59	7.41
1.06	5.13	473.73	56.09	51.08	8.93
1.06	5.45	480.94	58.61	53.13	9.34
1.06	5.86	489.43	61.14	55.71	8.88
0.84	6.86	462.33	36.36	36.28	0.21
0.84	7.02	465.15	36.72	36.82	0.28
0.84	7.21	468.25	37.09	37.44	0.94
0.84	7.44	471.92	37.46	38.18	1.93
0.84	7.68	475.71	37.82	38.98	3.07
0.84	7.96	479.91	38.19	39.90	4.47
0.84	8.26	484.44	38.55	40.93	6.19
0.84	8.61	489.44	38.92	42.14	8.28
0.84	8.98	494.62	39.29	43.46	10.62
0.91	7.03	463.46	41.69	40.82	2.08
0.91	7.24	467.01	42.07	41.58	1.17
0.91	7.51	471.20	42.55	42.51	0.10
0.91	7.81	475.75	43.20	43.56	0.83
0.91	8.17	481.10	44.03	44.87	1.90
0.91	8.57	486.86	45.13	46.34	2.69
0.91	9.03	493.29	46.57	48.11	3.30
1.01	6.99	462.76	45.48	44.72	1.67
1.01	7.27	467.23	47.60	45.76	3.87
1.01	7.59	472.17	49.71	46.96	5.53
1.01	7.99	478.17	51.83	48.49	6.44
1.01	8.47	485.09	53.94	50.38	6.61
1.01	9.08	493.42	56.06	52.84	5.74
0.82	9.13	461.07	31.53	32.95	4.49
0.82	9.31	463.43	31.78	33.36	4.97
0.82	9.52	465.96	32.05	33.81	5.48
0.82	9.74	468.72	32.34	34.30	6.06
0.82	9.99	471.74	32.66	34.87	6.75
0.82	10.28	475.10	33.00	35.52	7.65
0.82	10.61	478.86	33.37	36.27	8.70
0.82	10.97	482.83	33.77	37.10	9.86
0.82	11.34	486.89	34.21	37.97	10.98
0.82	11.76	491.32	34.68	38.97	12.36
0.82	12.21	495.95	35.19	40.07	13.86
0.91	9.12	461.23	37.86	38.46	1.59
0.91	9.38	464.49	39.31	39.11	0.50

0.91	9.68	468.05	40.75	39.84	2.25
0.91	10.02	472.17	42.20	40.72	3.51
0.91	10.42	476.71	43.65	41.72	4.41
0.91	10.88	481.87	45.10	42.94	4.78
0.91	11.43	487.78	46.55	44.40	4.62
0.91	12.08	494.46	48.00	46.16	3.83
1.03	9.41	465.06	48.30	43.37	10.21
1.03	9.82	469.89	49.72	44.45	10.59
1.03	10.31	475.59	51.14	45.82	10.40
1.03	10.88	481.87	52.56	47.41	9.80
1.03	11.59	489.38	53.98	49.46	8.37
1.03	12.41	497.56	55.40	51.88	6.35
0.84	11.46	462.29	31.91	32.95	3.27
0.84	11.71	464.78	32.09	33.39	4.05
0.84	11.98	467.47	32.31	33.87	4.84
0.84	12.29	470.40	32.58	34.40	5.58
0.84	12.62	473.60	32.90	35.01	6.41
0.84	13.01	477.16	33.29	35.69	7.21
0.84	13.43	480.99	33.76	36.48	8.04
0.84	13.89	485.05	34.34	37.31	8.66
0.84	14.40	489.42	35.03	38.28	9.28
0.84	14.97	494.17	35.87	39.38	9.78
0.84	15.61	499.35	36.89	40.63	10.14
0.93	11.58	464.20	40.52	38.45	5.12
0.93	11.94	467.78	41.69	39.17	6.05
0.93	12.38	471.99	42.86	40.04	6.58
0.93	12.92	476.98	44.03	41.13	6.59
0.93	13.54	482.56	45.21	42.41	6.18
0.93	14.27	488.83	46.38	43.95	5.23
0.93	15.10	495.75	47.55	45.77	3.75
1.04	11.37	461.70	45.94	41.08	10.59
1.04	11.77	465.58	47.17	41.88	11.21
1.04	12.25	470.21	48.40	42.91	11.35
1.04	12.82	475.44	49.64	44.11	11.14
1.04	13.50	481.50	50.87	45.58	10.40
1.04	14.35	488.67	52.10	47.45	8.92
1.04	15.33	496.63	53.34	49.71	6.81

Appendix E

Laminar Flame Speed from Experiments and Fitting with New Correlation for 25 *iso*-Octane and 75 *n*-Heptane blend

phi	P (atm)	T (K)	LFS(experments) (cm/s)	LFS(fit) (cm/s)	% error, abs (%)
0.80	2.37	473.78	51.86	46.82	9.71
0.80	2.44	477.42	52.66	47.79	9.25
0.80	2.53	481.81	53.46	49.04	8.27
0.80	2.63	486.55	54.26	50.46	6.99
0.80	2.76	492.44	55.06	52.30	5.01
0.80	2.91	499.01	55.87	54.52	2.42
0.80	3.08	506.00	56.67	57.03	0.63
0.89	2.40	475.02	59.78	54.60	8.67
0.89	2.51	480.00	60.78	56.17	7.59
0.89	2.63	485.50	61.78	57.97	6.17
0.89	2.77	492.06	62.78	60.32	3.92
0.89	2.96	500.20	63.78	63.44	0.53
0.89	3.19	509.39	64.79	67.32	3.90
1.02	2.41	477.57	61.49	61.98	0.80
1.02	2.54	483.65	62.95	64.15	1.91
1.02	2.70	490.87	64.71	66.91	3.40
1.02	2.90	499.53	66.81	70.55	5.59
1.02	3.17	510.44	69.33	75.66	9.13
1.12	2.46	477.81	61.93	61.10	1.35
1.12	2.60	484.36	62.38	63.43	1.68
1.12	2.75	490.82	63.14	65.87	4.32
1.12	2.95	499.31	64.40	69.35	7.69
1.12	3.20	509.06	66.50	73.85	11.06
0.84	4.57	473.58	44.40	44.50	0.22
0.84	4.70	476.94	45.31	45.36	0.11
0.84	4.86	480.83	46.24	46.35	0.25
0.84	5.03	485.16	47.19	47.52	0.71
0.84	5.26	490.57	48.16	49.11	1.97
0.84	5.52	496.50	49.15	50.97	3.71
0.84	5.82	502.91	50.16	53.06	5.79
0.84	6.14	509.69	51.19	55.46	8.33
0.92	4.73	473.68	50.54	49.70	1.67
0.92	4.90	477.96	51.77	50.88	1.72
0.92	5.11	482.91	53.09	52.35	1.40
0.92	5.37	488.90	54.52	54.18	0.62
0.92	5.68	495.70	56.06	56.45	0.70
0.92	6.04	503.20	57.72	59.19	2.54
0.92	6.48	512.09	59.50	62.81	5.56
1.03	4.65	474.07	52.22	54.31	4.01
1.03	4.83	478.67	53.85	55.72	3.47
1.03	5.06	484.17	55.87	57.53	2.98
1.03	5.37	491.15	58.40	59.96	2.68
1.03	5.73	498.99	61.55	62.86	2.12
1.03	6.22	508.96	65.47	67.04	2.40
1.18	4.72	476.56	56.30	51.56	8.42
1.18	4.95	482.10	58.52	53.17	9.14
1.18	5.25	488.96	60.74	55.37	8.84
1.18	5.62	496.96	62.96	58.10	7.72
1.18	6.07	506.00	65.18	61.43	5.75
0.84	6.91	474.59	39.61	40.95	3.39

0.84	7.10	477.86	40.13	41.72	3.97
0.84	7.31	481.30	40.65	42.55	4.68
0.84	7.56	485.38	41.17	43.60	5.89
0.84	7.83	489.70	41.70	44.73	7.27
0.84	8.14	494.39	42.22	46.04	9.05
0.84	8.49	499.65	42.74	47.59	11.35
0.84	8.88	505.21	43.26	49.34	14.05
0.84	9.33	511.42	43.79	51.42	17.43
0.91	7.01	475.38	46.07	46.29	0.49
0.91	7.26	479.42	46.91	47.36	0.97
0.91	7.55	484.07	47.81	48.64	1.74
0.91	7.88	489.33	48.49	50.18	3.49
0.91	8.28	495.24	49.39	52.01	5.31
0.91	8.73	501.77	49.95	54.18	8.46
0.91	9.27	509.18	52.25	56.86	8.81
1.01	6.88	473.83	49.61	50.37	1.54
1.01	7.13	478.08	52.08	51.57	0.97
1.01	7.46	483.39	54.55	53.15	2.57
1.01	7.89	489.92	57.02	55.22	3.16
1.01	8.42	497.82	59.49	57.93	2.63
1.01	9.08	506.98	61.96	61.37	0.95
1.15	7.07	474.99	54.75	48.54	11.34
1.15	7.39	480.19	56.69	49.97	11.85
1.15	7.81	486.51	58.64	51.82	11.63
1.15	8.31	493.90	60.58	54.15	10.62
1.15	8.92	502.24	62.53	57.02	8.81
0.94	9.25	474.87	44.25	45.27	2.29
0.94	9.56	478.71	46.05	46.24	0.42
0.94	9.93	483.24	47.85	47.46	0.81
0.94	10.38	488.52	49.66	48.96	1.41
0.94	10.93	494.85	51.46	50.86	1.17
0.94	11.60	502.16	53.26	53.23	0.06
0.94	12.39	510.26	55.06	56.11	1.90
1.03	9.42	477.14	53.89	49.19	8.72
1.03	9.86	482.57	55.52	50.73	8.63
1.03	10.40	488.90	56.27	52.63	6.47
1.03	11.05	496.14	57.19	54.96	3.89
1.03	11.84	504.51	59.37	57.92	2.45
1.15	9.07	473.36	50.71	45.55	10.17
1.15	9.43	477.88	52.86	46.70	11.65
1.15	9.88	483.24	54.12	48.15	11.03
1.15	10.43	489.56	55.94	49.95	10.71
1.15	11.09	496.77	56.73	52.17	8.03
1.15	11.90	505.24	60.03	55.02	8.34
0.93	11.49	476.20	44.32	43.67	1.47
0.93	11.88	480.14	45.68	44.66	2.24
0.93	12.37	484.88	47.05	45.89	2.46
0.93	12.94	490.36	48.42	47.40	2.11
0.93	13.62	496.54	49.78	49.21	1.15
0.93	14.40	503.38	51.15	51.37	0.42
0.93	15.30	510.90	52.52	53.97	2.75
1.04	11.66	477.61	50.68	47.57	6.14
1.04	12.16	482.56	52.05	48.92	6.02
1.04	12.76	488.21	53.51	50.55	5.53
1.04	13.50	494.99	55.07	52.63	4.42
1.04	14.41	502.83	56.73	55.27	2.58
1.04	15.50	511.82	58.51	58.59	0.13
1.16	11.68	477.44	52.75	44.59	15.48
1.16	12.21	482.55	53.60	45.89	14.39
1.16	12.84	488.47	54.30	47.50	12.52
1.16	13.61	495.29	55.62	49.48	11.04
1.16	14.54	503.20	57.98	51.98	10.35
1.16	15.69	512.43	61.39	55.20	10.09
0.87	2.74	488.97	52.64	57.02	8.33
0.87	2.85	493.88	54.60	58.77	7.65
0.87	2.98	499.29	56.56	60.79	7.47
0.87	3.14	505.92	58.52	63.43	8.39
0.87	3.34	513.54	60.49	66.72	10.31
0.87	3.57	522.26	62.45	70.94	13.59
1.03	2.54	486.25	63.03	65.49	3.91
1.03	2.66	491.89	63.76	67.71	6.20
1.03	2.81	498.10	64.70	70.34	8.72
1.03	2.99	505.67	65.93	73.77	11.88
0.86	4.60	487.75	47.32	50.80	7.36
0.86	4.75	491.56	48.61	51.95	6.88
0.86	4.93	496.18	49.89	53.45	7.15

0.86	5.14	501.26	51.17	55.21	7.90
0.86	5.39	507.15	52.45	57.33	9.31
0.86	5.68	513.72	53.74	59.91	11.47
0.86	6.01	521.09	55.02	63.08	14.65
0.95	4.71	490.26	54.50	57.69	5.86
0.95	4.93	495.82	55.95	59.64	6.60
0.95	5.19	502.12	57.47	62.04	7.95
0.95	5.49	508.94	59.06	64.85	9.81
0.95	5.84	516.71	60.71	68.29	12.48
0.95	6.28	525.82	62.45	72.83	16.62
1.05	4.62	488.33	58.45	60.32	3.19
1.05	4.84	494.05	60.61	62.40	2.96
1.05	5.12	500.63	63.18	65.01	2.90
1.05	5.47	508.71	66.24	68.47	3.37
1.05	5.91	518.39	69.88	73.05	4.53
0.92	6.84	487.94	48.53	51.27	5.65
0.92	7.07	492.06	49.46	52.57	6.29
0.92	7.36	496.80	50.60	54.12	6.96
0.92	7.70	502.40	51.99	56.06	7.83
0.92	8.11	508.86	53.67	58.45	8.91
0.92	8.58	515.87	55.72	61.29	9.99
0.92	9.13	523.84	58.22	64.80	11.31
1.02	6.98	489.34	54.82	56.37	2.83
1.02	7.29	494.41	57.15	58.11	1.68
1.02	7.69	500.93	59.48	60.50	1.71
1.02	8.19	508.71	61.81	63.58	2.87
1.02	8.81	517.75	64.14	67.55	5.32
1.17	6.99	490.92	57.28	53.89	5.92
1.17	7.36	496.97	59.42	55.90	5.92
1.17	7.80	503.83	61.65	58.36	5.33
1.17	8.32	511.72	63.97	61.44	3.96
1.17	8.98	521.02	66.38	65.46	1.39
0.94	9.37	490.61	49.02	50.75	3.53
0.94	9.71	494.92	50.58	52.10	3.00
0.94	10.12	500.02	52.21	53.77	2.98
0.94	10.65	506.36	53.94	55.99	3.80
0.94	11.28	513.52	55.76	58.72	5.30
0.94	12.05	521.85	57.67	62.20	7.85
1.04	9.18	487.76	54.81	53.37	2.63
1.04	9.60	493.11	56.66	55.10	2.75
1.04	10.09	499.09	58.51	57.15	2.32
1.04	10.69	506.13	60.36	59.74	1.02
1.04	11.41	514.20	62.21	63.01	1.29
1.04	12.31	523.68	64.06	67.27	5.01
1.18	9.14	488.70	53.40	49.91	6.53
1.18	9.51	493.43	55.65	51.34	7.74
1.18	10.00	499.42	57.90	53.26	8.02
1.18	10.61	506.44	60.14	55.69	7.40
1.18	11.35	514.63	62.39	58.79	5.77
1.18	12.24	523.89	64.63	62.71	2.97
0.93	11.41	489.58	46.16	48.39	4.84
0.93	11.79	493.58	47.88	49.57	3.54
0.93	12.27	498.42	49.60	51.07	2.96
0.93	12.85	504.17	51.32	52.96	3.20
0.93	13.56	510.82	53.04	55.32	4.31
0.93	14.37	518.11	54.76	58.12	6.14
0.93	15.31	526.21	56.48	61.57	9.01
1.05	11.31	488.38	51.59	51.68	0.17
1.05	11.75	492.90	53.50	53.08	0.79
1.05	12.30	498.44	55.41	54.90	0.92
1.05	12.98	505.00	57.32	57.22	0.18
1.05	13.81	512.59	59.23	60.13	1.52
1.05	14.81	521.30	61.14	63.81	4.37
1.18	11.24	487.67	52.21	47.46	9.10
1.18	11.67	492.01	52.33	48.70	6.93
1.18	12.21	497.36	55.42	50.32	9.21
1.18	12.87	503.67	57.31	52.35	8.66
1.18	13.68	511.01	59.04	54.91	7.00
1.18	14.68	519.62	62.30	58.22	6.55
0.83	9.03	460.90	32.77	34.92	6.57
0.83	9.23	463.49	33.05	35.41	7.15
0.83	9.44	466.10	33.36	35.92	7.67
0.83	9.68	469.03	33.70	36.50	8.31
0.83	9.96	472.42	34.06	37.20	9.21
0.83	10.26	475.99	34.46	37.95	10.13

0.83	10.61	479.99	34.89	38.84	11.32
0.92	9.28	463.41	42.53	41.03	3.53
0.92	9.59	467.21	43.80	41.87	4.41
0.92	9.94	471.38	45.14	42.82	5.13
0.92	10.37	476.40	46.57	44.03	5.45
0.92	10.88	482.15	48.09	45.49	5.41
0.92	11.51	488.84	49.70	47.32	4.80
0.92	12.25	496.47	51.42	49.56	3.61
1.04	9.29	464.10	48.74	45.08	7.51
1.04	9.73	469.36	50.62	46.35	8.43
1.04	10.22	475.04	52.50	47.82	8.92
1.04	10.83	481.86	54.38	49.68	8.64
1.04	11.56	489.53	56.26	51.94	7.67
1.04	12.42	498.20	58.14	54.73	5.87
0.82	2.47	460.87	47.04	43.97	6.53
0.82	2.57	465.48	48.24	45.08	6.54
0.82	2.67	470.05	49.44	46.23	6.48
0.82	2.78	474.87	50.64	47.47	6.26
0.82	2.92	480.44	51.84	49.01	5.46
0.82	3.08	487.08	53.04	51.01	3.84
0.82	3.27	494.29	54.24	53.31	1.72
0.91	2.44	460.90	56.97	50.58	11.21
0.91	2.55	465.97	57.89	51.96	10.25
0.91	2.69	472.13	59.02	53.73	8.97
0.91	2.85	478.97	60.45	55.85	7.61
0.91	3.04	486.82	62.23	58.46	6.06
0.91	3.29	496.26	64.45	61.86	4.02
1.02	2.49	459.07	56.09	54.37	3.07
1.02	2.60	464.06	58.05	55.79	3.89
1.02	2.73	469.44	60.01	57.42	4.32
1.02	2.91	476.98	61.97	59.86	3.41
1.02	3.13	485.44	63.92	62.80	1.75
1.02	3.40	495.26	65.88	66.56	1.03
1.16	2.55	459.05	51.56	52.22	1.28
1.16	2.66	463.75	53.10	53.49	0.73
1.16	2.78	468.96	55.02	55.03	0.02
1.16	2.95	475.57	57.41	57.01	0.69
1.16	3.16	483.33	60.39	59.57	1.35
1.16	3.42	492.72	64.09	62.98	1.74
0.86	4.75	461.18	42.64	41.74	2.11
0.86	4.90	464.73	43.38	42.55	1.92
0.86	5.07	468.64	44.14	43.48	1.50
0.86	5.27	473.14	44.93	44.54	0.86
0.86	5.50	478.39	45.75	45.88	0.28
0.86	5.78	484.18	46.59	47.45	1.86
0.86	6.09	490.63	47.46	49.35	3.98
0.86	6.45	497.60	48.36	51.47	6.43
0.94	4.68	460.51	50.11	46.64	6.93
0.94	4.86	464.84	50.78	47.69	6.09
0.94	5.08	469.93	51.59	49.01	4.99
0.94	5.34	475.90	52.56	50.69	3.56
0.94	5.65	482.54	53.73	52.61	2.08
0.94	6.01	489.96	55.13	54.95	0.32
1.05	4.67	459.86	52.76	49.36	6.45
1.05	4.89	464.92	53.87	50.69	5.90
1.05	5.12	470.32	55.30	52.11	5.76
1.05	5.43	477.09	57.17	54.08	5.40
1.05	5.79	484.59	59.62	56.45	5.32
1.05	6.27	494.01	62.80	59.69	4.96
0.83	6.93	460.59	35.84	36.66	2.28
0.83	7.10	463.37	36.33	37.21	2.42
0.83	7.31	466.83	36.82	37.91	2.97
0.83	7.51	470.11	37.31	38.60	3.47
0.83	7.76	473.89	37.81	39.43	4.27
0.83	8.02	477.84	38.30	40.32	5.28
0.83	8.32	482.31	38.79	41.39	6.69
0.83	8.67	487.28	39.28	42.62	8.51
0.83	9.03	492.24	39.78	43.92	10.41
0.83	9.46	498.00	40.27	45.53	13.07
0.91	6.91	460.58	41.20	41.70	1.22
0.91	7.14	464.34	42.04	42.54	1.20
0.91	7.39	468.37	43.01	43.47	1.06
0.91	7.70	473.17	44.13	44.63	1.12
0.91	8.03	478.20	45.42	45.91	1.07
0.91	8.42	483.82	46.91	47.41	1.07
0.91	8.88	490.23	48.62	49.24	1.28

0.91	9.42	497.35	50.60	51.43	1.64
1.01	7.08	463.24	48.70	46.66	4.19
1.01	7.38	467.96	50.96	47.83	6.13
1.01	7.75	473.70	53.21	49.35	7.26
1.01	8.24	480.80	55.45	51.35	7.40
1.01	8.84	489.17	57.68	53.90	6.55
1.01	9.56	498.54	59.91	57.04	4.78
0.85	11.41	461.67	32.65	34.64	6.10
0.85	11.66	464.18	32.92	35.11	6.67
0.85	11.92	466.79	33.25	35.61	7.09
0.85	12.25	469.95	33.63	36.24	7.76
0.85	12.59	473.20	34.07	36.90	8.29
0.85	12.98	476.84	34.59	37.66	8.86
0.85	13.42	480.85	35.19	38.54	9.51
0.85	13.92	485.23	35.90	39.53	10.13
0.85	14.48	490.01	36.73	40.69	10.78
0.85	15.09	495.06	37.70	41.97	11.32
0.93	11.43	461.79	41.82	39.53	5.47
0.93	11.77	465.17	43.09	40.25	6.59
0.93	12.20	469.32	44.37	41.15	7.26
0.93	12.74	474.38	45.65	42.31	7.32
0.93	13.38	480.16	46.92	43.72	6.83
0.93	14.11	486.51	48.20	45.34	5.93
0.93	14.95	493.47	49.47	47.27	4.45
1.04	11.60	462.68	47.99	42.94	10.51
1.04	12.06	467.13	49.17	43.95	10.61
1.04	12.62	472.36	50.44	45.20	10.38
1.04	13.29	478.39	51.80	46.74	9.76
1.04	14.11	485.44	53.27	48.66	8.65
1.04	15.12	493.63	54.84	51.08	6.86

Appendix F

Laminar Flame Speed from Experiments and Fitting with New Correlation for *n*-Heptane

phi	P (atm)	T (K)	LFS(experments) (cm/s)	LFS(fit) (cm/s)	% error, abs (%)
0.87	2.48	487.97	58.43	59.48	1.80
0.87	2.58	492.84	60.30	61.31	1.67
0.87	2.71	498.73	62.18	63.65	2.37
0.87	2.87	505.89	64.05	66.69	4.12
0.87	3.06	513.89	65.92	70.50	6.95
0.87	3.29	523.49	67.80	75.56	11.45
0.98	2.48	487.12	65.41	66.82	2.15
0.98	2.61	493.20	67.37	69.38	2.98
0.98	2.76	500.08	69.34	72.42	4.44
0.98	2.96	508.85	71.31	76.73	7.61
1.11	2.46	490.79	67.35	70.18	4.21
1.11	2.60	497.56	69.09	73.19	5.93
1.11	2.79	506.18	71.10	77.43	8.90
0.85	4.69	489.04	50.88	51.98	2.17
0.85	4.84	493.01	51.41	53.26	3.59
0.85	5.04	497.86	52.04	54.94	5.57
0.85	5.26	503.25	52.77	56.94	7.90
0.85	5.53	509.54	53.64	59.39	10.72
0.93	4.58	487.05	58.05	57.88	0.29
0.93	4.78	492.18	58.76	59.76	1.70
0.93	5.02	498.14	59.66	62.03	3.98
0.93	5.29	504.71	60.78	64.75	6.54
0.93	5.63	512.44	62.19	68.19	9.65
0.93	6.04	521.27	63.95	72.60	13.52
1.05	4.72	491.12	57.07	63.54	11.34
1.05	4.97	497.27	60.75	66.03	8.69
1.05	5.27	504.35	64.61	69.16	7.05
1.05	5.66	513.22	68.63	73.35	6.88
1.05	6.17	523.92	72.84	79.17	8.69
1.19	4.78	489.09	60.73	58.03	4.45
1.19	5.02	494.93	62.95	60.15	4.45
1.19	5.34	502.14	65.38	62.95	3.71
1.19	5.73	510.65	68.03	66.65	2.04
1.19	6.21	520.55	70.94	71.41	0.66
0.90	6.93	488.11	48.91	52.03	6.38
0.90	7.17	492.25	49.58	53.38	7.67
0.90	7.46	497.11	50.46	55.04	9.08
0.90	7.79	502.34	51.61	56.93	10.32
0.90	8.19	508.68	53.13	59.39	11.78
0.90	8.66	515.69	55.11	62.35	13.14
0.90	9.21	523.55	57.72	65.98	14.31
0.99	7.20	491.00	55.23	58.01	5.03
0.99	7.53	496.36	58.20	59.97	3.05
0.99	7.96	503.13	61.16	62.63	2.40
0.99	8.53	511.65	64.13	66.30	3.38
0.99	9.21	521.27	67.10	70.95	5.74
1.15	6.96	488.38	58.21	55.57	4.53
1.15	7.29	493.76	60.40	57.43	4.92
1.15	7.71	500.53	62.79	59.94	4.54
1.15	8.24	508.44	65.41	63.15	3.46
1.15	8.89	517.80	68.27	67.35	1.35
0.93	9.16	489.59	50.60	52.23	3.21
0.93	9.51	494.14	52.72	53.72	1.90

0.93	9.92	499.27	54.83	55.50	1.21
0.93	10.47	505.98	56.95	57.99	1.83
0.93	11.14	513.70	59.06	61.11	3.47
0.93	11.93	522.32	61.18	64.98	6.22
1.05	9.42	491.93	60.30	56.78	5.84
1.05	9.91	497.97	60.74	58.96	2.93
1.05	10.50	505.05	61.77	61.72	0.09
1.05	11.23	513.31	63.56	65.24	2.64
1.05	12.14	522.96	66.43	69.86	5.16
1.19	9.27	490.79	55.49	51.81	6.63
1.19	9.71	496.31	58.09	53.63	7.69
1.19	10.27	502.87	60.70	55.93	7.86
1.19	10.95	510.67	63.31	58.92	6.94
1.19	11.80	519.74	65.92	62.77	4.78
0.93	11.28	488.83	50.42	50.03	0.77
0.93	11.70	493.27	53.38	51.42	3.67
0.93	12.21	498.52	54.70	53.16	2.82
0.93	12.83	504.58	55.78	55.29	0.89
0.93	13.58	511.66	58.08	57.98	0.17
0.93	14.45	519.46	57.97	61.26	5.67
0.93	15.48	528.23	59.61	65.35	9.63
1.06	11.54	491.76	55.67	54.57	1.98
1.06	12.09	497.35	58.15	56.51	2.83
1.06	12.78	504.03	60.02	58.98	1.74
1.06	13.64	511.94	62.61	62.18	0.68
1.06	14.65	520.84	63.03	66.17	4.99
0.81	2.40	474.87	49.11	49.89	1.58
0.81	2.48	478.94	50.39	51.09	1.39
0.81	2.58	483.65	51.67	52.58	1.75
0.81	2.70	488.96	52.95	54.32	2.59
0.81	2.84	495.33	54.23	56.51	4.21
0.81	3.02	502.81	55.51	59.35	6.92
0.81	3.20	510.28	56.79	62.48	10.02
0.90	2.50	476.67	58.88	57.50	2.35
0.90	2.63	482.68	60.55	59.56	1.63
0.90	2.77	489.17	62.21	61.96	0.40
0.90	2.96	497.30	63.88	65.19	2.06
0.90	3.18	506.11	65.55	69.07	5.38
1.03	2.44	474.18	59.70	62.60	4.86
1.03	2.56	479.91	62.45	64.69	3.59
1.03	2.72	487.09	65.21	67.47	3.47
1.03	2.91	495.02	67.96	70.83	4.22
1.03	3.16	505.35	70.71	75.70	7.06
1.12	2.41	473.45	59.02	61.73	4.59
1.12	2.53	478.93	61.95	63.68	2.80
1.12	2.69	486.04	64.88	66.38	2.31
1.12	2.88	494.31	67.81	69.84	3.00
1.12	3.14	504.52	70.74	74.51	5.33
0.85	4.53	472.54	45.96	46.50	1.17
0.85	4.66	476.04	46.94	47.46	1.11
0.85	4.83	480.08	47.92	48.57	1.35
0.85	5.02	484.83	48.91	50.03	2.30
0.85	5.25	490.29	49.89	51.68	3.59
0.85	5.52	496.49	50.87	53.79	5.75
0.85	5.83	503.17	51.85	56.17	8.32
0.85	6.18	510.55	52.83	59.04	11.75
0.94	4.61	474.85	51.77	53.09	2.54
0.94	4.80	479.59	53.43	54.56	2.12
0.94	5.05	485.64	55.09	56.61	2.76
0.94	5.33	492.00	56.75	58.83	3.67
0.94	5.68	499.71	58.41	61.72	5.67
0.94	6.08	508.21	60.07	65.35	8.79
1.04	4.66	475.36	55.57	56.79	2.19
1.04	4.89	480.95	57.48	58.61	1.97
1.04	5.17	487.52	59.87	60.94	1.79
1.04	5.52	495.19	62.86	63.84	1.55
1.04	5.95	504.42	66.60	67.75	1.73
0.84	6.73	472.65	40.31	42.20	4.69
0.84	6.90	475.60	40.67	42.92	5.54
0.84	7.09	478.93	41.06	43.77	6.60
0.84	7.32	482.75	41.49	44.78	7.92
0.84	7.58	486.92	41.97	45.92	9.42
0.91	6.89	472.86	44.49	47.24	6.18
0.91	7.11	476.53	45.58	48.24	5.83
0.91	7.38	480.91	46.83	49.47	5.65

0.91	7.70	485.97	48.26	50.99	5.66
0.91	8.07	491.68	49.90	52.80	5.81
0.91	8.50	497.99	51.77	54.94	6.13
0.91	9.01	505.13	53.91	57.56	6.78
1.02	7.07	473.72	52.22	51.96	0.51
1.02	7.37	478.47	54.65	53.38	2.32
1.02	7.75	484.48	57.09	55.28	3.17
1.02	8.26	492.06	59.53	57.87	2.79
1.02	8.88	500.77	61.97	61.13	1.36
1.02	9.64	510.89	64.41	65.36	1.48
1.15	6.86	472.61	54.66	49.60	9.25
1.15	7.15	477.45	57.06	50.98	10.66
1.15	7.56	483.86	59.44	52.91	10.99
1.15	8.06	491.28	61.79	55.33	10.45
1.15	8.64	499.58	64.12	58.28	9.10
1.15	9.36	509.20	66.43	62.09	6.54
0.94	9.07	473.56	49.42	46.75	5.40
0.94	9.42	477.96	51.43	47.95	6.77
0.94	9.82	482.88	53.52	49.34	7.81
0.94	10.32	488.81	55.68	51.13	8.17
0.94	10.93	495.86	57.91	53.42	7.76
0.94	11.72	504.38	60.23	56.44	6.30
1.03	9.32	474.80	55.26	50.14	9.26
1.03	9.76	480.17	56.62	51.70	8.69
1.03	10.28	486.28	58.12	53.59	7.79
1.03	10.93	493.68	59.75	56.06	6.17
1.03	11.71	501.94	61.54	59.07	4.02
1.03	12.66	511.53	63.50	62.96	0.85
1.15	9.36	475.67	53.88	47.66	11.54
1.15	9.80	480.86	56.21	49.11	12.64
1.15	10.35	487.24	58.55	51.00	12.90
1.15	11.03	494.76	60.88	53.40	12.29
1.15	11.86	503.42	63.21	56.42	10.74
0.94	11.30	473.36	43.85	44.78	2.13
0.94	11.67	477.14	46.46	45.76	1.51
0.94	12.12	481.62	48.11	46.97	2.36
0.94	12.66	486.82	49.55	48.45	2.22
0.94	13.29	492.75	50.72	50.23	0.97
0.94	14.05	499.48	52.12	52.42	0.58
0.94	14.93	507.01	53.46	55.07	3.02
1.03	11.39	473.78	51.42	48.06	6.53
1.03	11.86	478.44	53.19	49.36	7.21
1.03	12.43	483.95	54.95	50.95	7.28
1.03	13.12	490.42	56.71	52.96	6.61
1.03	14.00	498.19	58.48	55.59	4.93
1.03	15.04	506.92	60.24	58.83	2.34
0.83	2.38	454.39	47.07	44.35	5.78
0.83	2.46	458.22	48.40	45.25	6.51
0.83	2.55	462.53	49.73	46.32	6.87
0.83	2.68	467.96	51.06	47.73	6.52
0.83	2.81	473.85	52.39	49.37	5.76
0.83	2.98	480.67	53.72	51.39	4.34
0.83	3.16	487.93	55.05	53.71	2.44
0.92	2.44	458.91	59.87	52.09	13.00
0.92	2.57	464.90	61.02	53.79	11.84
0.92	2.72	471.51	62.17	55.82	10.22
0.92	2.91	479.48	63.32	58.40	7.77
0.92	3.14	488.81	64.47	61.77	4.18
1.04	2.34	454.02	58.46	55.04	5.84
1.04	2.46	459.88	60.08	56.76	5.53
1.04	2.61	466.37	61.70	58.75	4.79
1.04	2.77	473.36	63.33	61.11	3.51
1.04	2.99	482.27	64.95	64.29	1.02
1.04	3.26	492.47	66.57	68.38	2.72
1.18	2.47	454.09	46.42	51.41	10.75
1.18	2.57	458.72	48.61	52.64	8.29
1.18	2.69	463.67	51.31	54.03	5.30
1.18	2.84	469.72	54.66	55.88	2.23
1.18	3.03	477.27	58.80	58.25	0.93
1.18	3.28	486.43	63.92	61.48	3.82
0.84	4.73	455.39	41.19	39.81	3.35
0.84	4.86	458.56	41.67	40.48	2.85
0.84	5.02	462.29	42.18	41.32	2.04
0.84	5.19	466.24	42.72	42.24	1.12
0.84	5.41	471.05	43.31	43.38	0.15
0.84	5.66	476.36	43.93	44.71	1.78

0.84	5.94	482.11	44.60	46.25	3.71
0.84	6.24	488.22	45.31	48.01	5.95
0.92	4.67	456.13	48.06	45.32	5.69
0.92	4.84	460.19	49.04	46.27	5.65
0.92	5.05	465.07	50.02	47.49	5.05
0.92	5.30	470.71	51.00	49.01	3.89
0.92	5.61	477.41	51.98	50.89	2.10
0.92	5.95	484.49	52.96	53.12	0.30
0.92	6.34	492.06	53.94	55.61	3.10
1.02	4.88	458.82	51.50	49.92	3.06
1.02	5.10	463.71	52.38	51.23	2.20
1.02	5.36	469.58	53.65	52.92	1.35
1.02	5.68	476.33	55.45	54.94	0.92
1.02	6.09	484.40	58.02	57.60	0.72
0.82	7.05	457.45	35.42	36.02	1.70
0.82	7.23	460.35	35.74	36.59	2.37
0.82	7.42	463.37	36.08	37.20	3.10
0.82	7.64	466.69	36.46	37.89	3.91
0.82	7.87	470.23	36.86	38.65	4.87
0.82	8.14	474.27	37.29	39.56	6.09
0.82	8.45	478.74	37.76	40.61	7.55
0.82	8.80	483.61	38.27	41.81	9.25
0.82	9.18	488.75	38.81	43.15	11.20
0.90	6.91	456.34	42.04	41.04	2.38
0.90	7.11	459.59	42.84	41.76	2.53
0.90	7.36	463.51	43.79	42.65	2.61
0.90	7.65	468.01	44.90	43.72	2.63
0.90	7.97	472.86	46.21	44.92	2.80
0.90	8.37	478.67	47.76	46.45	2.75
0.90	8.84	485.13	49.58	48.26	2.67
0.90	9.42	492.78	51.72	50.57	2.22
0.98	6.82	457.04	47.01	45.71	2.77
0.98	7.09	461.32	49.62	46.75	5.78
0.98	7.42	466.54	52.22	48.09	7.92
0.98	7.83	472.79	54.82	49.77	9.21
0.98	8.37	480.69	57.43	52.07	9.33
0.98	9.01	489.40	60.03	54.85	8.64
0.82	9.12	457.77	32.77	34.83	6.30
0.82	9.30	460.12	33.07	35.27	6.66
0.82	9.54	463.04	33.40	35.84	7.30
0.82	9.80	466.16	33.77	36.47	7.98
0.82	10.09	469.58	34.17	37.17	8.79
0.82	10.39	473.06	34.62	37.92	9.53
0.82	10.75	477.08	35.12	38.82	10.53
0.82	11.12	481.17	35.67	39.77	11.51
0.82	11.54	485.73	36.28	40.87	12.66
0.82	12.02	490.64	36.96	42.15	14.03
0.92	9.12	457.96	42.43	40.71	4.05
0.92	9.40	461.42	43.72	41.47	5.16
0.92	9.74	465.53	45.11	42.39	6.03
0.92	10.13	470.08	46.58	43.48	6.66
0.92	10.61	475.52	48.16	44.83	6.92
0.92	11.21	481.97	49.84	46.54	6.62
0.92	11.89	489.11	51.63	48.58	5.90
1.03	9.09	459.40	50.24	45.24	9.94
1.03	9.50	464.33	52.12	46.44	10.90
1.03	9.97	469.90	54.01	47.87	11.36
1.03	10.58	476.74	55.89	49.74	11.01
1.03	11.28	484.35	57.78	51.98	10.05
1.03	12.15	493.10	59.66	54.81	8.13
0.84	11.44	457.80	31.59	34.68	9.80
0.84	11.70	460.32	31.97	35.15	9.94
0.84	11.97	463.05	32.39	35.68	10.16
0.84	12.29	466.08	32.87	36.29	10.40
0.84	12.63	469.32	33.41	36.94	10.58
0.84	13.01	472.76	34.02	37.67	10.73
0.84	13.43	476.59	34.71	38.51	10.94
0.84	13.91	480.74	35.49	39.46	11.19
0.84	14.45	485.32	36.37	40.56	11.51
0.84	15.06	490.39	37.36	41.85	12.02
0.84	15.75	495.87	38.48	43.33	12.60
0.93	11.70	461.52	42.78	40.79	4.65
0.93	12.10	465.43	44.20	41.66	5.76
0.93	12.61	470.22	45.62	42.78	6.23
0.93	13.20	475.56	47.03	44.07	6.29
0.93	13.89	481.64	48.45	45.67	5.75

0.93	14.71	488.51	49.86	47.58	4.57
0.93	15.65	496.01	51.28	49.83	2.82
1.05	11.83	463.69	50.31	44.49	11.58
1.05	12.35	468.60	51.50	45.69	11.29
1.05	13.00	474.51	52.84	47.20	10.68
1.05	13.80	481.42	54.35	49.10	9.66
1.05	14.75	489.31	56.05	51.47	8.18
1.05	15.89	498.28	57.97	54.41	6.15

Bibliography

[1] G.E. Andrews and D. Bradley. Determination of laminar burning velocity: A critical review. *Combustion and Flame*, 18:133, 1972.

[2] J. K. Bechtold and M. Matalon. Effects of stoichiometry on stretched premixed flames. *Combustion and Flame*, 119(3):217 – 232, 1999.

[3] J. Beeckmann, O. Rohl, and N. Peters. Experimental and numerical investigation of iso-octane, methanol and ethanol regarding laminar burning velocity at elevated pressure and temperature. *SAE Technical Paper 2009-01-1774*, 2009.

[4] K. J. Bosschaart and L. P. H. de Goey. Detailed analysis of the heat flux method for measuring burning velocities. *Combustion and Flame*, 132(1-2):170 – 180, 2003.

[5] C.T. Bowman, M. Frenklach, W. R. Gardiner, and G. Smith. *The GRI 3.0 Chemical Kinetics Mechanism*, `www.me.berkeley.edu/gri_mech/`, 1999.

[6] D. Bradley, R. A. Hicks, M. Lawes, C. G. W. Sheppard, and R. Woolley. The measurement of laminar burning velocities and markstein numbers for iso-octane-air and iso-octane-n-heptane-air mixtures at elevated tem-

peratures and pressures in an explosion bomb. *Combustion and Flame*, 115(1-2):126 – 144, 1998.

[7] D. Bradley, M. Lawes, and M.S. Mansour. Explosion bomb measurements of ethanol-air laminar gaseous flame characteristics at pressures up to 1.4mpa. *Combustion and Flame*, 156(7):1462 – 1470, 2009.

[8] S. G. Bryce, R. Lindsay, I. Galliard, and A. R. Glover. Fuels development for formula one. *SAE Technical Paper 942540*, 1994.

[9] Catherine A. Daly, John M. Simmie, Judith Wrmel, Nabiha Djebali, and Claude Paillard. Burning velocities of dimethyl ether and air. *Combustion and Flame*, 125(4):1329 – 1340, 2001.

[10] F.N. Egolfopoulos, P. Cho, and C.K. Law. Laminar flame speeds of methane/air mixtures under reduced and elevated pressures. *Combustion and Flame*, 76:375–391, 1989.

[11] F.N. Egolfopoulos, D.X. Du, and C.K. Law. A study on ethanol oxidation kinetics in laminar premixed flames, flow reactors, and shock tubes. *Proceedings of the Combustion Institute*, 24:833–841, 1992.

[12] F.N. Egolfopoulos, D.L. Zhu, and C.K. Law. Experimental and numerical determination of laminar flame speeds: Mixtures of c2-hydrocarbons with oxygen and nitrogen. *Proceedings of the Combustion Institute*, 23:471–478, 1990.

[13] M. Elia, M. Ulinski, and M. Metghalchi. Laminar burning velocity of methane-air-diluent mixtures. *Journal of engineering for gas turbines and power*, 123:190–196, 2001.

[14] C.R. Ferguson and J.C. Keck. On laminar flame quenching and its application to spark ignition engines. *Combustion and Flame*, 28:197, 1977.

[15] D.H. France and R. Pritchard. Laminar burning velocity measurements using a laser-doppler anemometer. *Journal of Institute of Fuel*, 44:79, 1976.

[16] J. E. Freeh, K. Kumar, Y. Huang, and C. J. Sung. Laminar flame speeds of preheated iso-octane/air and n-decane/air flames using digital particle image velocimetry. In *40th AIAA/ASME/SAE/ASEE Joint Propulsion Conference and Exhibit*, 2004.

[17] G.J. Gibbs and H.F. Calcote. Effect of molecular structure on burning velocity. *Journal of Chemical Engineering and Data*, 4:226, 1959.

[18] Irvin Glassman. *Combustion*. Academic Press, 1996.

[19] X. J. Gu, M. Z. Haq, M. Lawes, and R. Woolley. Laminar burning velocity and markstein lengths of methane-air mixtures. *Combustion and Flame*, 121(1-2):41 – 58, 2000.

[20] O.L. Gulder. Laminar burning velocities of methanol, isooctane and isooctane/methanol blends. *Combustion Science and Technology*, 33:179, 1983.

[21] Omer L. Gulder. Correlations of laminar combustion data for alternative s.i. engine fuels. *SAE Technical Paper 841000*, 1984.

[22] Panfeng Han, M. David Checkel, Brian A. Fleck, and Natalie L. Nowicki. Burning velocity of methane/diluent mixture with reformer gas addition. *Fuel*, 86(4):585 – 596, 2007.

[23] Takashi Hara and Kimitoshi Tanoue. Laminar flame speeds of ethanol, n-heptane, iso-octane air mixtures. *JSAE Paper 20068518*, 2006.

[24] M. I. Hassan, K. T. Aung, and G. M. Faeth. Measured and predicted properties of laminar premixed methane/air flames at various pressures. *Combustion and Flame*, 115(4):539 – 550, 1998.

[25] C. Hasse, M. Bollig, N. Peters, and H. A. Dwyer. Quenching of laminar iso-octane flames at cold walls. *Combustion and Flame*, 122(1-2):117 – 129, 2000.

[26] T. Hirasawa, C. J. Sung, A. Joshi, Z. Yang, H. Wang, and C. K. Law. Determination of laminar flame speeds using digital particle image velocimetry: Binary fuel blends of ethylene, n-butane, and toluene. *Proceedings-Combustion Institute*, 29:1427–1434, 2002.

[27] Y. Huang, C. J. Sung, and J. A. Eng. Laminar flame speeds of primary reference fuels and reformer gas mixtures. *Combustion and Flame*, 139:239–251, 2004.

[28] Zuohua Huang, Qian Wang, Jinrong Yu, Yong Zhang, Ke Zeng, Haiyan Miao, and Deming Jiang. Measurement of laminar burning velocity of dimethyl ether-air premixed mixtures. *Fuel*, 86(15):2360 – 2366, 2007.

[29] Zuohua Huang, Yong Zhang, Ke Zeng, Bing Liu, Qian Wang, and Deming Jiang. Measurements of laminar burning velocities for natural gas-hydrogen-air mixtures. *Combustion and Flame*, 146(1-2):302 – 311, 2006.

[30] S. Jerzembeck, N. Peters, P. Pepiot-Desjardins, and H. Pitsch. Laminar burning velocities at high pressure for primary reference fuels and gasoline: Experimental and numerical investigation. *Combustion and Flame*, 156(2):292 – 301, 2009.

[31] G. Jomaas, C.K. Law, and J.K. Bechtold. On transition to cellularity in expanding spherical flames. *Journal of Fluid Mechanics*, 583:1–26, 2007.

[32] R. J. Kee, J. F. Grcar, M. D. Smooke, and J. A. Miller. Sandia report sand85-8240.

[33] R. J. Kee, F. M. Rupley, and J. A. Miller. Sandia report sand89-8009.

[34] R. J. Kee, J. Warnatz, and J. A. Miller. Sandia report sand83-8209.

[35] Andrew P. Kelley, Grunde Jomaas, and Chung K. Law. Critical radius for sustained propagation of spark-ignited spherical flames. *Combustion and Flame*, 156(5):1006 – 1013, 2009.

[36] Kenneth K. Kuo. *Principles of Combustion*. John Wiley & Sons, Inc., 2nd edition, 2004.

[37] S. Y. Liao, D. M. Jiang, and Q. Cheng. Determination of laminar burning velocities for natural gas. *Fuel*, 83(9):1247 – 1250, 2004.

[38] S.Y. Liao, D.M. Jiang, Z.H. Huang, and K. Zeng. Characterization of laminar premixed methanol-air flames. *Fuel*, 85(10-11):1346 – 1353, 2006.

[39] P.A. Libby and K.N.C. Bray. Implications of the laminar flamelet model in premixed turbulent combustion. *Combustion and Flame*, 39:33–41, 1980.

[40] S.K. Marley and W.L. Roberts. Measurements of laminar burning velocity and markstein number using high-speed chemiluminescence imaging. *Combustion and Flame*, 141(4):473 – 477, 2005.

[41] M. Metghalchi and J.C. Keck. Burning velocities of air with methanol, isooctane, and indolene at high pressure and temperature. *Combustion and Flame*, 48:191, 1982.

[42] David B. Rhodes and James C. Keck. Laminar burning speed measurements of indolene-air-diluent mixtures at high pressures and temperatures. *SAE Technical Paper 850047*, 1985.

[43] Thomas W. III Ryan and Samuel S. Lestz. The laminar burning velocity of issooctane, n-heptane, methanol, methane, and propane at elevated

temperature and pressures in the presence of a diluent. *SAE Technical Paper 800103*, 1980.

[44] Khizer Saeed and C R Stone. The modelling of premixed laminar combustion in a closed vessel. *Combustion Theory and Modelling*, 8(4):721–743, 2004.

[45] Khizer Saeed and C.R. Stone. Measurements of the laminar burning velocity for mixtures of methanol and air from a constant-volume vessel using a multizone model. *Combustion and Flame*, 139(1-2):152 – 166, 2004.

[46] Y. Saso, D. L. Zhu, H. Wang, C. K. Law, and N. Saito. Laminar burning velocities of trifluoromethane-methane mixtures: Experiment and numerical simulation. *Combustion and Flame*, 114(3-4):457 – 468, 1998.

[47] S.P. Sharma, D.D. Agrawal, and C.P. Gupta. The pressure and temperature dependence of burning velocity in a spherical combustrion bomb. *Eighteenth Symposium (International) on Combustion*, page 493, 1981.

[48] Rudolf H. Stanglmaier, Charles E. Roberts, Darius Mehta, Christopher J. Chadwell, J. Corwin Snyder, Matthew Watkins, and Noyes L. Avery. Measurement of laminar burning velocity of multi-component fuel blends for use in high-performance si engines. *SAE Technical Paper 2003-01-3185*, 2003.

[49] R. Stone, A. Clarke, and P. Beckwith. Correlations for the laminar-burning velocity of methane/diluent/air mixtures obtained in free-fall experiments. *Combustion and Flame*, 114(3-4):546 – 555, 1998.

[50] Toni Tahtouh, Fabien Halter, and Christine Mounam-Rousselle. Measurement of laminar burning speeds and markstein lengths using a novel methodology. *Combustion and Flame*, 156(9):1735 – 1743, 2009.

[51] V. Tufano, S. Crescitelli, and G. Russo. Overall kinetic parameters and laminar burning velocity from pressure measurements in closed vessels. *Combustion Science and Technology*, 31:119, 1983.

[52] C.M. Vagelopoulos and F.N. Egolfopoulos. Laminar flame speeds and extinction strain rates of mixtures of carbon monoxide with hydrogen, methane, and air. *Proceedings of the Combustion Institute*, 25:1317–1323, 1994.

[53] Ching-Hua Wang, Gwo-Jiun Ueng, and Mei-Shyong Tsay. An experimental determination of the laminar burning velocities and extinction stretch rates of benzene/air flames. *Combustion and Flame*, 113(1-2):242 – 248, 1998.

[54] The NASA Computer Program CEA (Chemical Equilibrium with Applications). `http://www.grc.nasa.gov/WWW/CEAWeb/`.

[55] Carl L. Yaws. *Chemical Properties Handbook*. McGraw-Hill Professional, 1998.

[56] Zhiyuan Zhang, Zuohua Huang, Xiangang Wang, Jun Xiang, Xibin Wang, and Haiyan Miao. Measurements of laminar burning velocities and markstein lengths for methanol-air-nitrogen mixtures at elevated pressures and temperatures. *Combustion and Flame*, 155(3):358 – 368, 2008.

[57] D.L. Zhu, F.N. Egolfopoulos, and C.K. Law. Experimental and numerical determination of laminar flame speeds of methane/(ar, n2, co2)-air mixtures as function of stoichiometry, pressure, and flame temperature. *Proceedings of the Combustion Institute*, 22:1537–1545, 1988.

Vita

Jung Joo Byun was born in Seoul, Rep. of Korea on 16 November 1976, as a son of Dr. Hee Joon Byun and Hye Sik Shin. In 1995, he entered Hongik University in Seoul and received the degree of Bachelor of Science with a major in Mechanical Engineering in 2002. He entered Korea Advanced Institute of Science and Technology(KAIST) in Daejeon in 2002 and received the degree of Master of Science with a major in Mechanical Engineering in 2004. During the following one and half years, he worked in Hongik University's annexed science and technology laboratory as a researcher. In August 2005, he entered The Graduate School of The University of Texas at Austin. During his Ph.D study, from September 2007 to September 2009, he worked as a student intern at Southwest Research Institute(SwRI) in San Antonio, TX. He married Hye Jin Jung in 2007 and had a baby girl, Elaina in 2011.

Permanent address: Samsung Hillstate APT 211-202
50 Samsung 2-dong
Gangnam-gu Seoul, 135-877 South Korea

This dissertation was typeset with LaTeX[†] by the author.

[†]LaTeX is a document preparation system developed by Leslie Lamport as a special version of Donald Knuth's TeX Program.